Fall 2010

Robust frequency-domain turbo equalization for multiple-input multiple-output (MIMO) wireless communications

Jian Zhang

ROBUST FREQUENCY-DOMAIN TURBO EQUALIZATION FOR MULTIPLE-INPUT MULTIPLE-OUTPUT (MIMO) WIRELESS COMMUNICATIONS

by

JIAN ZHANG

A DISSERTATION

Presented to the Faculty of the Graduate School of the

MISSOURI UNIVERSITY OF SCIENCE & TECHNOLOGY

In Partial Fulfillment of the Requirements for the Degree

DOCTOR OF PHILOSOPHY

in

ELECTRICAL ENGINEERING

2010

Approved by

Yahong Rosa Zheng, Advisor
Steve Grant
Randy H. Moss
R. Joe Stanley
Sanjay Madria

PUBLICATION DISSERTATION OPTION

This dissertation consists of the following five published or submitted papers , formatted in the style used by the Missouri University of Science and Technology, listed as follows:

Paper 1, J. Zhang and Y. R. Zheng, "Improved Frequency-Domain Channel Estimation and Equalization for MIMO Wireless Communications," has been published in Int. J. Wireless Inf. Networks, vol.16, pp.12-21, June 2009.

Paper 2, J. Zhang, Y. R. Zheng, C. Xiao, and K. B. Letaief, "Channel equalization and symbol detection for single carrier MIMO systems in the presence of multiple carrier frequency offsets," has been published in IEEE Trans. Veh. Technol., vol.59, pp.2021-2030, May 2010.

Paper 3, J. Zhang and Y. R. Zheng, "Layered frequency-domain equalization for single carrier MIMO systems with multiple carrier frequency offsets," has been published in Proc. IEEE GlobeCom'09, Dec. 2009.

Paper 4, J. Zhang and Y. R. Zheng, "Frequency-Domain Turbo Equalization with Soft-Successive Interference cancellation for single carrier MIMO underwater acoustic communications," IEEE Trans. Wireless Commun., in revision, June 2010.

Paper 5, J. Zhang and Y. R. Zheng, "Bandwidth-Efficient Frequency-Domain Equalization for Single Carrier Multiple-Input Multiple-Output Underwater Acoustic Communications," will be published by Journal of the Acoustic Society of America, Oct. 2010.

ABSTRACT

This dissertation investigates single carrier frequency-domain equalization (SC-FDE) with multiple-input multiple-output (MIMO) channels for radio frequency (RF) and underwater acoustic (UWA) wireless communications. It consists of five papers, selected from a total of 13 publications. Each paper focuses on a specific technical challenge of the SC-FDE MIMO system.

The first paper proposes an improved frequency-domain channel estimation method based on interpolation to track fast time-varying fading channels using a small amount of training symbols in a large data block. The second paper addresses the carrier frequency offset (CFO) problem using a new group-wise phase estimation and compensation algorithm to combat phase distortion caused by CFOs, rather than to explicitly estimate the CFOs. The third paper incorporates layered frequency-domain equalization with the phase correction algorithm to combat the fast phase rotation in coherent communications. In the fourth paper, the frequency-domain equalization combined with the turbo principle and soft successive interference cancelation (SSIC) is proposed to further improve the bit error rate (BER) performance of UWA communications. In the fifth paper, a bandwidth-efficient SC-FDE scheme incorporating decision-directed channel estimation is proposed for UWA MIMO communication systems. The proposed algorithms are tested by extensive computer simulations and real ocean experiment data. The results demonstrate significant performance improvements in four aspects: improved channel tracking, reduced BER, reduced computational complexity, and enhanced data efficiency.

ACKNOWLEDGMENTS

I would like to express my gratitude to all the people who helped me through the journey of PhD study.

First, I would like to thank my advisor, Dr. Yahong Rosa Zheng, for inspiring my interests in the wonderful world of wireless communications, for developing my professional research skills, for cultivating my independent scientific thinking, and for supporting me both technically and financially. Her meticulous scientific attitude, strict academic requirement, and valuable comments on my research work and technical writing imposed a deep influence on my career development. I would also like to express my appreciation to Dr. Chengshan Xiao, for his guidance in the joint research projects during the past three and half years. I acknowledge the support of Office of Naval Research and National Science Foundation for sponsoring the research projects.

I am very grateful to the members of my advisory committee, Drs. Steve Grant, Randy H. Moss, R. Joe Stanley, and Sanjay Madria, for their precious time and valuable advice in examining this dissertation.

I would like to thank all the students in the Communication and Real-Time Signal Processing lab at Missouri S&T for their kind assistance on my research work, and thank all my friends in Rolla for their help during my Ph.D. years.

Finally, I wish to express my heartful thanks to both sides of my family for their unselfish love and everlasting support. Particularly, I would like to thank my dearest parents, for bring me up and shaping my character of great virtue, and thank my parents-in-law for providing me encouragement and experience of overcoming difficulties. I would also like to offer my extraordinary thanks to my wife, Tiange Shao, for her generous love, constant encouragement, and full support.

TABLE OF CONTENTS

Page

LIST OF ILLUSTRATIONS

PAPER 3

PAPER 4

PAPER 5

LIST OF TABLES

1. INTRODUCTION

1.1 BACKGROUND

Multiple-input multiple-output (MIMO) technology is a promising theme for high data rate, high reliability wireless communications. The so-called multiple-input multiple-output refers to the physical layer of communication systems that employ multiple transmit antennas/elements and multiple receive antennas/elements, as shown in Fig. 1.1. Recent theoretic studies have shown that MIMO systems can provide significant capacity gain [1] without additional bandwidth or transmit power over traditional single-input and single-output (SISO) systems. In quasi-static flat Rayleigh fading channels, the MIMO capacity grows linearly, rather than logarithmically, with the minimum number of transmit and receiver antennas. The tremendous MIMO channel capacity gain can be achieved by spatial multiplexing and diversity coding, thus improving data rate and reliability of wireless communication systems. However, the goal of applying MIMO technology to achieve high data rate with high reli-

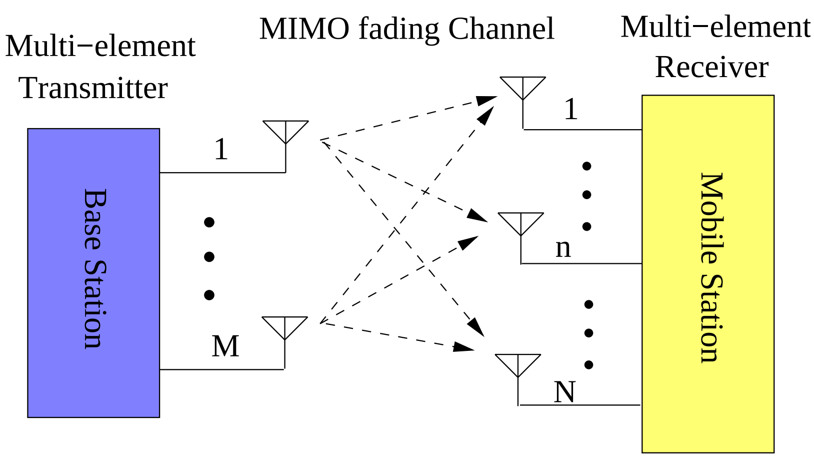

Figure 1.1 A typical MIMO system

ability in a wireless communication system is impeded by several challenges. In general, a wireless channel is a triply-selective fading channel in practice. Firstly, the propagation between each transmit and each receive element consists of a large number of reflectors and/or scatters, which results in multiple “echoes” of the transmitted signals at receivers. This multipath delay spread effect is referred to as the frequency selective channel. Secondly, the motion of the transmitter/receiver and the movement of objects in the propagation environment also give rise to the Doppler spread, which indicates the time varying nature of the channel. This effect is called as time selective channel. Last, the angle spread at the multiple transmitter and receiver elements leads to the space selective effect. These three selectiveness are intertwined with each other, causing significant technical challenges in practical MIMO transceiver design.

In particular, the frequency selectiveness caused by multi-path delay effect can result in severe inter-symbol interference (ISI), which increases the complexity of receiver and degrades the performance of communications if not dealt with properly. The time selectiveness associated with Doppler spread can lead to fast time-varying channel responses and Doppler modulation, which imposes much difficulty on channel synchronization. Besides, carrier frequency offset (CFO) causes significant performance degradation if the Doppler spread is large. CFO is often caused by the local oscillator mismatch in radio frequency (RF) communications or instantaneous time-varying Doppler shift in underwater acoustic communications. The CFOs can result in severe phase distortion on coherent communications. The space selectiveness in a MIMO system results in the co-channel interference (CCI) which has to be removed for correct detection of data streams from different transmit elements. These three dispersions (ISI, Doppler modulation/CFO, and CCI) are also intertwined causing formidable difficulties in MIMO transceiver design.

Channel estimation is the first problem to be addressed in the receiver. However, due to the existence of CCI and Doppler spread, a specified approach should be developed to estimate all channels separately, track the fast time varying channels, and combat the effect of CFO. Another important issue in the receiver is to mitigate ISI and ICI. A common approach to combat ISI and CCI is by equalization. Traditional time-domain equalizers suffer from high computational complexity and slow convergence when the channel length is long and CCI is severe, because the complexity grows quadratically with the number of receiver elements and the number of channel taps. In high data-rate communication systems, these numbers are on the order of ten and hundred, respectively. TDE is then computationally prohibitive in practice and with intolerable slow convergence. Frequency-domain methods have to be used to solve the problem.

There are mainly two frequency-domain equalization methods for modern high data rate wireless communications: orthogonal frequency division multiplexing (OFDM) and single carrier with FDE (SC-FDE). These two types of systems share the common functional components but differ in the replacement of inverse fast Fourier transform (IFFT) operations: in OFDM, IFFT is performed at transmitter; in SC, IFFT is performed at receiver. The function blocks for these two systems are shown in Fig. 1.2. In both schemes, data are transmitted in blocks, and cyclic prefix (CP) or zero padding (ZP) are inserted between blocks. The SC-FDE has a similar complexity and performance as the OFDM with the same bandwidth efficiency, but is less sensitive to carrier frequency offset (CFO) and nonlinear distortions.

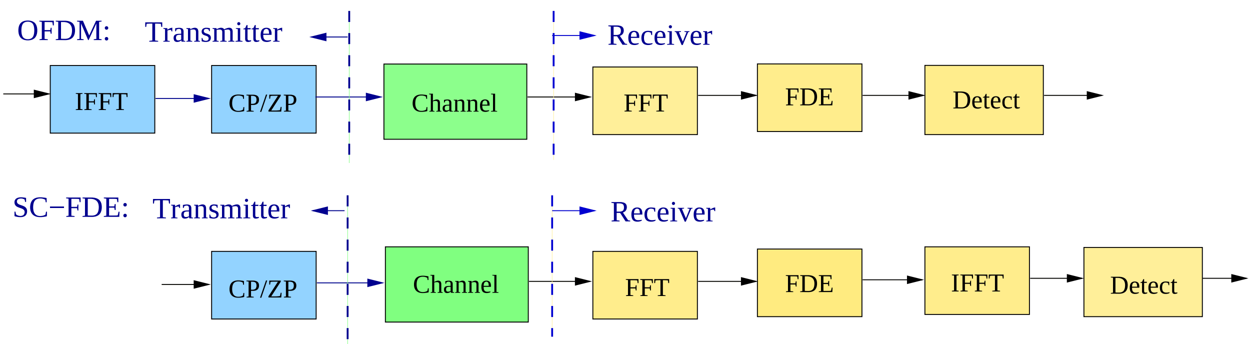

Figure 1.2 Function blocks of OFDM and SC-FDE

1.2 PROBLEM STATEMENT

This dissertation focuses on SC-FDE for MIMO wireless communications and its application to difficult RF and underwater channels. In a high data-rate MIMO SC-FDE system, the information bits or encoded bits are mapped into symbols based on the specified modulation scheme and then grouped into blocks appended by CPs or ZPs. The data streams from all branches are transmitted simultaneously in the same carrier. The RF channels normally have a few tens of taps. At receivers, CPs are removed or overlap-add is employed if ZPs are used in one data block, and fast Fourier Transform (FFT) is applied to convert the time-domain signal to frequency domain. The equalization is carried out in each frequency tone, and the equalized frequency-domain signal is converted to time domain to detect the symbols.

Specially, this dissertation investigates four technical challenges associated with high data-rate MIMO SC-FDE systems.

1. Channel estimation for fast time-varying MIMO channels. A common approach of estimating the channel impulse response is to insert known pilot symbols in the data streams and use the received pilot signals to estimate the channels. For MIMO architecture, all the subchannels corresponding to the transmitter and receiver pairs have to be estimated. Pilot-assisted channel estimation falls into three categories based on the construction of pilot blocks: (1) time domain nonorthogonal and frequency domain orthogonal, (2) time domain orthogonal and frequency domain nonorthogonal, (3) both time domain and frequency domain nonorthogonal. In the first method, pilot blocks are designed with mutually orthogonal spectral for each transmit element but are transmitted simultaneously from all transmit elements. In the second method, pilot blocks are uncorrelated for all transmit elements and transmitted sequentially in time. In the third method, independent pilot blocks with mutually nonorthogonal spectral are transmitted simultaneously, and a least square approach is employed to estimate channels. In my work, methods (1) and (3) are investigated to track the time-varying channel impulse responses.

2. BER performance improvement for MIMO system without increasing transmit power. Channel coding allows a reduction of transmit power to achieve the same error performance with respect to uncoded systems in the cost of increasing transmission bandwidth. Turbo code is one of the powerful channel coding schemes which approaches Shannon limits. Based on the principle of turbo code, turbo equalization is proposed to

combat ISI and reduce error rate in an iterative detection way. In the turbo equalization, channel decoder cooperates with the equalizer by exchanging the soft information on the coded bits and the confidence on the information bits is increased gradually. Therefore, turbo equalization [2][3] provides significant performance gain with low computational complexity. In order to further improve BER performance for MIMO systems, a novel detection scheme combining turbo equalization and layer detection [4][5] is investigated in this work.

3. Severe CFO mitigation. After equalization, the effect of CFO should be mitigated before making hard decision or soft decision on the symbols. CFO can cause severe phase errors on the equalized signals when the block size is large and/or the constellation size of the modulation is high in a SC-FDE system. Rather than directly estimating the CFO by training symbols, which costs amount of computation, efficient phase correction algorithms are applied after equalization to compensate the composite phase distortion.

4. Complexity and data efficiency. In order to reduce the complexity of receivers for MIMO systems over severely dispersive channels, the frequency-selective channels are divided into frequency-flat channels by discrete Fourier transform and equalization is implemented in frequency domain. Compared with time-domain equalization, frequency-domain equalization achieves better performance with significantly reduced complexity. However, FDE requires cyclic prefix or unique word to be inserted between the data blocks, which results in large transmission overhead in high data rate MIMO communications. A bandwidth-efficient SC-FDE scheme based on the overlap-save method is investigated to increase data efficiency while maintaining similar BER performance.

The developed MIMO channel estimation and equalization schemes are applied to underwater acoustic communication systems. Underwater acoustic channels impose more challenges than radio frequency (RF) environment. Acoustic propagation is characterized by three major factors: frequency-dependent attenuation, excessive delay spread, and significant time-varying Doppler shift. The attenuation of acoustic waves is approximately proportional to the square of the frequency, leading to extremely low carrier frequency, limited bandwidth and limited communication range. For example, in medium underwater acoustic communication systems operating over 1 to 10 kilometers, the available bandwidth is only on the order of several kHz. Another character of underwater acoustic channels is the severe multipath propagation that causes long delay spread of a few up to hundreds of milliseconds depending on the communication range and channel conditions. In addition, the time varying Doppler shift, caused by the relative motion between transducers and hydrophones, dynamic motion of water media, and varying sound speed, is another obstacle for UWA communications. The ratio of Doppler shift to carrier frequency is on the order of 10^{-3} to 10^{-4}, which is more significant than that of the RF counterpart (on the order of 10^{-6}). The significant Doppler shift results in not only rapid fluctuation of the fading channels but also compression or dilation of signal waveforms. These features make underwater acoustic channel considered as one of the worst physical links for communications, and achieving reliable wireless underwater communications over 5 kbps has been a challenging goal for the research community for decades. The proposed FDE schemes, phase correction algorithm and channel estimation methods are applied to these challenging channels to improve the data rate and reliability of UWA communications.

1.3 SUMMARY OF CONTRIBUTIONS

This thesis includes the technical novelties in the five publications. The complete publication list can be found in Section 3. The technical contributions are:

1. Improved frequency-domain MIMO channel estimation method using interpolation vectors for MIMO SC FDE systems. The proposed algorithm employs the least squares (LS) criterion to estimate frequency response of the pilot block. It then estimates frequency response of the data block by interpolating the channel frequency responses of two adjacent pilot blocks thus tracks the fast time-varying channel responses. The Chu sequence is adopted as the pilot signals since it has a constant magnitude in both frequency and time domains. This novel MIMO channel estimation method exploits the correlation of the channel response and effectively improves the accuracy of channel estimation without significantly increasing complexity. Simulation studies for 2×2,

2×4, 2×8, 4×4, 4×8, and 8×8 MIMO systems were considered and the frequency selective channel had several tens of taps. The simulation results showed that the estimated channels are very close to the true channels and the FDE using the estimated channels can achieve BER performance close to perfect known channels.

2. Combating multiple unknown CFOs in MIMO SC FDE. The degradation of performance caused by CFO in MIMO SC FDE systems boosts the necessity of mitigating the effect of CFO. It shows that the constellation of the equalized data is rotated due to multiple CFOs for large block size and high constellation size in single carrier transmission. As a result, the equalized data cannot be reliably detected without removing the phase distortion caused by the multiple unknown CFOs. Instead of estimating the CFOs directly, a novel and robust method is proposed to estimate the rotated phases and remove the rotated phases for the equalized data. The basic MMSE FDE and layered FDE were applied to evaluate the performance of the CFO mitigation algorithms. Simulation and experimental results demonstrate that the phase correction algorithm can effectively eliminate the effect of CFO.

3. Frequency-domain turbo equalization (FDTE) and multiuser detection with soft successive interference cancellation (SSIC) for MIMO SC FDE systems. In this turbo detection, the channel equalization and decoding are iteratively applied on the same block of data, and the extrinsic information on the coded bits are exchanged between these two modules. Different from the traditional MMSE FDE, the proposed turbo FDE feeds forward the extrinsic information of the coded bits represented by LLRs to the decoder and the extrinsic LLRs gleaned by the decoders are then fed back to the equalizer. The proposed scheme preferentially detects the data streams with higher power, and the interference induced by the strong streams are softly canceled out from the received data. The bit error rate of the detection is improved as the number of iterations increases.

4. Bandwidth-efficient MIMO SC FDE scheme incorporated with decision-directed channel estimation. The proposed FDE is executed based on the overlap-save method by

dividing a large data block into small subblocks. An overlapped window is formed, which consists of the current subblock and small parts of the previous and subsequent subblocks. The time-varying channel impulse responses are timely tracked by the detected subblock data. Therefore, a block with the length much larger than the channel coherence time can be equalized by the FDE with only one pilot block without performance degradation, thus improving the data efficiency at the cost of slightly increased computational complexity. At the same data efficiency, the proposed FDE significantly improves BER performance compared to the traditional FDE.

5. Application of MIMO SC FDE transceiver in underwater acoustic communication systems. MIMO SC FDE transceiver architectures with 2-4 transducers and 12 hydrophones have been employed in several medium range undersea experiments, including Reschedule Acoustic Communications Experiment(RACE) and Surface Process and Acoustic Communications Experiment(SPACE) conducted by Woods Hole Oceanographic Institution (WHOI) in March and October, 2008, respectively. The aforementioned pilot-assisted MIMO channel estimation algorithm, the phase correction algorithm, the FDTE-SSIC and the bandwidth-efficient FDE algorithms have been tested in these harsh underwater channels with memory of several tens to one hundred taps and several Hz Doppler spread. The results have shown that the proposed transceiver structures can support high data-rate underwater acoustic communications with low bit error rate.

1.4 REFERENCES

[1] G. J. Foschini and M. J. Gans,"On limits of wireless communications in a fading environment when using multiple antennas," *Wireless Personal Commun.*, vol. 6, pp.311-335, 1998.

[2] M. Tüchler, A. C. Singer, and R. Koetter,"Minimum mean squared error equalization using a priori information," *IEEE Trans. Signal Proc.*, vol. 50, pp. 673-683, Mar. 2002.

[3] Y. Wu, X. Zhu, and A. K. Nandi, "Low complexity adaptive turbo space-frequency equalization for single-carrier multiple-input multiple output systems," *IEEE Trans. Wireless Commun.*, vol. 7, pp. 2050-2056, June 2008.

[4] G. J. Foschini, "Layered space-time architecture for wireless communication in a fading environment when using multi-element antennas," *Bell Labs Tech. J.*, vol. 1, pp. 41-59, Autunm, 1996.

[5] X. Zhu and R. D. Murch, "Layered space-frequency equalization in a single-carrier MIMO system for frequency-selective channels," *IEEE Trans. Wireless Commun.*, vol. 3, pp. 701-708, May 2004.

PAPER

1. IMPROVED FREQUENCY-DOMAIN CHANNEL ESTIMATION AND EQUALIZATION FOR MIMO WIRELESS COMMUNICATIONS

Jian Zhang and Rosa Yahong Zheng

Abstract—This paper introduces an improved frequency-domain channel estimation method based on interpolation vectors for single-carrier frequency-domain equalization (SC-FDE) with the multiple-input multiple output (MIMO) scheme. The proposed algorithm is derived by employing the least squares (LS) criterion, and a specified application for the wide sense stationary uncorrelated scattering (WSSUS) Rayleigh fading channel is presented. The channel frequency-domain responses estimated at two adjacent pilot blocks are used to track the time-variant channel information, which can effectively improve the accuracy of channel estimation and without significantly increasing complexity. Maximum mean square error (MMSE) frequency-domain equalization based on the estimated channel is employed in the receiver to recover transmitted signals. This paper also investigates The training sequence design method for multiple transmit antennas and the noise variance estimation method. Numerical simulation results show that the proposed methods can perform very well for fading channels with long multipath delay and high Doppler spread.

1. INTRODUCTION

High data rate is one of the main aims in broadband wireless communication. However, a fundamental challenge of achieving this goal is mitigating the inter-symbol interference (ISI) resulting from multipath propagation. The classical approach to combat ISI is time domain equalization(TDE). However, its complexity, *i.e.*, the number of operations per detected symbol, grows linearly with the maximum channel impulse response length. Frequency-domain equalization(FDE), which has been promoted as a promising alternative technique for overcoming ISI, exhibits good performance with substantial computation reduction [1]. Thus, orthogonal frequency division multiplexing (OFDM) and single carrier with FDE systems have been the two primary techniques in future broadband wireless communications. They share common functional components but differ in the placement of inverse fast Fourier transform (IFFT) operation. In complexity and performance, SC-FDE is similar to OFDM, but it avoids many of the drawbacks inherent in OFDM systems, such as high peak-to average power ratio (PARA) and high sensitivity to carrier frequency offset. The dual-mode system, which uses OFDM in the downlink and SC in the uplink, has recently become popular. It can concentrate most computational complexity at the base station, thus, reducing the overload of subscribes.

In recent years, the combination of SC-FDE with multiple-input multiple output (MIMO) has received more attention in the literature [2] - [12]. The design of a SC-FDE based on minimum mean square error criterion for a spatial multiplexing (SM) MIMO system has been proposed in [2] and [3]. The application of SC-FDE to a space time block coded (STBC) system is also investigated in [11] and [12]. Whichever MIMO architecture is adopted, knowledge about the channel's frequency transfer function is required to design the equalizer. Adaptive FDE schemes based on the least mean squares (LMS) algorithm and the recursive least squares (RLS) algorithm for MIMO and single-input multiple output(SIMO) systems are studied in [4], [27], and [14]. In these adaptive algorithms, known pilot signals are transmitted prior to data transmission to probe the initial channel information in training mode. The estimator then switches to a decision-directed mode to track the channel information for different periods of time. However, the performance of the adaptive algorithms is not satisfactory for fast time-varying fading channels due to the weak correlation of the channel at different times.

This paper proposes a least-squares (LS) channel estimation algorithm for a MIMO SC-FDE system employing the interpolation method. Although the algorithm can be implemented in STBC architectures, the focus in this paper is on its application in SM architectures. The advantages of this channel estimation algorithm are twofold. First, because it takes advantage of the channel estimations at two neighboring pilots to obtain the interpolation vectors, the estimated channel information is more accurate than that obtained by adaptive algorithms. Second, the interpolation coefficients can be computed offline once the Doppler frequency spread and the noise variance are estimated. Thus, it has a complexity similar to adaptive algorithms. Obviously, the cost of this method is that processing the current frame's data must be delayed until the arrival of the next frame. The idea behind this method is similar to that behind the time-domain interpolation method introduced in [16] and [17], but it differs in that the algorithm is implemented in the frequency domain. This method has been employed in SIMO single carrier communication systems, and demonstrated to perform effectively even in fast time varying channel environments [15]. The design of training sequences in MIMO architecture will become complex due to the superposition of signals transmitted from different antennas. The method proposed in [19] is used here to assign the pilot sequences with particular formats to transmit antennas. The performance of this method is evaluated here in combination with the interpolation method for estimating the time-varying channel.

The following notions are generally used throughout the paper: lowercase bold fonts represent vectors or matrices in the time-domain, uppercase bold fonts denote vectors or matrices in the frequency domain, $\mathbf{I}_m$ is an $m \times m$ identity matrix, and superscripts $(\cdot)^*$, $(\cdot)^{-1}$, $(\cdot)^T$, and $(\cdot)^H$ denote the complex conjugate, inverse, transpose, and conjugate transpose, respectively.

2. SYSTEM MODEL AND MMSE-SCFDE FOR MIMO

2.1 MIMO Transceiver Architecture. Consider a spatial multiplexing MIMO system with n_T transmit antennas and n_R receive antennas. The baseband equivalent model is shown in Fig. 1. At the transmitter, a high-rate data stream is split into n_T independent branches by a serial-to-parallel (S/P) converter. At each branch, the data stream is grouped into blocks. After periodically inserting the cyclic prefixes (CPs), all blocks are transmitted simultaneously over the frequency selective channel using the same carrier. At the receive end, distorted receive signals are first processed by the front end of all antennas, then the CP is removed. Next, the received data are converted into frequency domain by applying fast Fourier transform (FFT). Frequency-domain channel estimation, equalization, and demultiplexing are then performed. Finally, an inverse fast Fourier transform (IFFT) is used to convert the frequency domain signal to time domain for demodulating. A parallel-to-serial (P/S) converter is applied to output the estimated data sequence serially.

The data must be organized blockwise for transmission in a MIMO-SCFDE system. The data structure used in this system is shown in Fig. 2. At the beginning of a frame,

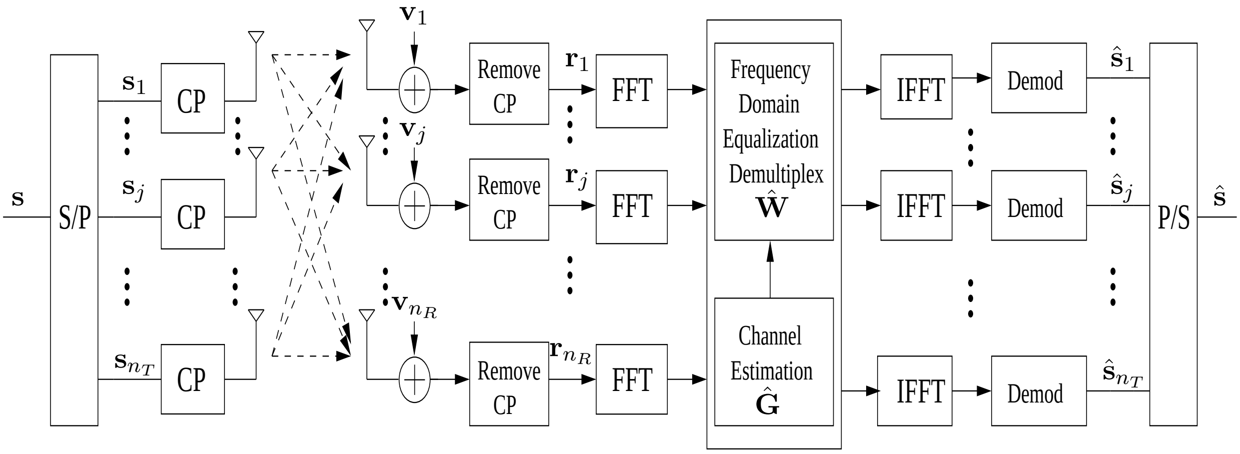

Figure 1 MIMO-SCFDE system with spatial multiplexing architecture

a pilot block is first transmitted to obtain an initial estimation of the channel's frequency domain response. The rest of the frame are data blocks. Each block consists of N data symbols and a length-N_c CP that is the copy of the last N_c symbols of the current block are appended. To eliminate inter-block interference (IBI), the constraint $N_c \geq L-1$ is necessary, where L represents the length of impulse response of the frequency selective fading channel. The period of one block is $T_b = (N + N_c)T_s$ and the frame duration is $T_f = N_f(N + N_c)T_s$, where T_s is the symbol period and N_f is the number of blocks in one frame.

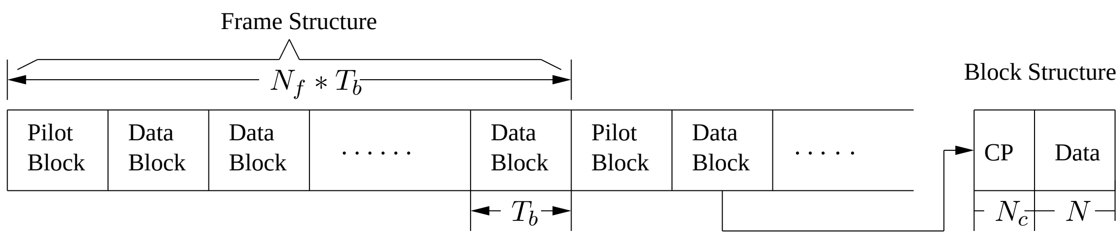

Figure 2 Frame structure

2.2 System Model. Let $\mathbf{s}_j = [s_j(1), \ldots, s_j(N)]^T$ be a data block to be transmitted from the j-th antenna. After removing CP at the i-th receive antenna, the received data block can be presented by

$$\mathbf{r}_i = \sum_{j=1}^{n_T} \mathbf{g}_{i,j}\mathbf{s}_j + \mathbf{v}_i \tag{1}$$

where $\mathbf{r}_i$ and $\mathbf{v}_i$ denote the length-N received data block and complex Gaussian noise vector added at i-th receive antenna with variance $\sigma^2/2$ per dimension. An $N \times N$ circulant channel matrix defined by the channel impulse response (CIR) between the i-th receive antenna and the j-th transmit antenna, $\mathbf{g}_{i,j}$, is expressed as

$$\mathbf{g}_{i,j} = \begin{bmatrix} g_{i,j}(1) & 0 & \dots & g_{i,j}(L) & \dots & g_{i,j}(2) \\ g_{i,j}(2) & g_{i,j}(1) & \ddots & \ddots & \ddots & \vdots \\ \vdots & \ddots & \ddots & \ddots & \ddots & g_{i,j}(L) \\ g_{i,j}(L) & \ddots & g_{i,j}(1) & 0 & \ddots & 0 \\ 0 & g_{i,j}(L) & \ddots & \ddots & \ddots & \ddots \\ \vdots & \ddots & \ddots & \ddots & \ddots & 0 \\ 0 & \dots & g_{i,j}(L) & \dots & \dots & g_{i,j}(1) \end{bmatrix}. \tag{2}$$

This equation is based on the significant assumption that the response of the frequency selective channel remains invariant for the duration of one block. A practical time-varying frequency selective fading channel generally varies even within one block. However, if the block time duration T_b is smaller than the channel coherence time, the fading channel can be supposed to be approximately time-invariant.

The MIMO system is expressed in matrix form as

$$\mathbf{r} = \mathbf{g}_M\mathbf{s} + \mathbf{v} \tag{3}$$

where $\mathbf{s} = [\mathbf{s}_1^T,\ \mathbf{s}_2^T,\ \dots,\ \mathbf{s}_{n_T}^T]^T$, $\mathbf{r} = [\mathbf{r}_1^T,\ \mathbf{r}_2^T,\ \dots,\ \mathbf{r}_{n_R}^T]^T$, $\mathbf{v} = [\mathbf{v}_1^T,\ \dots,\ \mathbf{v}_{n_R}^T]^T$. $\mathbf{g}_M$ is a matrix with a size of $(Nn_R) \times (Nn_T)$, given by

$$\mathbf{g}_M = \begin{bmatrix} \mathbf{g}_{1,1} & \cdots & \mathbf{g}_{1,n_T} \\ \vdots & \ddots & \vdots \\ \mathbf{g}_{n_R,1} & \cdots & \mathbf{g}_{n_R,n_T} \end{bmatrix} \tag{4}$$

Define $\mathbf{B}_K = \mathbf{I}_K \otimes \mathbf{F}_N$, where $\otimes$ denotes the Kronecker product and $\mathbf{F}_N$ is the normalized DFT matrix of size $N \times N$. The (m,n)-th element of $\mathbf{F}_N$ is given by $\frac{1}{\sqrt{N}} \exp\left(\frac{-j2\pi(m-1)(n-1)}{N}\right)$ for $m,\ n = 1,\ 2,\ \ldots,\ N$. Applying the DFT to the received signal and using the property $\mathbf{B}_{n_T}^H \mathbf{B}_{n_T} = \mathbf{I}_{Nn_T}$, the frequency-domain representation is obtained as expressed by equation (3):

$$\begin{aligned} \mathbf{R} = \mathbf{B}_{n_R}\mathbf{r} &= \mathbf{B}_{n_R}\mathbf{g}_M\mathbf{s} + \mathbf{B}_{n_R}\mathbf{v} \\ &= \mathbf{B}_{n_R}\mathbf{g}_M\mathbf{B}_{n_T}^H\mathbf{B}_{n_T}\mathbf{s} + \mathbf{B}_{n_R}\mathbf{v} \\ &= \mathbf{G}_M\mathbf{S} + \mathbf{V} \end{aligned} \tag{5}$$

where the DFT of transmitted data and received data are respectively denoted by $\mathbf{S} = \mathbf{B}_{n_T}\mathbf{s}$ and $\mathbf{R} = \mathbf{B}_{n_R}\mathbf{r}$. The block matrix $\mathbf{G}_M = \mathbf{B}_{n_R}\mathbf{g}_M\mathbf{B}_{n_T}^H$ is defined by:

$$\mathbf{G}_M = \begin{bmatrix} \mathbf{G}_{1,1} & \cdots & \mathbf{G}_{1,n_T} \\ \vdots & \ddots & \vdots \\ \mathbf{G}_{n_R,1} & \cdots & \mathbf{G}_{n_R,n_T} \end{bmatrix} \tag{6}$$

Because $\mathbf{g}_{i,j}$ is a circulant matrix, $\mathbf{G}_{i,j}$ will be a diagonal matrix whose elements correspond to the frequency response of the channel between the i-th receive antenna and the j-th transmit antenna. The notation $\mathbf{V}$ represents the frequency domain of the complex Gaussian white noise, which has the same variance as $\mathbf{v}$. The weights of the MMSE equalizer have been given according to MMSE criterion in [2]

$$\hat{\mathbf{W}}_{MMSE} = P_s\mathbf{G}_M^H[P_s\mathbf{G}_M\ \mathbf{G}_M^H + \sigma^2\mathbf{I}_{Nn_R}]^{-1} \tag{7}$$

where P_s is the average power of the transmit signal.

As shown in equation (7), the computation of the MMSE frequency-domain equalizer will become difficult as N and the number of antennas increase due to the inverse of the large matrix. Using the properties of matrix transformation, the computation can be simplified by decomposing equation (7) into each frequency bin. Hence, we define

$$\mathbf{G}^k = \begin{bmatrix} G_{1,1}(k) & \dots & G_{1,n_T}(k) \\ \vdots & \ddots & \vdots \\ G_{n_R,1}(k) & \dots & G_{n_R,n_T}(k) \end{bmatrix} \tag{8}$$

as a $n_R \times n_T$ matrix consisting of all the k-th diagonal elements of $\mathbf{G}_{i,j}$. The vectors $\mathbf{R}^k = [R_1(k),\ \dots,\ R_{n_R}(k)]^T$, $\mathbf{S}^k = [S_1(k),\ \dots,\ S_{n_T}(k)]^T$, and $\mathbf{V}^k = [V_1(k),\ \dots,\ V_{n_R}(k)]^T$represent the response of the k-th frequency tone of received signal, transmitted signal, and noise, respectively. Thus,

$$\mathbf{R}^k = \mathbf{G}^k\mathbf{S}^k + \mathbf{V}^k, \qquad k = 1,\ \dots,\ N \tag{9}$$

The frequency estimation of an equalized signal can be obtained by employing the aforementioned MMSE equalizer:

$$\hat{\mathbf{S}}^k = P_s(\hat{\mathbf{G}}^k)^H[P_s\hat{\mathbf{G}}^k(\hat{\mathbf{G}}^k)^H + \sigma^2\mathbf{I}_{n_R} + \varepsilon\mathbf{I}_{n_R}]^{-1}\mathbf{R}^k \tag{10}$$

where $\hat{\mathbf{G}}^k$ is the estimated channel transfer function and ε is minimum mean error of channel estimation. It should be noted that the channel equalizer given by equation (10) takes into account the channel estimation error ε, unlike equation (7).

Proof: Let $\mathbf{E}^k$ be the estimation error matrix. Then, $\mathbf{G}^k = \hat{\mathbf{G}}^k + \mathbf{E}^k$. Replacing $\mathbf{G}^k$ in equation (9) yields

$$\mathbf{R}^k = \hat{\mathbf{G}}^k\mathbf{S}^k + \mathbf{E}^k\mathbf{S}^k + \mathbf{V}^k \tag{11}$$

Let $\hat{\mathbf{W}}^k$ be the frequency-domain equalizer matrix for the k-th frequency bin, and let the output of the equalizer be given by $\hat{\mathbf{S}}^k = \hat{\mathbf{W}}^k\mathbf{R}^k$. The equalization error vector is denoted by:

$$\Delta(k) = \mathbf{S}^k - \hat{\mathbf{S}}^k = \mathbf{S}^k - \hat{\mathbf{W}}^k\mathbf{R}^k \tag{12}$$

To obtain $\hat{\mathbf{W}}^k$, the following optimal equation must be solved:

$$\hat{\mathbf{W}}^k_{opt} = \mathbf{argmin}_{\hat{\mathbf{W}}^k}\xi\{\Delta^H(k)\Delta(k)\} \tag{13}$$

where $\xi\{\cdot\}$ denotes the expectation operation. By taking the derivative with respect to $\hat{\mathbf{W}}^k$, the MMSE optimal equalizer matrix can be found by:

$$\begin{aligned}\hat{\mathbf{W}}^k_{opt} &= \xi\{\mathbf{S}^k(\mathbf{R}^k)^H\}\left[\xi\{\mathbf{R}^k(\mathbf{R}^k)^H\}\right]^{-1} \\ &= P_s(\hat{\mathbf{G}}^k)^H\left[P_s\hat{\mathbf{G}}^k(\hat{\mathbf{G}}^k)^H + \xi\{\mathbf{E}^k(\mathbf{E}^k)^H\} + \xi\{\mathbf{V}^k(\mathbf{V}^k)^H\}\right]^{-1} \\ &= P_s(\hat{\mathbf{G}}^k)^H\left[P_s\hat{\mathbf{G}}^k(\hat{\mathbf{G}}^k)^H + \varepsilon\mathbf{I}_{n_R} + \sigma^2\mathbf{I}_{n_R}\right]^{-1}. \end{aligned} \tag{14}$$

Thus, the output of the frequency domain equalizer is

$$\hat{\mathbf{S}}^k = \hat{\mathbf{W}}^k_{opt}\cdot\mathbf{R}^k \tag{15}$$

This completes the proof.

After obtaining the frequency-domain estimation of the transmitted data, IFFT is applied to convert them into time-domain estimation. The transmitted symbols will be recovered by passing the time-domain estimation through a demodulator. As indicated by equation (10), the knowledge about the channel and noise variance is generally required to design an MMSE equalizer in frequency domain. Given the correlation property of a fading channel's frequency response at different times [21], Section III below proposes a novel algorithm based on an interpolation vector. This algorithm can provide good channel estimation for the frequency-domain equalizer .

3. FREQUENCY DOMAIN CHANNEL ESTIMATION FOR MIMO-SCFDE

3.1 Pilot Design. A common approach to estimate channel information at the receiver end is to periodically insert pilot signals into data streams. The pilot sequence should have a constant amplitude over all frequency tones to avoid noise enhancement at certain frequencies. This work adopts the Chu sequence proposed in [22] for pilot sequences because it has a constant magnitude in both frequency and time domains and can effectively overcome the PAPR problem at the transmitter in many FDE systems.

Another problem in designing pilot sequences for multiple transmit antennas is distinguishing the pilot sequences of different antennas in time or frequency domain. A straightforward solution is to let each of the n_T transmitters sequentially transmit one pilot block while the others remain silent. However, this approach will lead to huge overhead for pilot blocks as the number of transmitters increases. Given the limitations of this approach, the orthogonal frequency component method is applied here. First, a length-N/n_T Chu sequence is generated as the basic training sequence denoted by $\mathbf{c} = \{c_1,\ c_2,\ \ldots, c_{N/n_T}\}$ and duplicated n_T times to get a length-N sequence as the pilot sequence of the first transmit antenna denoted by $\mathbf{p}_1 = [\mathbf{c},\ \ldots,\ \mathbf{c}]_{1\times N}$. As a result, $(n_T - 1)$ zeros will be inserted between adjacent frequency tones of the basic Chu sequence to generate a comb-shaped spectral [23], which is illustrated in Fig. 3. The frequency responses of pilot sequences for different antennas are orthogonal to each other, which can be easily implemented by multiplying a phase rotating component by the training sequence of the first antenna. Thus, the pilot for the m-th transmit antenna can be given by

$$p_m(k) = p_1(k)e^{j2\pi(k-1)(m-1)/N} \qquad k = 1,\ \ldots,\ N. \tag{16}$$

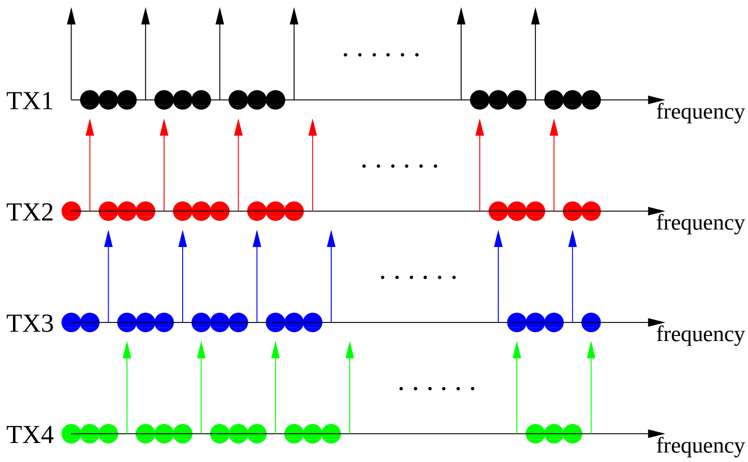

Figure 3 Frequency representation of pilot sequences for different antennas ($n_T = 4$)

3.2 Channel Estimation for Pilot Block. Bandwidth efficient algorithms such as the recursive reconstructive (RR) algorithm [20] and the simplified LS algorithm [19] have been proposed for channel estimation. The latter has lower implementation complexity, and its estimation performance is similar to that of the RR algorithm. The set of indices of nonzero frequency tones for the pilot block of the m-th antenna is defined as $\Psi_m = [m,\ m+n_T,\ \ldots,\ N-n_T+m]$. The received signal at the nth antenna can be expressed in frequency domain as follows:

$$Y_n(k) = \sum_{m=1}^{n_T} G_{n,m}(k)P_m(k) + V_n(k) \qquad k = 1,\ 2,\ \ldots,\ N \tag{17}$$

where $P_m(k)$ represents the k-th element of the DFT of pilot block $\mathbf{p}_m$. Due to the frequency orthogonality of different antennas' pilot blocks, $P_m(k) = 0$ except for $k \in \Psi_m$. Therefore, the above equation can be simplified to

$$Y_n(k) = G_{n,m}(k)P_m(k) + V_n(k) \qquad k \in \Psi_m. \tag{18}$$

The channel estimation procedures for the pilot block are described as follows:

(1) Obtain the initial estimation at the locations of nonzero frequency tones for the (n,m)-th sub-channel:

$$\tilde{G}_{n,m}(k) = \begin{cases} \frac{Y_n(k)}{P_m(k)} = G_{n,m}(k) + \frac{V_n(k)}{P_m(k)}, & k \in \Psi_m \\ 0, & \text{others} \end{cases} \tag{19}$$

(2) Multiply the scalar factor n_T by the initial estimation. This action recovers the total energy of null tones in frequency domain.

(3) Transform the result of step 2 into the time domain by IFFT and get $\tilde{\mathbf{g}}_{n,m}$, which is a periodic time-domain impulse response refraining n_T times. Since the dispersive channel has the length L, $\tilde{\mathbf{g}}_{n,m}(k)$ for $k = L+1,\ \ldots,\ N/n_T$ are supposed to be noise with a variance of σ_n^2. This fact enables a method of estimating noise variance. Note that the condition $N/n_T \geq L$ is required.

(4) Put $\tilde{\mathbf{g}}_{n,m}$ through a frequency-domain filter to reduce noise. The filter can be implemented by using a length-L window mask to remove the noise beyond the channel length [20].

(5) Convert the noise-reduced impulse response into the frequency domain and obtain the estimation of frequency transfer function over all frequency tones. The estimation of frequency function can be expressed as

$$\hat{\mathbf{G}}_{n,m} = \mathbf{G}_{n,m} + \hat{\mathbf{V}}_n = \mathbf{F}_N \mathbf{U} \tilde{\mathbf{g}}_{n,m} \tag{20}$$

where $\mathbf{U}$ is a diagonal windowing matrix whose first L elements in diagonal are 1 and whose other elements are zeros.

3.3 Channel Estimation for Data Block. This paper develops a novel channel estimation method based on interpolation vectors. This method uses the pilot blocks of two adjacent frames. Because the channel transfer function is assumed to be time-invariant in one block but time-variant between blocks, the channel response must be re-estimated and updated progressively. Let $\hat{\mathbf{G}}^1_{n,m}(k)$ and $\hat{\mathbf{G}}^{N_f+1}_{n,m}(k)$ be the estimated channel response at the pilot blocks of the current and next frames, respectively, both of which correspond to the k-th frequency bin of the (n,m)-th sub-channel. To consider the spatial correlation among receive antennas in the interpolation method, a column vector is defined as $\hat{\mathbf{Z}}_m(k) = \left[\hat{G}^1_{1,m}(k) \quad \ldots \hat{G}^1_{n_R,m}(k) \quad \hat{G}^{N_f+1}_{1,m}(k) \quad \ldots \hat{G}^{N_f+1}_{n,m}(k)\right]^T$, and the interpolation row vector is specified for the l-th block of the current frame as $\mathbf{C}^l_{n,m}(k)$. The channel frequency response for the data block can be calculated by

$$\hat{G}^l_{n,m}(k) = \mathbf{C}^l_{n,m}(k)\hat{\mathbf{Z}}_m(k), \qquad l = 2,\ 3,\ \ldots,\ N_f, \qquad k = 1,\ 2,\ \ldots,\ N. \tag{21}$$

The mean squared estimation error is then determined by

$$\epsilon^l_{n,m}(k) = \xi\left\{|e^l_{n,m}(k)|^2\right\} = \xi\left\{|G^l_{n,m}(k) - \hat{G}^l_{n,m}(k)|^2\right\}. \tag{22}$$

The interpolation vector $\mathbf{C}^l_{n,m}(k)$ can be solved by minimizing the mean square error. Taking the derivative of equation (22) with respect to $\mathbf{C}^l_{n,m}(k)$, the following optimal solution is obtained:

$$\mathbf{C}^l_{n,\ m}(k) = \mathbf{A}\mathbf{D}^{-1}, \tag{23}$$

$$\begin{aligned} \mathbf{A} &= \xi\{G^l_{n,\ m}(k)\hat{\mathbf{Z}}^H_m(k)\} = \begin{bmatrix} A_1 & \dots & A_{(2n_R)} \end{bmatrix}, \\ A_i &= \xi\{G^l_{n,\ m}(k)(\hat{G}^1_{i,\ m}(k))^*\}, \\ A_{i+n_R} &= \xi\{G^l_{n,\ m}(k)(\hat{G}^{N_f+1}_{i,\ m}(k))^*\}, \end{aligned} \tag{24}$$

$$\begin{aligned} \mathbf{D} &= \xi\{\hat{\mathbf{Z}}_m(k)\hat{\mathbf{Z}}^H_m(k)\} = \{D_{p,q}\}_{(2n_R)\times(2n_R)}, \\ D_{i,j} &= \xi\{\hat{G}^1_{i,m}(k)(\hat{G}^1_{j,m}(k))^*\}, \\ D_{i+n_R,j} &= D^*_{j,i+n_R} \;=\; \xi\{\hat{G}^{N_f+1}_{i,m}(k)(\hat{G}^1_{j,m}(k))^*\}, \\ D_{i+n_R,j+n_R} &= \xi\{\hat{G}^{N_f+1}_{i,m}(k)(\hat{G}^{N_f+1}_{j,m}(k))^*\}, \end{aligned} \tag{25}$$

for $i,\ j = 1,\ \dots,\ n_R$ and $p,\ q = 1,\ \dots,\ 2n_R$. It is clear that the interpolation vector depends only on the second-order statistics of the channel rather than the instantaneous channel coefficients. For many practical fading channels, the second-order statistics remain stationary for fixed Doppler frequencies and antenna settings, which is beneficial because the interpolation vectors can be obtained through off-line training for each base station sector. Some statistic fading models, such as isotropic or non-isotropic scattering Rayleigh/Ricean/Nakagami models, can be used to compute the interpolation vectors for different scenarios. The computed interpolation vectors can then be selected and used directly for channel estimation of the data block in equation (21), which leads to great computational savings in real-time processing. Below, the commonly accepted WSSUS Rayleigh fading channel is considered as an application example of the proposed method. The second-order statistical properties for frequency selective Rayleigh fading channels are discussed in [26]. The interpolation vectors for this type of channel have a closed form solution due to the decomposition property of triply-selective channels. The elements in equations (24) and (25) are defined as

$$
\begin{aligned}
A_i &= J_0(\omega_d(l-1)T_b)\rho^{Rx}_{n,i} f_h(k), \\
A_{i+n_R} &= J_0(\omega_d(N_f-l+1)T_b)\rho^{Rx}_{n,i} f_h(k), \\
D_{i,j} = D_{i+n_R,j+n_R} &= \rho^{Rx}_{i,j} f_h(k) + \frac{L}{N}\mu_{i,j}, \\
D_{i+n_R,j} &= J_0(\omega_d N_f T_b)\rho^{Rx}_{i,j} f_h(k)
\end{aligned} \tag{26}
$$

where $J_0(\cdot)$ is the zero-order Bessel function of the first kind, $\omega_d = 2\pi f_d$ is the maximum Doppler frequency, and $\rho^{Rx}_{i,j}$, the spatial correlation coefficient between the i,j-th sub-channel, does not normally change much over time. The noise correlation $\mu_{i,j} = \sigma_i^2$ for $i = j$ and zero for $i \neq j$. The Fourier transform of the inter-tap correlation $f_h(k)$ is defined as

$$
f_h(k) = \sum_{t_1=1}^{L}\sum_{t_2=1}^{L} Q_{t_1,t_2}\exp\left(\frac{-j2\pi(t_1-t_2)(k-1)}{N}\right) \tag{27}
$$

where Q_{t_1,t_2} is the inter-tap correlation between the t_1-th tap and the t_2-th tap of the fading channel. Because the inter-tap correlation may change slightly faster than the spatial correlation, more frequent adjustment is required. The proof of equation (26) is as follows:

Proof: According to [26], the correlation between the p-th block and q-th block for k-th frequency bin can be expressed by

$$
\begin{aligned}
\xi\left\{\mathbf{G}^p_{n_1,m}(k)(\mathbf{G}^q_{n_2,m}(k))^*\right\} &= \sum_{t_1=1}^{L}\sum_{t_2=1}^{L}\xi\left\{\mathbf{g}^p_{n_1,m}(t_1,\frac{N}{2})(\mathbf{g}^q_{n_2,m}(t_2,\frac{N}{2}))^*\right\}\exp\left(\frac{-j2\pi(t_1-t_2)(k-1)}{N}\right) \\
&= J_0[2\pi f_d(p-q)T_b]\rho^{Rx}_{n_1,n_2}\sum_{t_1=1}^{L}\sum_{t_2=1}^{L} Q_{t_1,t_2}\exp\left(\frac{-j2\pi(t_1-t_2)(k-1)}{N}\right) \\
&= J_0[2\pi f_d(p-q)T_b]\rho^{Rx}_{n_1,n_2} f_h(k)
\end{aligned} \tag{28}
$$

The equation $\xi\left\{\mathbf{g}^p_{n_1,m}(t_1,i_1)(\mathbf{g}^q_{n_2,m}(t_2,i_2))^*\right\} = Q_{t_1,t_2}\rho^{Rx}_{n1,n2}J_0[2\pi f_d(pT_b+i_1-qT_b-i_2)]$ is used here. By Substituting equation (28) into equations (24) and (25), equation (26) can be derived.

$$
\begin{aligned}
A_i &= \xi\{G^l_{n,m}(k)(\hat{G}^1_{i,m}(k))^*\} = \xi\{G^l_{n,m}(k)(G^1_{i,m}(k) + \hat{V}^1_i(k))^*\} \\
&= \xi\{G^l_{n,m}(k)G^1_{i,m}(k)\} = J_0(\omega_d(l-1)T_b)\rho^{Rx}_{n,i} f_h(k)
\end{aligned}
$$

$$
\begin{aligned}
A_{i+n_R} &= \xi\{G^l_{n,m}(k)(\hat{G}^{N_f+1}_{i,m}(k))^*\} = \xi\{G^l_{n,m}(k)(G^{N_f+1}_{i,m}(k) + \hat{V}^{N_f+1}_i(k))^*\} \\
&= \xi\{G^l_{n,m}(k)G^{N_f+1}_{i,m}(k)\} = J_0(\omega_d(N_f - l + 1)T_b)\rho^{Rx}_{n,i} f_h(k)
\end{aligned}
$$

$$
\begin{aligned}
D_{i,j} &= \xi\{\hat{G}^1_{i,m}(k)(\hat{G}^1_{j,m}(k))^*\} \\
&= \xi\{(G^1_{i,m}(k) + \hat{V}^1_i(k))(G^1_{j,m}(k) + \hat{V}^1_j(k))^*\} \\
&= \xi\{G^1_{i,m}(k)(G^1_{j,m}(k))^*\} + \xi\{\hat{V}^1_i(k)(\hat{V}^1_j(k))^*\} \\
&= \rho^{Rx}_{i,j} f_h(k) + \frac{L}{N}\mu_{i,j}
\end{aligned}
$$

$$
\begin{aligned}
D_{i+n_R,j} &= \xi\{\hat{G}^{N_f+1}_{i,m}(k)(\hat{G}^1_{j,m}(k))^*\} \\
&= \xi\{(G^{N_f+1}_{i,m}(k) + \hat{V}^{N_f+1}_i(k))(G^1_{j,m}(k) + \hat{V}^1_j(k))^*\} \\
&= \xi\{G^{N_f+1}_{i,m}(k)(G^1_{j,m}(k))^*\} + \xi\{\hat{V}^{N_f+1}_i(k)(\hat{V}^1_j(k))^*\} \\
&= J_0(\omega_d N_f T_b)\rho^{Rx}_{i,j} f_h(k)
\end{aligned}
$$

This completes the proof.

3.4 Noise Variance Estimation. As mentioned previously, $\tilde{\mathbf{g}}_{n,m}(k)$ are supposed to be the noise components for $k = L+1, \ \ldots, \ N/n_T$. Thus, the noise variance estimation can be obtained for the n-th receive antenna from $\tilde{\mathbf{g}}_{n,m}(k)$:

$$
\hat{\sigma}^2_n = \frac{1}{2(N/n_T - L)} \sum_{k=L+1}^{N/n_T} \left[|\tilde{\mathbf{g}}^1_{n,m}(k)|^2 + |\tilde{\mathbf{g}}^{N_f+1}_{n,m}(k)|^2 \right] \tag{29}
$$

4. SIMULATION EXPERIMENTS

In all computational simulations, a 60-tap frequency selective Rayleigh fading channel model was used. The average power of the first 20 taps ramped up linearly, whereas the last 40 taps ramped down linearly. The total average power of the fading channel was normalized to unit. The lengths of the data block and CP were specified as $N = 256$ and $N_c = 64$, respectively, and symbol duration was set to be $T_s = 0.25\mu s$. The first experiment used an SM system with 4 transmit antennas and 4 receive antennas. The data was modulated by QPSK, and the maximum Doppler spread f_d was set at 20Hz. The estimated channel frequency responses (CFRs) at an arbitrary time are shown in Fig. 4 for a pilot block and in Fig. 5 for a data block. The estimated channel frequency response can be very close to the practical channel response when SNR=10dB. The validity of the proposed noise variance estimation algorithm is illustrated in Fig. 6. Basically, the estimated noise variance is identical to the actual noise variance and its deviation is very small in the range of SNR. Here, SNR is defined as the average signal-to-noise ratio at each subchannel, which is determined by SNR $= \frac{\xi(|r_{i,j}|^2)}{\sigma^2} = \frac{1}{\sigma^2}$, where the transmit signal and fading channels are all normalized to unit power. In the second experiment, the bit error rate (BER) performances were investigated for various MIMO architectures, including 2×2, 4×4, and 8×8. The transmit data were modulated by QPSK, 8PSK, and 16QAM. The simulation results are shown in Figs. 7 – 9. The QPSK modulation performs better than the other two modulation methods in the same MIMO SC-FDE system and the BER performances obtained by the estimated channel response degrade 1–2 dB in contrast to the curves obtained based on the perfect channel information. Additionally, the diversity gain is illustrated by fixing the number of transmit antennas and increasing the number of receiver antennas. Figures 10 and 11 illustrate that performance can be significantly improved by adding more receive antennas in the receiver.

Finally, simulations were conducted with varied maximum Doppler frequency f_d, the results of which are shown in Fig. 12. The performances become worse with each increment of f_d. When $f_d = 300$Hz, the bit error rate approaches 10^{-3} at SNR $= 20$dB and change little at SNR=24dB. It is understandable because of two reasons. On the one hand, a

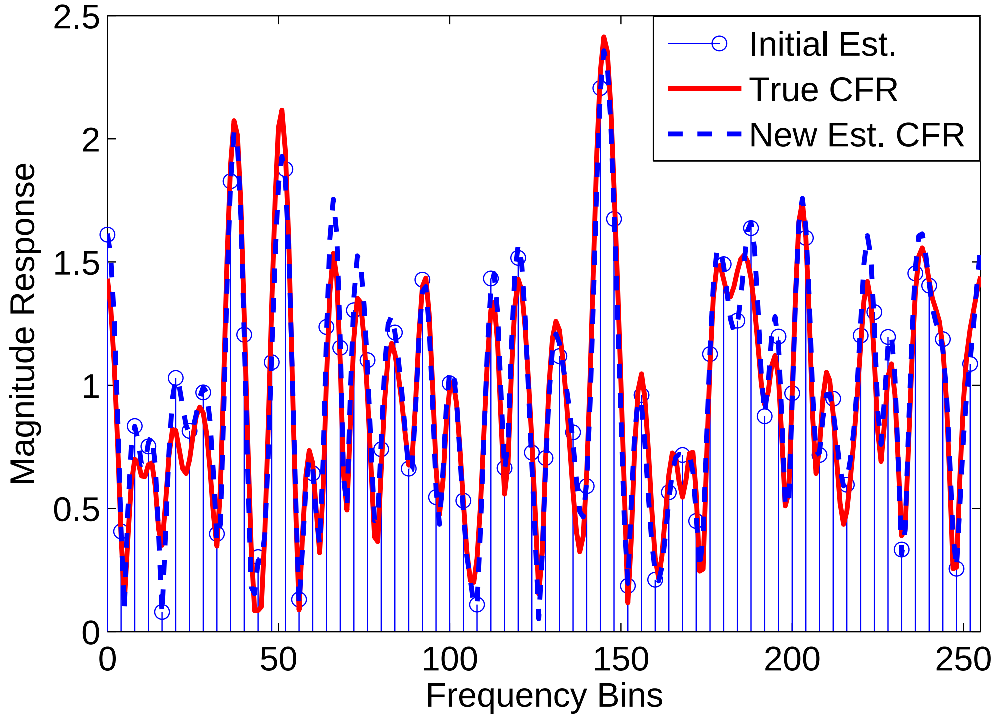

Figure 4 Channel estimation of pilot block for sub-channel $\mathbf{G}_{1,1}$ when SNR=10dB, f_d=20Hz, 4×4 MIMO architecture

large f_d means that the channel varies rapidly and the coherence time of the fading channel is very small and can no longer support the assumption that the channel frequency-domain response remains invariant for one block's duration. On the other hand, the channel becomes less correlated in this situation and our algorithm does not perform as well as it did for a small Doppler spread.

5. CONCLUSION

In this paper, we present a novel algorithm for estimating a frequency selective fading channel based on the interpolation vector for MIMO SC-FDE. Unlike common adaptive algorithms, this one takes advantage of the correlation of fading channel's frequency-domain response. The interpolation vectors can be computed in advance if the second-order statistics relating to the channel are known. The combination of SM with SC-FDE is an attractive potential technique for future high-rate wireless communication because of its high capacity gain and ability to combat ISI. Simulation results have shown that a MIMO SC-FDE based

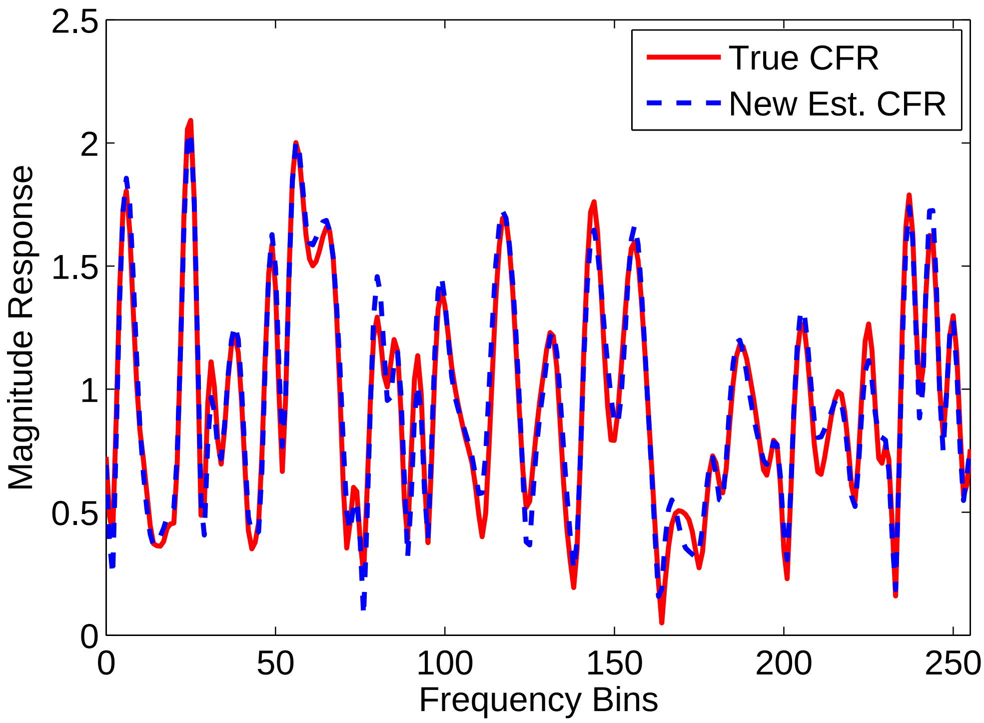

Figure 5 Channel estimation of data block for sub-channel $\mathbf{G}_{2,1}$ when SNR=10dB, f_d=20Hz, 4×4 MIMO architecture

on the estimated channel can perform well under the conditions of long channel response and fast time varying channel.

6. REFERENCES

[1] D. Falconer, S. L. Ariyavisitakul, A. Benyamin-Seeyar, and B. Eidson, "Frequency domain equalization for single-carrier broadband wireless systems," *IEEE Commun. Mag.*, vol. 40, no. 4, pp. 58-66, Apr. 2002.

[2] J. P. Coon and M. A. Beach, "An investigation of MIMO single carrier frequency-domain MMSE equalizer," in *London Communication Symposium*, 2002, pp.237-240.

[3] P. Vandenameele, L. V. der Perre, B. Gyselinckx, M. Engels, M. Moonen, and H. De Main, "A single-carrier frequency domain SDMA basestation,"in *Proc. IEEE ICASSP, Piscataway*, NJ, May 2000, vol. 6, pp. 3714-3717.

[4] J. Coon, S. Armour, M. Beach, and J. McGeehan, "Adaptive frequency-domain equalization for single carrier multiple-input multiple-output wireless transmissions," *IEEE Trans. Signal Processing*, vol. 53, no. 8, pp. 3247-3256, Aug. 2005.

[5] Y. Zhu and K. B. Letaief, "Single-carrier frequency-domain equalization with noise prediction for MIMO systems," *IEEE Trans. Commun.*,vol. 55, no. 5, pp. 1063-1076, May 2007.

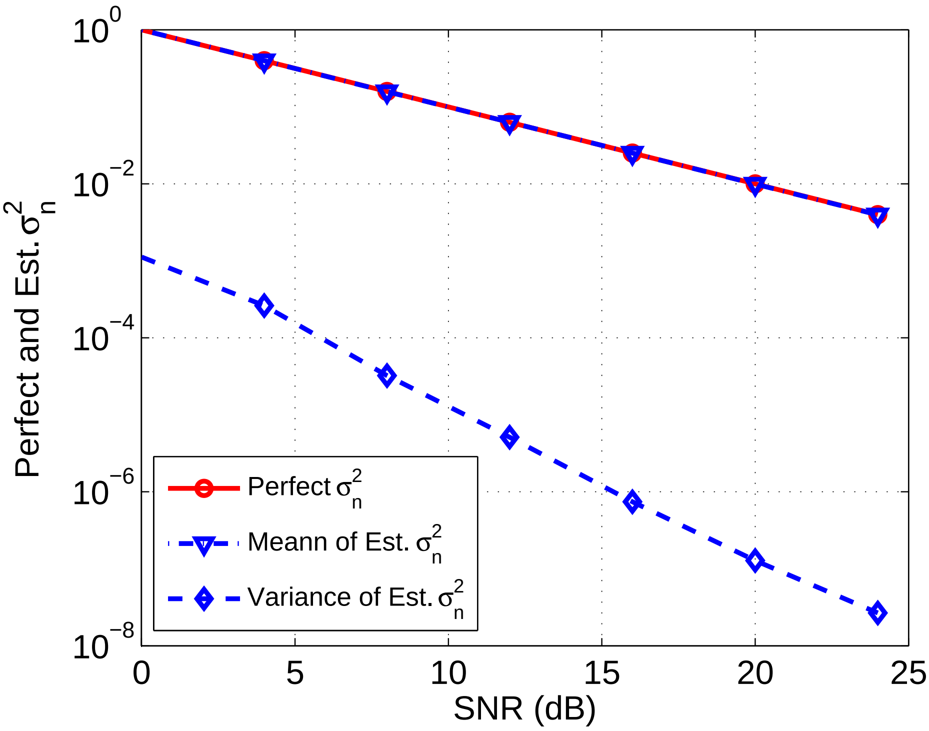

Figure 6 Performance of the proposed noise variance estimation algorithm

[6] J. Coon, J. Siew, M. Beach, A. Nix, S. Armour, and J. McGeehan,"A comparison study of MIMO-OFDM and MIMO-SCFDE in WLAN environments," *Proc. IEEE Global Telecommun. Conf.*, vol. 6, Dec.2003, pp. 3296-3301.

[7] M. Mendicute, J. Altuna, V. Atxa,and J. M. Zabalegui, "Performance comparision of OFDM and FDE single-carrier modulation for spatial multiplexing MIMO sytems," in *Proc. IEEE 5th Workshop on Signal Processing Advances in Wireless Communications*, July 2004, pp. 532-535.

[8] S. Reinhardt, T. Buzid, and M. Huemer, "Receiver structures for MIMO-SC/FDE systems," in *Proc. IEEE VTC Spring*, May 2006, vol. 3, pp. 1401-1405.

[9] S. Reinhardt, T. Buzid, and M.Huemer, "MIMO extensions for SC/FDE systems," in *Proc. European Conf. Wireless Technology*, Oct. 2005, pp. 109-112.

[10] G. Kadel, "Diversity and equalization in frequency domain-a robust and flexible receiver technology for broadband mobile communication systems," in *Proc.IEEE VTC Spring*, May 1997, vol. 2, pp.894-898.

[11] N. Al-Dhahir, "Single carrier frequency-domain equalization for space-time block coded transmissions over frequency-selective fading channels," *IEEE Commun. Lett.*, vol. 5, no. 7, pp. 304-306, July 2001.

[12] X. Xin, C. Yueming, and X. Youyun, "Space diversity schemes for STBC-Based SC/FDE systems and SC/Pre-FDE systems," in *Proc.ISCIT*, Oct. 2005, vol. 1, pp.325-329.

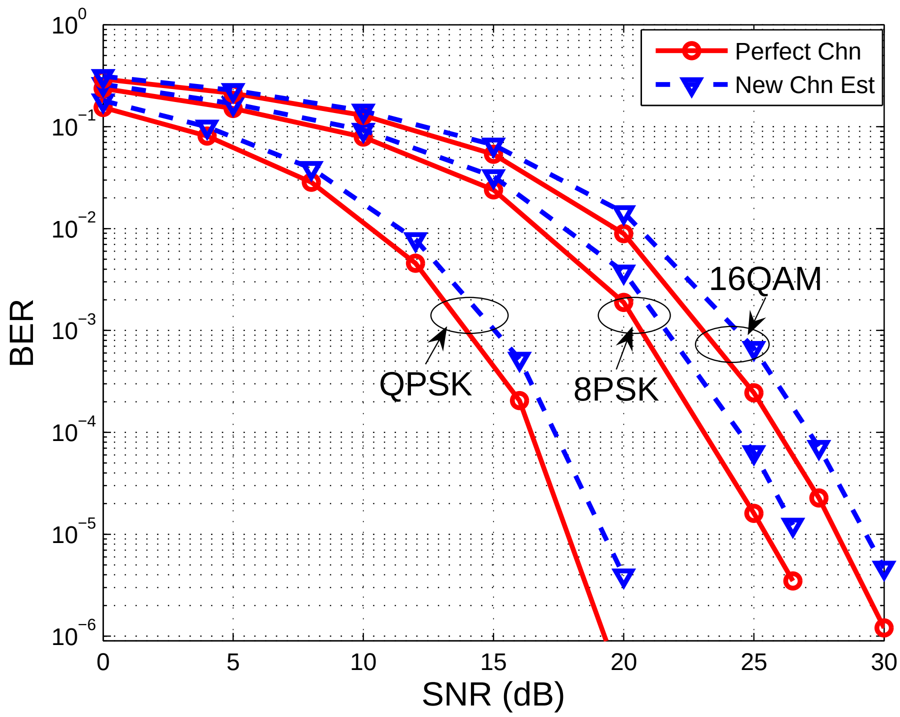

Figure 7 BER versus SNR for QPSK, 8PSK and 16QAM with MIMO 2x2 architecture

[13] M. V. Clark,"Adaptive frequency-domain equalization and diversity combining for broadband wireless communications," *IEEE J. Select. Areas Commun.*, vol. 16, no. 8, pp. 1385-1395, Oct. 1998.

[14] M. Morelli, L. Sanguinetti, and U. Mengali, "Channel estimation for adaptive frequency-domain equalization," *IEEE Trans. Wireless Commun.*, vol. 4, no. 5, pp. 2508-2518, Sept. 2005.

[15] J. Coon, M. Sandell, M. Beach, and J. McGreehan, "Channel and noise variance estimation and tracking algorithms for unique-word based single-carrier systems," *IEEE Trans. Wireless Commun.*, vol. 5, pp. 1488-1496, June 2006.

[16] J. Wu, C. Xiao, and J. C. Oliver, "Time-varying and frequency-selective channel estimation with unequally spaced pilot symbols," *Int. J. Wireless Inform. Networks*, vol. 11, no. 2, pp. 93-104, Arp. 2004.

[17] C. Xiao and J. C. Oliver, "Nonselective fading channel estimation with non-uniformly spaced pilot symbols," *Int. J. Wireless Inform. Networks*, vol. 7, pp. 177-185, July 2000.

[18] Y. R. Zheng and C. Xiao,"Frequency-domain channel estimation and equalization for broadband wireless communications," in *Proc. ICC*, 2007.

[19] J. Siew, J. Coon, R. J. Piechocki, A. Dowler, A. Nix, M. Beach, S. Armour, and J. McGeehan, "A channel estimation algorithm for MIMO-SCFDE," *IEEE Commun. Lett.*, vol. 8, no. 9, pp. 555-557, Sep 2004.

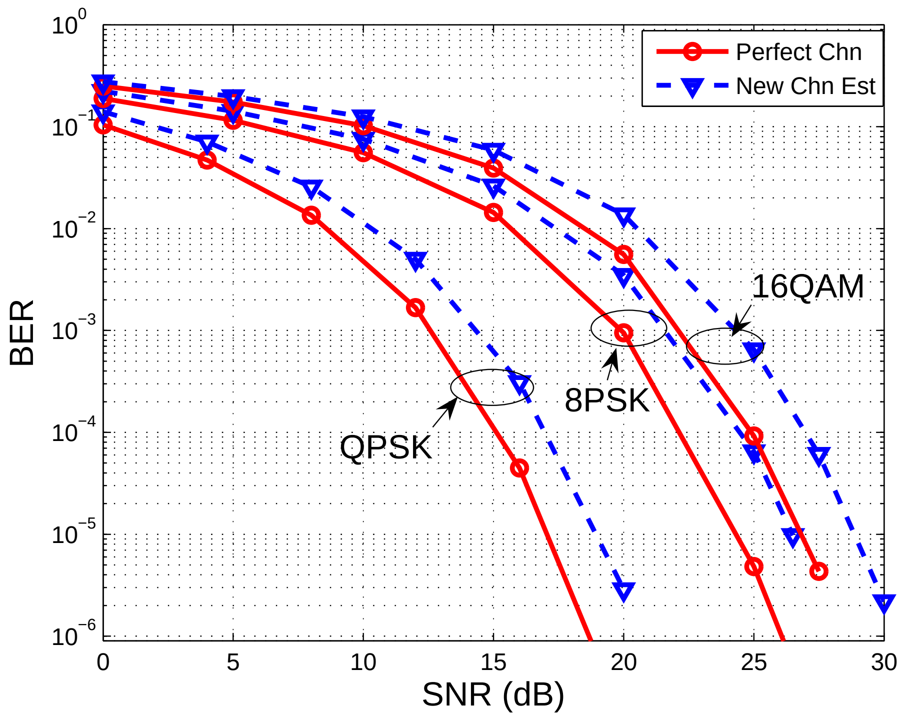

Figure 8 BER versus SNR for QPSK, 8PSK and 16QAM with MIMO 4x4 architecture

[20] J. Siew, J. Coon, R. Piechocki, A. Nix, M. Beach, S. Armour, and J. McGeehan,"A bandwidth efficient channel estimation algorithms for MIMO-SCFDE," in *Proc. VTC Fall*, Oct. 2003, vol. 2, pp. 1142-1146.

[21] Y. Li, L. J. Cimini, and N. R. Sollenberger, "Robust channel estimation for OFDM systems with rapid dispersive fading channels," *IEEE Trans.Commnu.*, vol. 46, pp. 902-915, July 1998.

[22] D. C. Chu,"Polyphase codes with good periodic correlation properties,"*IEEE Trans. Inform. Theory*, vol. IT-18, pp. 531-532, July 1972.

[23] A. V. Oppenheim, R. W. Schafer, and J. R. Buck, *Discrite-time signal processing*, 2nd Ed., Prentice Hall, 1999.

[24] A. Chini, "Multicarrier modulation in frequency selective fading channels," Ph.D. dissertion, Carleton University, Ottawa, Canada, 1994.

[25] C. Xiao, J. Wu, S.-Y. Leong, Y. R. Zheng, and K. B. Letaief, "A Discrete-Time Model for Triply Selective MIMO Rayleigh Fading Channels," *IEEE Trans. Wireless Commun.*, vol. 3, no. 5, pp. 1678-1688, Sept. 2004.

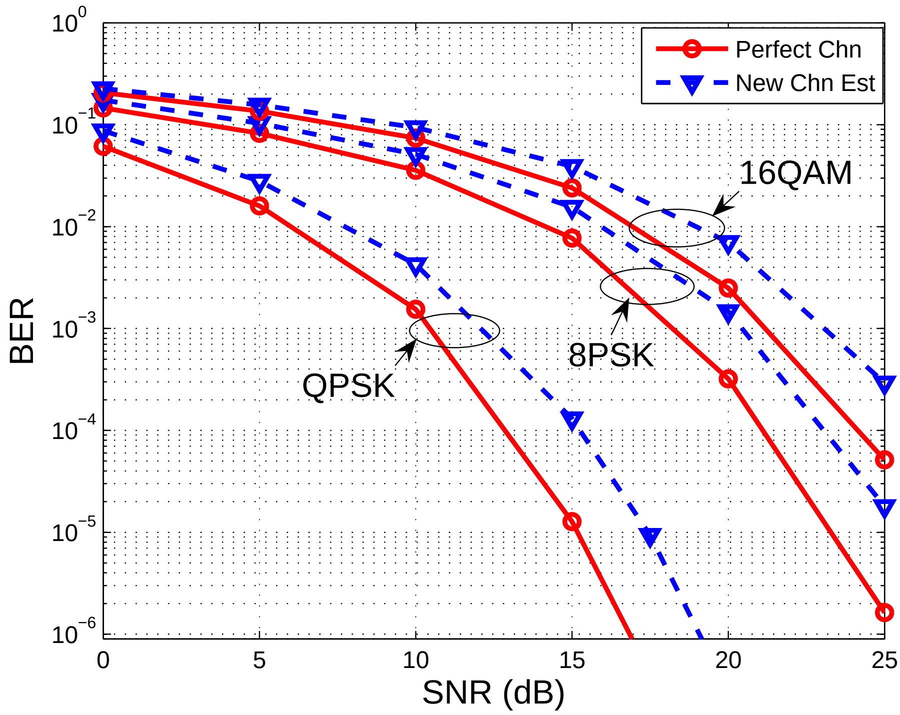

Figure 9 BER versus SNR for QPSK, 8PSK and 16QAM with MIMO 8x8 architecture

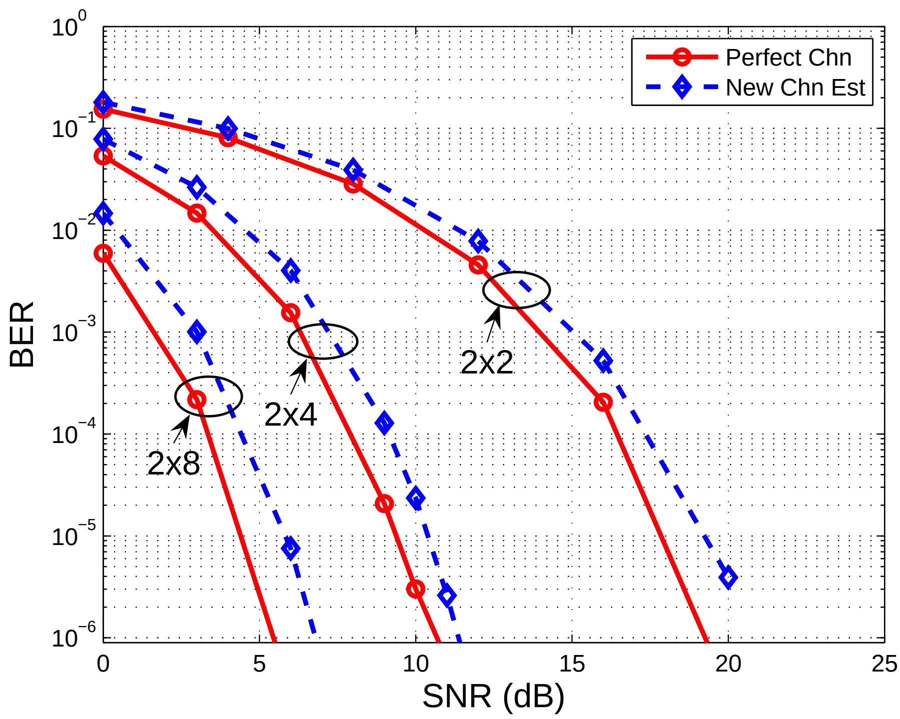

Figure 10 BER versus SNR for MIMO 2x2, 2x4, 2x8 architectures with QPSK modulation

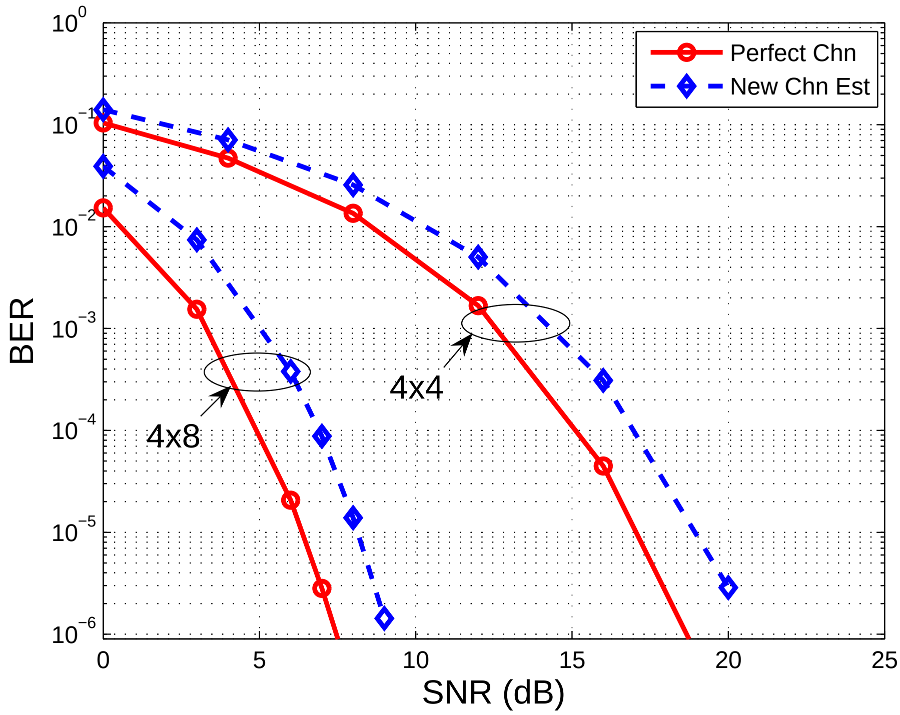

Figure 11 BER versus SNR for MIMO 4x4, 4x8 architectures with QPSK modulation

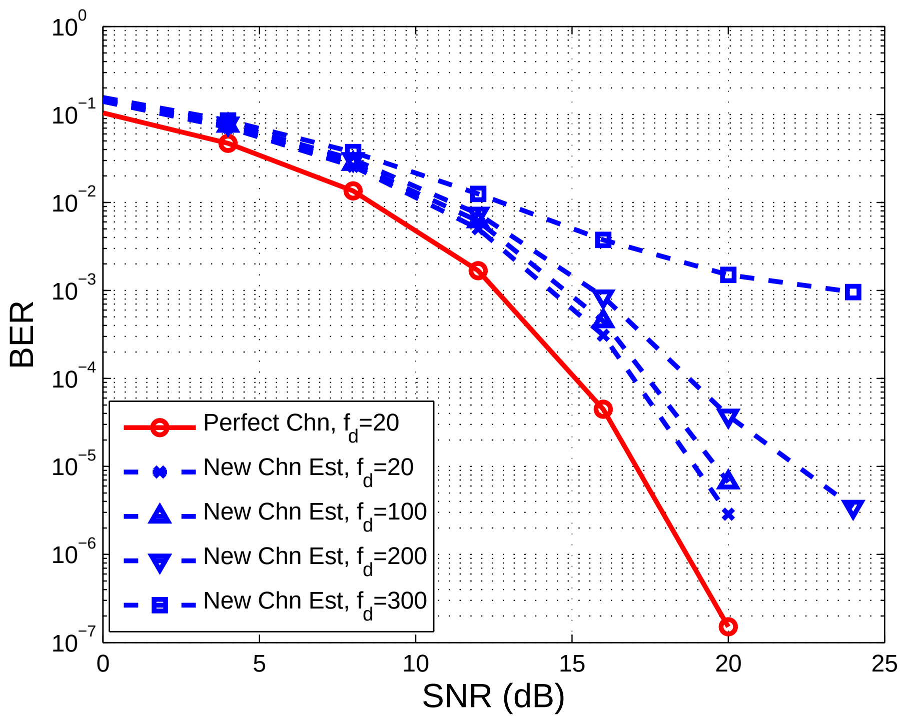

Figure 12 BER versus SNR for MIMO 4x4 with different f_d

2. CHANNEL EQUALIZATION AND SYMBOL DETECTION FOR SINGLE CARRIER MIMO SYSTEMS IN THE PRESENCE OF MULTIPLE CARRIER FREQUENCY OFFSETS

Jian Zhang, Yahong Rosa Zheng, Chengshan Xiao, and Khaled Ben Letaief

Abstract—A new frequency-domain channel equalization and symbol detection scheme is proposed for multiple-input multiple-output (MIMO) single carrier broadband wireless systems in the presence of severely frequency-selective channel fading and multiple unknown carrier frequency offsets (CFOs). Multiple CFOs cause severe phase distortion in the equalized data for large block lengths and/or constellation sizes, thus, yielding poor detection performance. Instead of explicitly estimating the CFOs and then compensating them, the proposed scheme estimates the rotated phases (not frequencies) caused by multiple unknown CFOs, then removes the phase rotations from the equalized data before symbol detection. The estimation accuracy of the phase rotation is improved by utilizing a group-wise method rather than symbol-by-symbol methods. This work differs from other related work in OFDM studies in that it can combat multiple CFOs that are time-varying within each block. Numerical examples for 4×2 and 8×4 single carrier systems with QPSK and 8PSK modulation illustrate the effectiveness of the proposed scheme in terms of scatter plots of constellation, mean square error (MSE) and bit error rate (BER).

I. INTRODUCTION

Single carrier (SC) frequency-domain equalization (FDE) is a promising approach for mitigating inter-symbol interference (ISI). In recent years, it has attracted considerable attention for both single-input single-output (SISO) and multiple-input multiple-output (MIMO) broadband wireless systems. Compared with time-domain equalization, SC-FDE has higher computational efficiency and better convergence properties to achieve the same or better performance over severely frequency-selective fading channels [1]. Compared with the widely adopted orthogonal frequency division multiplexing (OFDM), SC-FDE exhibits similar or better performance at comparable complexity while avoiding some problems inherent in OFDM, such as sensitivity to carrier frequency offsets and peak-to-average power ratio [2]. Accordingly, SC-FDE has been proposed in several standards, including the IEEE 802.16e [3, 4].

Carrier frequency offset (CFO), typically caused by local oscillator mismatch between transmitter and receiver, has been considered as a major impairment for OFDM because it destroys the orthogonality between sub-carriers and induces inter-carrier interference (ICI). To alleviate this effect, CFO has to be estimated and then mitigated at the receiver, which naturally introduces additional complexity to the receiver. The estimation of CFO in an OFDM system has been investigated extensively in the literature [5]- [12]. Such previous work can be categorized into data-aided and blind estimation depending on whether training sequences are used or not. In a data-aided approach, reference OFDM symbols are transmitted periodically and the CFO can be estimated based on the maximum-likelihood (ML) criterion [5]- [7] or least square (LS) criterion [8]. In blind estimation, several algorithms with efficient bandwidth utilization have been proposed by exploiting the redundancy in cyclic prefix (CP) [9], or the null subcarriers [10]- [12], or recently proposed hybrid time-frequency-domain method [13].

Generally, SC-FDE has less sensitivity to CFOs than OFDM for small block lengths and constellation sizes. Therefore, the CFO problem has received little attention, and fewer work has investigated the impact of CFOs on SC-FDE systems. However, when the block length or constellation size increases, the impact of CFOs on SC-FDE systems can not be ignored. Recently, Wang and Dong have examined the effect of CFO on the performance of SC-FDE over ultra-wideband (UWB) channels [14] under the assumption that the frequency offset is constant. In [15], a joint frequency-domain equalization and carrier synchronization method has been proposed for a single carrier SISO system. In this paper, we show that CFO can be quite troublesome for SC-FDE MIMO systems if the discrete Fourier transform (DFT) block length is large and/or the constellation size of the modulation is high. In a wireless communication system, the misalignment of carrier frequencies may lead to frequency offsets of up to a few hundred Hertz. As a result, the time-varying CFO can cause severe phase errors on the received signal, and the performance of the SC reception will degrade with the increase of block length or constellation size, especially for phase shift keying modulated symbols. Therefore, it is equally important for SC systems to take into account the impact of CFO in this situation.

The main contribution of this paper is that we propose a new phase estimation and compensation algorithm to combat the phase distortion caused by CFOs and reliably detect equalized data. In this algorithm, the equalized data block is divided into small groups, and the average rotating phase for each group is estimated in a decision-directed method. The phase distortions are compensated by the estimated rotating phases in the group-wise way. The phase correction method is combined with an improved least square (LS) frequency-domain (FD) channel estimation algorithm based on an interpolation method to track the time-varying channels. This approach differs from related work in several ways. First, unlike most work focusing on OFDM systems, our approach circumvents the direct estimation of the multiple CFOs. This dramatically reduces computational complexity and phase errors in the estimation of fading channel coefficients. Second, the combined effect of multiple CFOs after FD equalization is eliminated in a group-wise manner, rather than on a symbol-wise basis. The group-wise phase rotation estimation and compensation method is more robust to noise perturbation. Furthermore, existing CFO estimation algorithms assume a constant CFO during each block of transmission. In contrast, the method presented here can cope with multiple CFOs that are time-varying within one block without directly tracking the CFO. Another contribution of the paper is that we propose a new system model for the analysis of CFOs in MIMO SC-FDE systems. The model separates the phase variation of each frequency tone from the estimated channel frequency responses, thus, leading to better analysis of phase rotation caused by CFOs.

Simulation results demonstrate that excellent performance is achieved by adopting the proposed receiver structure for SC transmission of QPSK and 8PSK with large block lengths over fast frequency-selective fading channels. For a MIMO 4×2 communication system with constant CFO impairment, the performance of the proposed scheme degrades 0.5 dB compared with the case without CFO. For a MIMO 8×4 system, our algorithm can deal with the CFOs up to 250 Hz, and the time-varying CFOs can also be combatted.

The remainder of this paper is organized as follows. Section II describes the system model and develops the frequency representation. Sections III and IV present the bandwidth efficient FD channel estimation scheme and MMSE FDE for a MIMO system in the presence of CFO. Section V provides a novel phase correction algorithm, and Section VI presents the numerical results. Finally, our conclusions are drawn in Section VII.

II. SYSTEM MODEL AND PRELIMINARIES

Consider a broadband MIMO wireless system with N_t transmitter antennas and N_r receiver antennas. The baseband equivalent signal received at the m-th antenna can be expressed in the discrete-time domain as

$$y_m(k) = \sum_{n=1}^{N_t}\sum_{l=1}^{L} h_{m,n}(l,k) x_n(k+1-l) e^{j(2\pi f_{m,n,k} k T_s + \theta_{m,n})} + v_m(k) \quad (30)$$

where $x_n(k)$ is the k-th symbol from the n-th transmit antenna, $h_{m,n}(l,k)$ is the impulse response of the frequency-selective time-varying fading channel linking the n-th transmit antenna and m-th receive antenna with l being the tap index and k being the time index [16], $f_{m,n,k}$ and $\theta_{m,n}$ are, respectively, the time-varying carrier frequency offset and the initial timing error phase between the m-th receive antenna and the n-th transmit antenna, $v_m(k)$ is the additive white Gaussian noise with average power σ^2, T_s is the symbol interval, and L is the fading channel length in terms of T_s. It is noted that the fading channel coefficients $h_{m,n}(l,k)$ combine the effects of the transmit pulse-shape filter, physical multipath fading channel response, and the receive matched filter.

To facilitate frequency-domain channel equalization for the system described in (30), the transmitted data sequence $\{x_n(k)\}$ is partitioned into blocks of size N. A copy of the last N_{cp} symbols is appended at the front of the block as a cyclic prefix (CP). The length of CP N_{cp} is chosen to be at least $L-1$ to avoid inter-block interference (IBI). The CP-appended data block is given by

$$\mathbf{x}_n^{bk} = \left[x_n(-N_{cp}+1) \cdots x_n(0)\, x_n(1) \cdots x_n(N) \right]^T \quad (31)$$

and the corresponding received signal $\mathbf{y}_m^{bk}$ of the block is denoted by

$$\mathbf{y}_m^{bk} = \Big[y_m(-N_{cp}+1) \cdots y_m(0)\, y_m(1) \cdots y_m(N) \Big]^T \tag{32}$$

where the superscript $[\cdot]^T$ is the transpose.

At the receiver, the CPs are discarded to yield the received signal vector expressed by

$$\begin{bmatrix} \mathbf{y}_1 \\ \vdots \\ \mathbf{y}_{N_r} \end{bmatrix} = \begin{bmatrix} \mathbf{D}_{1,1}\mathbf{A}_{1,1} & \cdots & \mathbf{D}_{1,N_t}\mathbf{A}_{1,N_t} \\ \vdots & \ddots & \vdots \\ \mathbf{D}_{N_r,1}\mathbf{A}_{N_r,1} & \cdots & \mathbf{D}_{N_r,N_t}\mathbf{A}_{N_r,N_t} \end{bmatrix} \begin{bmatrix} \mathbf{x}_1 \\ \vdots \\ \mathbf{x}_{N_t} \end{bmatrix} + \begin{bmatrix} \mathbf{v}_1 \\ \vdots \\ \mathbf{v}_{N_r} \end{bmatrix} \tag{33}$$

where $\mathbf{x}_n = \big[x_n(1) \cdots x_n(N)\big]^T$, $\mathbf{y}_m = \big[y_m(1) \cdots y_m(N)\big]^T$, and $\mathbf{v}_m = \big[v_m(1) \;\cdots\; v_m(N)\big]^T$. The matrix $\mathbf{A}_{m,n}$ is given by (34) and $\mathbf{D}_{m,n}$ is defined as follows

$$\mathbf{A}_{m,n} = \begin{bmatrix} h_{m,n}(1,1) & 0 & \cdots & 0 & h_{m,n}(L,N+1) \cdots & h_{m,n}(2,N+1) \\ h_{m,n}(2,2) & h_{m,n}(1,2) & 0 & \ddots & \ddots & \ddots & \vdots \\ \vdots & \ddots & \ddots & \ddots & \ddots & \ddots & h_{m,n}(L,N+L-1) \\ h_{m,n}(L,L) & \ddots & \ddots & h_{m,n}(1,L) & 0 & \ddots & 0 \\ 0 & h_{m,n}(L,L+1) & \ddots & \ddots & \ddots & \ddots & \vdots \\ \vdots & \ddots & \ddots & \ddots & \ddots & \ddots & 0 \\ 0 & \cdots & 0 & h_{m,n}(L,N) & \cdots & \cdots & h_{m,n}(1,N) \end{bmatrix} \tag{34}$$

$$\mathbf{D}_{m,n} = \mathrm{diag}\left\{ e^{j(2\pi f_{m,n,1} T_s + \theta_{m,n})} \cdots e^{j(2\pi f_{m,n,N} N T_s + \theta_{m,n})} \right\}. \tag{35}$$

Let $\mathbf{F}_N$ denote the normalized DFT matrix of size $N \times N$, i.e., its (p,q)-th element is given by $\frac{1}{\sqrt{N}} \exp\left(\frac{-j2\pi(p-1)(q-1)}{N}\right)$. Thus, $\mathbf{F}_N^H \mathbf{F}_N = \mathbf{I}_N$ with $\mathbf{I}_N$ being the $N \times N$ identity matrix, where the superscript $[\cdot]^H$ denotes conjugate transpose. By left multiplying (33) by

$\text{diag}\{\mathbf{F}_N \ \cdots \ \mathbf{F}_N\}$, one obtains the frequency-domain representation as

$$\begin{bmatrix} \mathbf{Y}_1 \\ \vdots \\ \mathbf{Y}_{N_r} \end{bmatrix} = \begin{bmatrix} \mathbf{\Phi}_{1,1}\mathbf{H}_{1,1} & \cdots & \mathbf{\Phi}_{1,N_t}\mathbf{H}_{1,N_t} \\ \vdots & \ddots & \vdots \\ \mathbf{\Phi}_{N_r,1}\mathbf{H}_{N_r,1} & \cdots & \mathbf{\Phi}_{N_r,N_t}\mathbf{H}_{N_r,N_t} \end{bmatrix} \begin{bmatrix} \mathbf{X}_1 \\ \vdots \\ \mathbf{X}_{N_t} \end{bmatrix} + \begin{bmatrix} \mathbf{V}_1 \\ \vdots \\ \mathbf{V}_{N_r} \end{bmatrix} \tag{36}$$

where $\mathbf{Y}_m \triangleq \mathbf{F}_N \mathbf{y}_m$, $\mathbf{X}_n \triangleq \mathbf{F}_N \mathbf{x}_n$, $\mathbf{V}_m \triangleq \mathbf{F}_N \mathbf{v}_m$, $\mathbf{H}_{m,n} = \mathbf{F}_N \mathbf{A}_{m,n} \mathbf{F}_N^H$, and $\mathbf{\Phi}_{m,n} = \mathbf{F}_N \mathbf{D}_{m,n} \mathbf{F}_N^H$.

Remark 1: For a given L, if N is chosen to have the block time duration $(N+L-1)T_s$ less than the channel coherence time, then the channel impulse response for one block can be considered invariable, so that $\mathbf{A}_{m,n}$ is a circulant matrix and $\mathbf{H}_{m,n}$ is a diagonal matrix with the i-th diagonal element being $H_{m,n;i} = \sum_{l=1}^{L} h_{m,n}(l, N/2) \exp\left(\frac{-j2\pi(l-1)(i-1)}{N}\right)$, i.e., $\mathbf{H}_{m,n} = \text{diag}\{H_{m,n;1} \ \ H_{m,n;2} \ \ \cdots \ \ H_{m,n;N}\}$.

Remark 2: Although $\mathbf{\Phi}_{m,n}$ is generally a non-diagonal matrix, it can be approximated to a diagonal one when the block time duration is less than one third of the quantity $1/\max(f_{m,n,k})$. This condition is obtained by an engineering approach based on our extensive simulation results, which leads to little difference on the diagonal entries of $\mathbf{D}_{m,n}$ and $\mathbf{\Phi}_{m,n} = \mathbf{F}_N \mathbf{D}_{m,n} \mathbf{F}_N^H = \mathbf{F}_N [\lambda_{m,n}\mathbf{I} + \mathbf{\Gamma}_{m,n}]\mathbf{F}_N^H$, where $\lambda_{m,n} = \frac{1}{N}\sum_{k=1}^{N} e^{j(2\pi f_{m,n,k} k T_s + \theta_{m,n})}$ and $\mathbf{\Gamma}_{m,n} = \text{diag}\{e^{j(2\pi f_{m,n,1} T_s + \theta_{m,n})} - \lambda_{m,n}, \cdots, e^{j(2\pi f_{m,n,N} N T_s + \theta_{m,n})} - \lambda_{m,n}\}$. Since $\mathbf{\Gamma}_{m,n}$ is a matrix with small values on the diagonal entries if the block time duration requirement is satisfied, $\mathbf{F}_N \mathbf{\Gamma}_{m,n} \mathbf{F}_N^H$ is negligible. Therefore, $\mathbf{\Phi}_{m,n}$ can be reasonably approximated to a diagonal matrix with identical diagonal elements of $\{\mathbf{\Phi}_{m,n}(i,i)\}_{i=1}^{N} = \lambda_{m,n}$.

The above two properties of the single carrier frequency-domain representation enable effective channel estimation and equalization.

III. FD CHANNEL ESTIMATION

There are two commonly used methods [17, 18] for MIMO channel estimation assisted by training symbols. The first one is referred to as time-domain and frequency-domain orthogonal training method, which estimates the fading channel by sequentially transmitting one small block of N_{ts} training symbols appended by CPs with length of N_{cp} ($N_{cp} < N_{ts}$) from each transmit antenna, while all other transmit antennas remain silent. The total time duration of training blocks for MIMO channel estimation with N_t transmit antennas is $N_t(N_{ts} + N_{cp})T_s$. However, this approach results in a large overhead for transmission. The other method is regarded as a bandwidth efficient method because each antenna transmits training blocks overlapped in time domain but orthogonal in frequency domain. In this method, a length-N_{ts}/N_t ($N_{ts}/N_t \geq L$) Chu sequence [22] is generated as the basic training sequence denoted by $\mathbf{s}_t$. The length-N_{ts} pilot sequence of the first antenna can be constructed by simply duplicating $\mathbf{s}_t$ for N_t times. As a result, $N_t{-}1$ zeros are inserted between adjacent frequency tones of the basic Chu sequence to shape a comb-like spectrum. Then $N_t - 1$ phase-shifted sequences can be built as the pilot sequences of the other $N_t - 1$ antennas, whose k-th symbol is multiplied by $e^{j2\pi(k-1)(m-1)/N_{ts}}$ with $m = 2, \cdots, N_t$. Although these N_t sequences are transmitted simultaneously at the N_t transmit antennas, they are orthogonal in the $N_t N_{ts}$ frequency tones as shown in [17], and the channel can be estimated with a bit higher bandwidth efficiency compared with the former training method.

A. FD Channel Estimation for Pilot Block. This paper adopts the second training method and selects the number of training symbols N_{ts} such that the training block time duration $(N_{ts}{+}N_{cp})T_s$ is smaller than one third of the quantity $1/\max(f_{m,n,k})$ for all m and n. The non-diagonal elements of $\mathbf{\Phi}_{m,n}$, i.e., $\mathbf{\Phi}_{m,n}(p,q)$ with $p \neq q$, are then negligible compared with the diagonal elements $\mathbf{\Phi}_{m,n}(p,p)$. Therefore, the frequency-domain representation (36) of the received pilot signal at m-th antenna can be simplified as

$$\begin{aligned} Y_m(p) &= \sum_{n=1}^{N_t} \mathbf{\Phi}_{m,n}(p,p) H_{m,n;p} X_n(p) + V_m(p) \\ &= \sum_{n=1}^{N_t} \lambda_{m,n} H_{m,n;p} X_n(p) + V_m(p), \; p = 1, \cdots, N_{ts} \end{aligned} \tag{37}$$

where $\lambda_{m,n} = \frac{1}{N_{ts}} \sum_{k=1}^{N_{ts}} e^{j(2\pi f_{m,n,k} k T_s + \theta_{m,n})}$ is a complex-valued unknown parameter with amplitude close to the unit.

By defining the set of indices of nonzero frequency tones for the pilot sequence of the n-th transmit antenna as $\mathbf{\Psi}_n = \{n, \; n + N_t, \; \ldots, \; N_{ts} - N_t + n\}$ and applying the frequency orthogonality of pilot blocks, we simplify the equation (37) to

$$Y_m(i) = \lambda_{m,n} H_{m,n;i} X_n(i) + V_m(i), \qquad i \in \mathbf{\Psi}_n. \tag{38}$$

Hence, the FD channel estimation for pilot blocks can be described according to the following steps:

1) Obtain the initial estimation at the locations of nonzero frequency tones for the (m,n)-th sub-channel

$$\lambda_{m,n}\tilde{H}_{m,n;i} = \begin{cases} \frac{Y_m(i)}{X_n(i)}, & i \in \mathbf{\Psi}_n \\ 0, & \text{others.} \end{cases} \tag{39}$$

2) Multiply the scalar factor N_t with the initial estimation. This step recovers the total energy of null tones in the frequency domain.

3) Convert the result of 2) into the time-domain representation by IFFT which is a periodic impulse response repeating N_t times.

4) Use an L-size window mask to remove the noise beyond the channel length [20], yielding $\lambda_{m,n}\tilde{\mathbf{h}}_{m,n}$.

5) Transform the noise-reduced impulse response back into the frequency domain, and obtain the estimation of frequency-domain transfer function over all frequency tones. The estimation of frequency function can be expressed as

$$\lambda_{m,n}\hat{\mathbf{H}}_{m,n} = \lambda_{m,n}\text{diag}\{\mathbf{F}_{N}[1:L]\mathbf{F}^{H}_{N_{ts}}[1:L]\tilde{\mathbf{H}}_{m,n}\} \tag{40}$$

where $\mathbf{F}_N[1{:}L]$ denotes the first L columns of $\mathbf{F}_N$ (the N-point DFT matrix), $\tilde{\mathbf{H}}_{m,n} = [\tilde{H}_{m,n,1}, \cdots, \tilde{H}_{m,n,N_{ts}}]^T$, and $\lambda_{m,n}\hat{\mathbf{H}}_{m,n} = \lambda_{m,n}\text{diag}\{\hat{H}_{m,n;1} \ \ \hat{H}_{m,n;1} \ \cdots \ \hat{H}_{m,n;N}\}$.

B. Channel Estimation for Data Block. We employ the frame structure designed in [22], where one frame contains N_f blocks composed of one small pilot block with length of N_{ts} and $(N_f - 1)$ N-symbol data blocks. The estimated N-point transfer function matrices of the pilot blocks at the current frame and the next frame are then denoted as $\hat{\mathbf{H}}_{m,n,1}$

and $\hat{\mathbf{H}}_{m,n,N_f+1}$, respectively, for (m,n)-th subchannel, which can be used to estimate the transfer function matrices of the data blocks of the current frame via the interpolation method proposed in [21,22]. To simplify the description, this sub-section drops the index of subchannel and simplifies $\hat{\mathbf{H}}_{m,n,1}$ and $\hat{\mathbf{H}}_{m,n,N_f+1}$ as $\hat{\mathbf{H}}_1$ and $\hat{\mathbf{H}}_{N_f+1}$, respectively.

Define a column vector $\hat{\mathbf{H}}(i) = [\hat{H}_{1;i} \quad \hat{H}_{N_f+1;i}]^T$ as the estimated i-th tone of channel frequency response at pilot blocks of the adjacent frames, and let $\mathbf{C}_p(i)$ be an interpolation row vector corresponding to the p-th block in the current frame. The transfer function of the p-th block of the current frame is then estimated by

$$\hat{H}_{p;i} = \mathbf{C}_p(i)\hat{\mathbf{H}}(i), \qquad p = 1,\ 2,\ \cdots,\ N_f - 1 \tag{41}$$

and the estimated error is given by

$$e_p(i) = H_{p;i} - \hat{H}_{p;i} = H_{p;i} - \mathbf{C}_p(i)\hat{\mathbf{H}}(i). \tag{42}$$

The optimal solution for $\mathbf{C}_p(i)$ can be derived by minimizing the mean square estimation errors

$$\begin{aligned} \mathbf{C}_p(i) &= \mathcal{E}\left\{H_{p;i}\hat{\mathbf{H}}^H(i)\right\}\left[\mathcal{E}\left\{\hat{\mathbf{H}}(i)\hat{\mathbf{H}}^H(i)\right\}\right]^{-1} \\ &= \left[\mathcal{E}\left\{H_{p;i}H_{1;i}^*\right\} \quad \mathcal{E}\left\{H_{p;i}H_{N_f+1;i}^*\right\}\right] \cdot \\ &\quad \begin{bmatrix} \mathcal{E}\left\{|H_{1;i}|^2\right\} + \frac{\sigma^2 L}{N} & \mathcal{E}\left\{H_{1;i}H_{N_f+1;i}^*\right\} \\ \mathcal{E}\left\{H_{N_f+1;i}H_{1;i}^*\right\} & \mathcal{E}\left\{\left|H_{N_f+1;i}\right|^2\right\} + \frac{\sigma^2 L}{N} \end{bmatrix}^{-1} \end{aligned} \tag{43}$$

where $\mathcal{E}$ represents expectation of random variables.

It is noted that the interpolation vector only depends on the second-order statistics of the channel which often remain stationary. The variance of noise can be estimated at receivers by the method introduced in [21]. Therefore, the interpolation vector can be obtained off-line to save the computation for channel estimation in real-time processing. In this paper, the commonly used wide sense stationary uncorrelated scattering (WSSUS) Rayleigh fading channel is considered as the channel model, and the subchannels are assumed to be independent of each other. Hence, the interpolation row vector is simplified as

$$\mathbf{C}_p = \begin{bmatrix} J_0(\omega_d(p-1)T_b) \\ J_0(\omega_d(N_f+1-p)T_b) \end{bmatrix}^T \begin{bmatrix} 1+\frac{\sigma^2 L}{N} & J_0(\omega_d N_f T_b) \\ J_0(\omega_d N_f T_b) & 1+\frac{\sigma^2 L}{N} \end{bmatrix}^{-1} \tag{44}$$

where $J_0(\cdot)$ is the zero-order Bessel function of the first kind, $\omega_d = 2\pi f_d$ is the maximum angular Doppler frequency, and $T_b = (N + N_{cp})T_s$.

IV. FD CHANNEL EQUALIZATION

In the data transmission mode, we choose the data block time duration $(N + N_{cp})T_s$ smaller than the channel coherence time. Therefore, the frequency-domain channel matrices $\{\mathbf{H}_{m,n}\}$ are diagonal.

Based on the estimated channel transfer functions, we define $\mathcal{H}$ as

$$\mathcal{H} = \begin{bmatrix} \lambda_{1,1}\hat{\mathbf{H}}_{1,1} & \cdots & \lambda_{1,N_t}\hat{\mathbf{H}}_{1,N_t} \\ \vdots & \ddots & \vdots \\ \lambda_{N_r,1}\hat{\mathbf{H}}_{N_r,1} & \cdots & \lambda_{N_r,N_t}\hat{\mathbf{H}}_{N_r,N_t} \end{bmatrix}. \tag{45}$$

By applying the linear minimum mean square error (LMMSE) criterion, we obtain the FD equalized block as

$$\begin{bmatrix} \hat{\mathbf{X}}_1 \\ \vdots \\ \hat{\mathbf{X}}_{N_t} \end{bmatrix} = \mathcal{H}^H \left(\mathcal{H}\mathcal{H}^H + \sigma^2 \mathbf{I}_{N_r N}\right)^{-1} \begin{bmatrix} \mathbf{Y}_1 \\ \vdots \\ \mathbf{Y}_{N_r} \end{bmatrix}. \tag{46}$$

It is important to note that (46) is not computationally efficient due to the inversion of the $N_r N \times N_r N$ matrix. However, taking into consideration of the diagonal property of $\mathbf{H}_{m,n}$ and $\hat{\mathbf{H}}_{m,n}$, we can obtain a much more computationally efficient MMSE FD equalizer as follows

$$\begin{bmatrix} \hat{X}_1(i) \\ \vdots \\ \hat{X}_{N_t}(i) \end{bmatrix} = \mathcal{H}_i^H \left(\mathcal{H}_i \mathcal{H}_i^H + \sigma^2 \mathbf{I}_{N_r} \right)^{-1} \begin{bmatrix} Y_1(i) \\ \vdots \\ Y_{N_r}(i) \end{bmatrix} \qquad i = 1, 2, \cdots, N \tag{47}$$

where

$$\mathcal{H}_i = \begin{bmatrix} \lambda_{1,1} \hat{H}_{1,1;i} & \cdots & \lambda_{1,N_t} \hat{H}_{1,N_t;i} \\ \vdots & \ddots & \vdots \\ \lambda_{N_r,1} \hat{H}_{N_r,1;i} & \cdots & \lambda_{N_r,N_t} \hat{H}_{N_r,N_t;i} \end{bmatrix}. \tag{48}$$

As can be seen from (47), the modified MMSE FD equalization involves N-times inversions of $N_r \times N_r$ matrices, making it much more computationally efficient and numerically robust than (46), which involves the inversion of an $N_r N \times N_r N$ matrix.

Substituting (36) into (46) and keeping in mind that $\mathbf{\Phi}_{m,n}$ is a diagonally dominant matrix when the data block time duration $(N + N_{cp})T_s$ is smaller than one third of $1/\max(f_{m,n,k})$, the equalized block data for the n-th transmit antenna is given by

$$\hat{\mathbf{X}}_n = \left(\sum_{m=1}^{N_r} \mathbf{\Delta}_{m,n} \mathbf{\Phi}_{m,n} \right) \mathbf{X}_n + \hat{\mathbf{V}}_n \tag{49}$$

where $\mathbf{\Delta}_{m,n}$ is related to the fading channel and equalizer coefficients, which is a diagonal matrix when $N_t = 1$ and approximates to be a diagonal matrix when $N_t \neq 1$. The proof of this equation for $N_t = 1$ has been provided in [23], and the proof for the MIMO system is shown in Appendix.

Applying inverse DFT to the equalized data vector $\hat{\mathbf{X}}_n$, we have the equalized time-domain data vector $\hat{\mathbf{x}}_n$ given by

$$\begin{aligned}
\hat{\mathbf{x}}_n = \mathbf{F}_N^H \hat{\mathbf{X}}_n = & \sum_{m=1}^{N_r} \mathbf{F}_N^H \boldsymbol{\Delta}_{m,n} \boldsymbol{\Phi}_{m,n} \mathbf{X}_n + \mathbf{F}_N^H \hat{\mathbf{V}}_n \\
= & \sum_{m=1}^{N_r} \mathbf{F}_N^H \boldsymbol{\Delta}_{m,n} \mathbf{F}_N \mathbf{D}_{m,n} \mathbf{F}_N^H \mathbf{F}_N \mathbf{x}_n + \hat{\mathbf{v}}_n \\
= & \sum_{m=1}^{N_r} (\mathbf{F}_N^H \boldsymbol{\Delta}_{m,n} \mathbf{F}_N) \mathbf{D}_{m,n} \mathbf{x}_n + \hat{\mathbf{v}}_n. \qquad (50)
\end{aligned}$$

Since $\boldsymbol{\Delta}_{m,n}$ is approximately a diagonal matrix, all the diagonal elements of $\left(\mathbf{F}_N^H \boldsymbol{\Delta}_{m,n} \mathbf{F}_N\right)$ are approximately identical and equal to $\gamma_{m,n} = \frac{1}{N}\text{trace}\,(\boldsymbol{\Delta}_{m,n})$. When the data block time duration is less than the channel coherence time, all the non-diagonal elements of $\left(\mathbf{F}_N^H \boldsymbol{\Delta}_{m,n} \mathbf{F}_N\right)$ are insignificant comparing to $\gamma_{m,n}$. Therefore, the k-th symbol of $\hat{\mathbf{x}}_n$ can be expressed by

$$\begin{aligned}
\hat{x}_n(k) = & \left[\sum_{m=1}^{N_r} \gamma_{m,n} e^{j(2\pi f_{m,n,k} k T_s + \theta_{m,n})} \right] x_n(k) + \hat{v}_n(k) \\
= & |\beta_n(k)| e^{j\angle \beta_n(k)} x_n(k) + \hat{v}_n(k) \qquad (51)
\end{aligned}$$

where $\beta_n(k) = \sum_{m=1}^{N_r} \gamma_{m,n} e^{j\left(2\pi f_{m,n,k} k T_s + \theta_{m,n}\right)}$.

From (51), we conclude that the complex-valued symbol-wise scaling factor $\beta_n(k)$ is actually a diversity combining factor determined by the N_r-receive channel transfer functions, CFOs, time-error phases, and Doppler. In other words, the equalized data symbol $\hat{x}_n(k)$ is an amplitude-scaled and phase-rotated version of the transmitted data symbol $x_n(k)$. The rotating phase $\angle\beta_n(k)$ is a collection of all the contributions from the CFOs $f_{m,n,k}$ and timing-error phases $\theta_{m,n}$ of all the N_r fading channels. For each individual fading channel, the rotating phase $\angle\beta_{m,n}(k) = 2\pi f_{m,n,k} k T_s + \theta_{m,n} + \angle\gamma_{m,n}$, which represents the m-th channel's CFO-driven shifting phase, timing-error phase, and the channel transfer function effect. This is a physical interpretation of the single carrier frequency-domain equalized data.

If $x(k)$ is phase shift keying (PSK) modulated data, then the time-varying rotating phase $\angle\beta_{m,n}(k)$ must be compensated at the receiver after FDE and before demodulation and detection. This process will be discussed in detail in the next section.

V. PHASE-COHERENT DETECTION

In this section, we present an effective and robust algorithm for estimating the phases $\angle\beta_n(k)$, which is crucial for successful data detection of PSK modulated symbols. The challenge of phase estimations is that we face multiple fading channels, in which each individual channel has different carrier frequency offset, timing-error phase and Doppler, and the rotating phases $\angle\beta_n(k)$ represents a nonlinearly composed effect of these random (or time-varying) factors of all the fading channels. Therefore, directly estimating these carrier frequency offsets, timing-error phases and Doppler will be very costly if any possible.

What we know from the nature of fading channels is that the carrier frequency offsets are either constants or changing gradually from time to time, i.e., they do not change arbitrarily in a short period of time. Therefore, the rotating phases $\angle\beta_n(k)$ are also changing gradually from time to time. We thus, treat $\angle\beta_n(k)$ quasi-stationary. That is, they are constants over a small number of N_s consecutive received symbols.

We partition the equalized N-symbol block data $\hat{\mathbf{x}}_n$ into N_g groups, each with N_s data symbols, except for the last group might have less than N_s symbols if N/N_g is not an integer.

Let $\psi_n(g)$ denote the estimated average rotating phase for the g-th group of $\{\angle\beta_n((g-1)N_s+1), \cdots, \angle\beta_n((g-1)N_s+N_s)\}$ with $g = 1, 2, \cdots, N_g$, and let $\psi_n(0)$ denote the initial rotating phase and $\Delta\psi_n(g)$ the phase difference $\psi_n(g)-\psi_n(g-1)$. Hence,

$$\psi_n(g)=\psi_n(g-1) + \Delta\psi_n(g), \quad g = 1, 2, \cdots, N_g. \tag{52}$$

For MPSK modulation with symbols taken from an M_m-ary constellation $\mathcal{A}_{\mathcal{M}} \triangleq \left\{\exp\left[\frac{j(m-1)2\pi}{M_m}\right], m=1,2,\cdots,M_m\right\}$, we define a phase quantization function $\mathbb{Q}[\phi]$ as

$$\mathbb{Q}[\phi]=\frac{2(m-1)\pi}{M_m}, \qquad \frac{2m\pi-3\pi}{M_m} < \phi \leq \frac{2m\pi-\pi}{M_m}, \quad m = 1, 2, \cdots, M_m. \tag{53}$$

We are now in a position to present our algorithm as follows.

Algorithm: Group-wise Rotating Phase Estimation

Step 1. Denote the first N_p symbols $\{x_n(k)\}_{k=1}^{N_p}$ of each N-symbol block data $\mathbf{x}_n$ at the n-th transmit antenna as pilot symbols for phase reference to determine the initial rotating phase $\psi_n(0)$ given by

$$\psi_n(0)=\frac{1}{N_p}\sum_{k=1}^{N_p}\big(\angle\hat{x}_n(k)-\angle x_n(k)\big). \tag{54}$$

Compensate the phase of the first group data by $e^{-j\psi_n(0)}$, yielding

$$\tilde{x}_n(1,k)=\hat{x}_n(k)e^{-j\psi_n(0)}, \quad k=1,2,\cdots,N_s. \tag{55}$$

Calculate the individual phase deviation from its nominal phase of each symbol in the first group

$$\varphi_n(1,k)=\angle\tilde{x}_n(1,k)-\mathbb{Q}\left[\angle\tilde{x}_n(1,k)\right], \; k=1,2,\cdots,N_s. \tag{56}$$

Calculate the average phase deviation, and compute the rotating phase for the first group as follows

$$\Delta\psi_n(1)=\frac{1}{N_s}\sum_{k=1}^{N_s}\varphi_n(1,k) \tag{57}$$

$$\psi_n(1)=\psi_n(0)+\Delta\psi_n(1). \tag{58}$$

Set $g=2$ for next step.

Step 2. Compensate the phase of the g-th group data by $e^{-j\psi_n(g-1)}$, yielding

$$\tilde{x}_n(g,k)=\hat{x}_n((g-1)N_s+k)e^{-j\psi_n(g-1)}, \; k=1,2,\cdots,N_s. \tag{59}$$

Calculate the individual phase deviation from its nominal phase of each symbol in the g-th group

$$\varphi_n(g,k)=\angle\tilde{x}_n(g,k)-\mathbb{Q}\left[\angle\tilde{x}_n(g,k)\right], \; k=1,2,\cdots,N_s. \tag{60}$$

Calculate the average phase deviation, and estimate the rotating phase for the g-th group as below

$$\Delta\psi_n(g) = \frac{1}{N_s}\sum_{k=1}^{N_s}\varphi_n(g,k) \tag{61}$$

$$\psi_n(g) = \psi_n(g-1) + \Delta\psi_n(g). \tag{62}$$

Step 3. Update $g=g+1$, and repeat Step 2 until $g=N_g$.

After estimating the N_g group phases of equalized block data from the n-th transmit antenna, we can compensate the phase rotation of the equalized data $\hat{x}_n$ in group basis:

$$\check{x}_n(g,k) = \hat{x}_n((g-1)N_s+k)e^{-j\psi_n(g)}, \quad \begin{array}{c} k=1,2,\cdots,N_s \\ g=1,2,\cdots,N_g \end{array}. \tag{63}$$

Finally, the binary information data of the block can be obtained via standard MPSK demodulation procedure on the phase-compensated signal $\check{x}_n(g,k)$ of the block. Different block data with different transmit antenna index n can be processed in a similar manner, details are omitted here for brevity.

We make two remarks before leaving this section.

Remark 3: The choice of N_s symbols in a group needs to satisfy the condition $2\pi\,|f_{d,n}|\,N_sT_s < \frac{\pi}{M_m}$ to ensure that the maximum rotating phase does not exceed a decision region of MPSK, where $|f_{d,n}|$ is the absolute value of the maximum composite CFO, in Hz, linking to the n-th transmit antenna.

Remark 4: The group-wise estimation of the rotating phase is insensitive to noise perturbations due to its averaging process (61), which is a low-pass filtering process.

VI. NUMERICAL RESULTS

In this section, two numerical examples of MIMO wireless systems with various system parameters and fading channels are presented to demonstrate the performance of the proposed algorithm. The first example is to show that the proposed receiver algorithm can provide good performance for frequency selective fading channels with a long delay spread and multiple unknown carrier frequency offsets. The second example is to study the effect of various CFOs and demonstrate the capability of dealing with time-varying CFOs by our algorithm. In both examples, the fading channels were simulated by the improved Clarke's Rayleigh fading model [24, 25] with multiple CFOs.

System A: We first considered a MIMO wireless system with 2 transmit antennas and 4 receive antennas. A 75-tap frequency selective Rayleigh fading channel was employed, where the average power of the first 25 taps ramps up linearly, and the last 50 taps ramps down linearly. The total average power of the fading channel was normalized to one, and the maximum Doppler spread was assumed to be 50 Hz. The lengths of training symbols N_{ts} and data blocks N were set at 256 and 4096, respectively. In one burst transmission, every antenna transmitted 6 frames, each of which consists of 1 pilot block and 2 data blocks. QPSK and 8PSK modulations were adopted with symbol period, $T_s = 0.125\ \mu s$. The multiple CFOs, listed in Table 1, were unknown to the receiver in the simulations.

Table 1 Multiple CFOs for the 4×2 wireless system

$\mathrm{CFO}_{1,1}$	−200 Hz	$\mathrm{CFO}_{1,2}$	170 Hz
$\mathrm{CFO}_{2,1}$	−190 Hz	$\mathrm{CFO}_{2,2}$	180 Hz
$\mathrm{CFO}_{3,1}$	−180 Hz	$\mathrm{CFO}_{3,2}$	190 Hz
$\mathrm{CFO}_{4,1}$	−170 Hz	$\mathrm{CFO}_{4,2}$	200 Hz

The scatter plot of the equalized 8PSK data with SNR=18 dB is depicted in Fig. 1, where these equalized symbols are phase-rotated forming a donut-like shape. They cannot be reliably demodulated directly after equalization. Figure 2 shows the scatter plot of the phase-corrected data, exhibiting clear gaps between eight constellation locations. The data can now be reliably demodulated using the conventional detection procedure.

In Fig. 3, the mean square error (MSE) is evaluated for equalized and phase corrected symbols, respectively. The phase corrected symbols have much lower MSE than that of the equalized symbols, which substantiates the effectiveness of our phase correction algorithm. The uncoded bit error rates are shown in Fig. 4 for three cases: 1) the channel coefficients are perfectly known to the receiver, and there is no CFO, *i.e.*, zero CFO, this case serves as a benchmark; 2) the channel coefficients are estimated by the interpolation-based algorithm discussed in Section III, and there is no CFO in the system; 3) the channel coefficients are

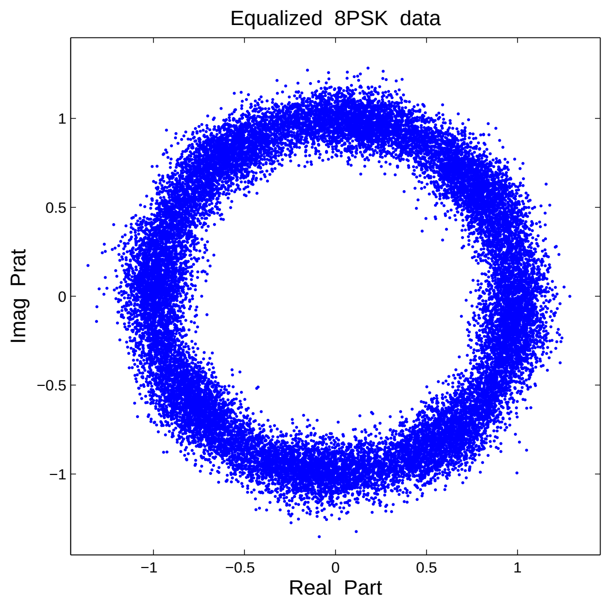

Figure 1 Scatter plot of equalized 8PSK signals of transmit antenna 2, SNR= 18 dB.

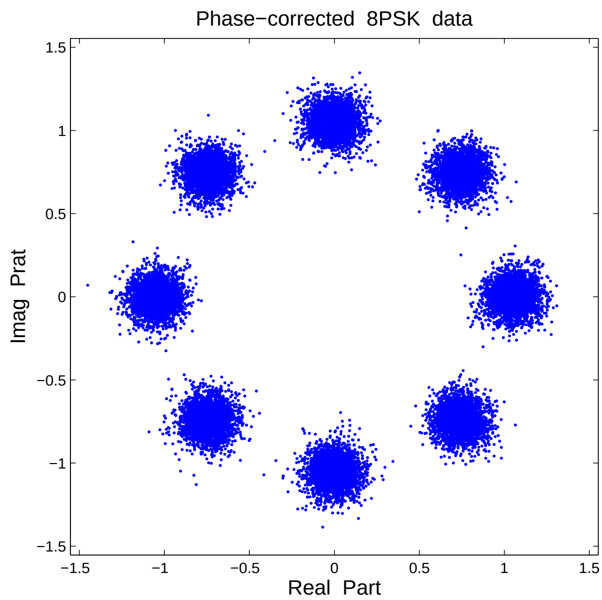

Figure 2 Scatter plot of equalized and phase-corrected 8PSK signals of transmit antenna 2, SNR= 18 dB.

estimated by the interpolation-based algorithm, and the multiple unknown CFOs are handled by the proposed phase correction method. In this figure, we can see that the performance of the second channel condition is 2 dB away for QPSK (1.5 dB for 8PSK) from that of the idealistic first channel condition when the BER is 10^{-3}. Also note that the performance of

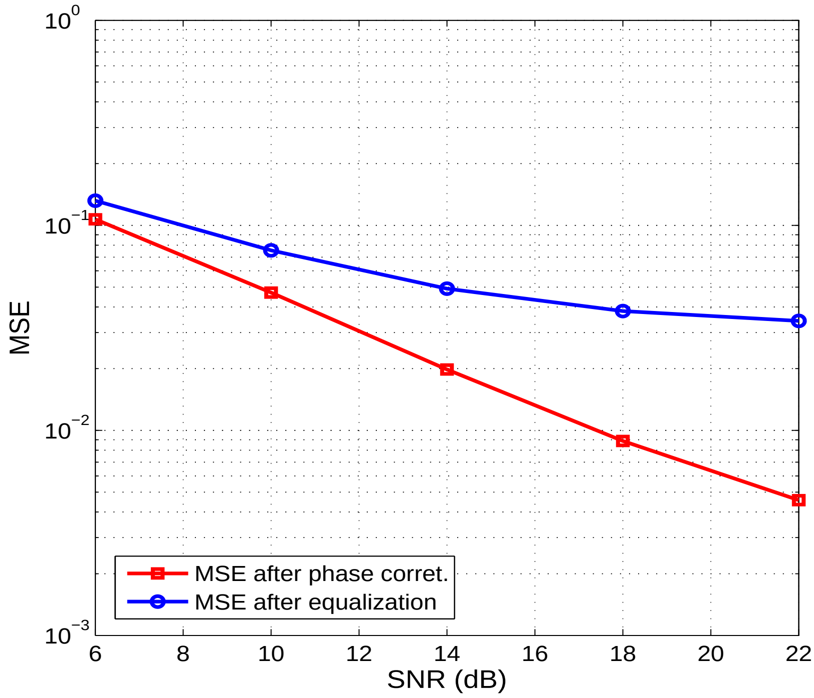

Figure 3 Mean square error for QPSK and 8PSK symbols after equalization and phase correction.

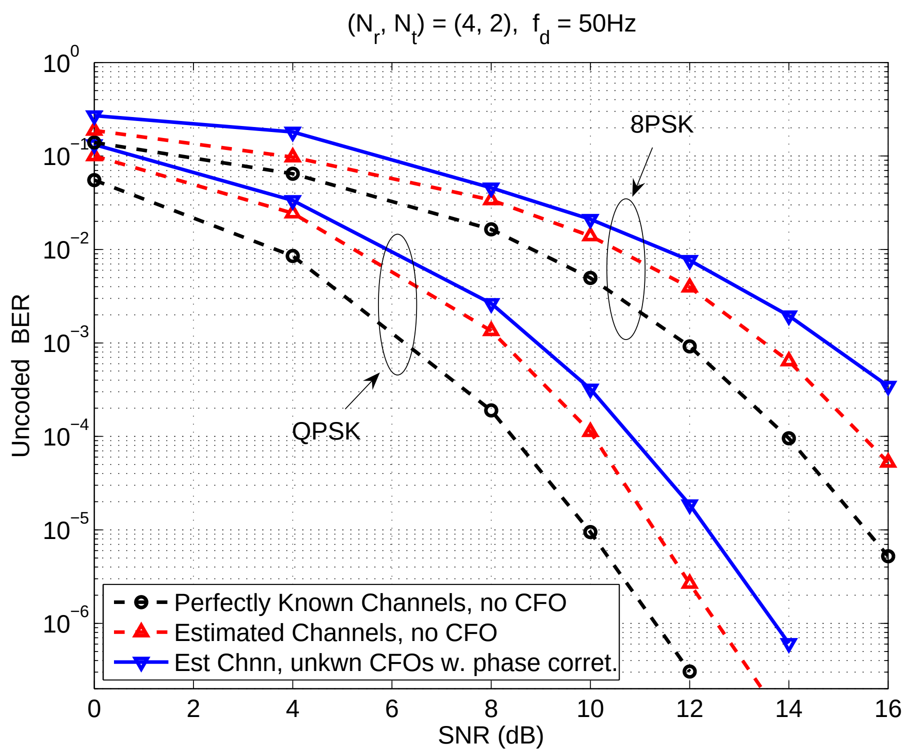

Figure 4 Uncoded bit error rate of equalized and phase-corrected QPSK and 8PSK modulated signals.

the third channel conditions (with multiple unknown CFOs) is only 0.5 dB away for QPSK (1 dB for 8PSK) from that of the second channel condition (with no CFO) when BER is 10^{-3}. Therefore, the proposed method is effective for mitigating the multiple unknown CFOs and extended ISI caused by severe frequency selective channel fading, especially when the DFT block size is large and/or the CFOs are significant.

System B: A different MIMO system with 4 transmit antennas and 8 receive antennas was investigated to study the effect of different CFOs on the BER and to evaluate the capability of compensating the time-varying CFOs of the proposed algorithm. The channels were assumed to be 20-tap frequency-selective Rayleigh fading channels whose l-th tap has average power given by $0.2225\exp(-0.2l)$. The maximum Doppler spread was set to 20 Hz in evaluating the effect of various CFOs. The maximum allowable CFO is determined by the block size and symbol period according to Remark 2 as $|f_{\text{CFO}}^{\max}| < \frac{1}{3} \cdot \frac{1}{NT_s}$. For time-varying CFOs, the BER performances were simulated under different maximum Doppler spreads. In one realization of the channel, 6 frames were transmitted, and we chose FFT size $N = 2048$, $N_{ts} = 256$ and 8PSK modulation with symbol interval, $T_s = 0.25\ \mu s$. In the first simulation experiment, the subchannels corresponding to the first and third transmitters were assumed to have identical CFOs f_{CFO} Hz, and the second and fourth transmitters were assumed to have same CFOs of $-f_{\text{CFO}}$ Hz.

Figure 5 presents the BER performance at various values of f_{CFO}, where the channels are estimated at the receiver. When f_{CFO} equals to 50 Hz and 100 Hz, the resulting performances are virtually identical to that of the CFO-free system. When f_{CFO} equals to 200 Hz and 250 Hz, the BER performances are less than 1 dB away from the CFO-free system. These results tell us that our phase correction algorithm is very effective to deal with multiple unknown CFOs which are ranging from small to moderate to high. It is noted that the second generation (2G) and third generation (3G) wireless communication standards specified that the CFO must be in the region from -200 Hz to 200 Hz.

All the examples presented so far assume that the multiple CFOs remain constant in one block. In order to evaluate the performance of the proposed algorithm for time-varying CFOs, we consider the situation that the subchannels corresponding to the same transmit

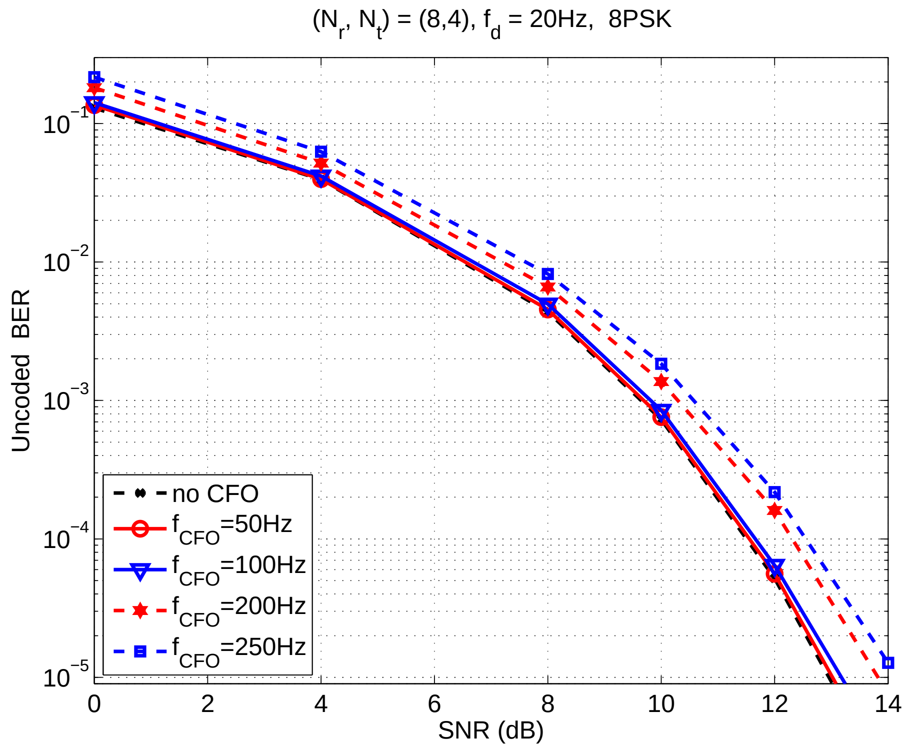

Figure 5 Uncoded bit error rate of equalized and phase-corrected 8PSK modulated signals for different CFOs.

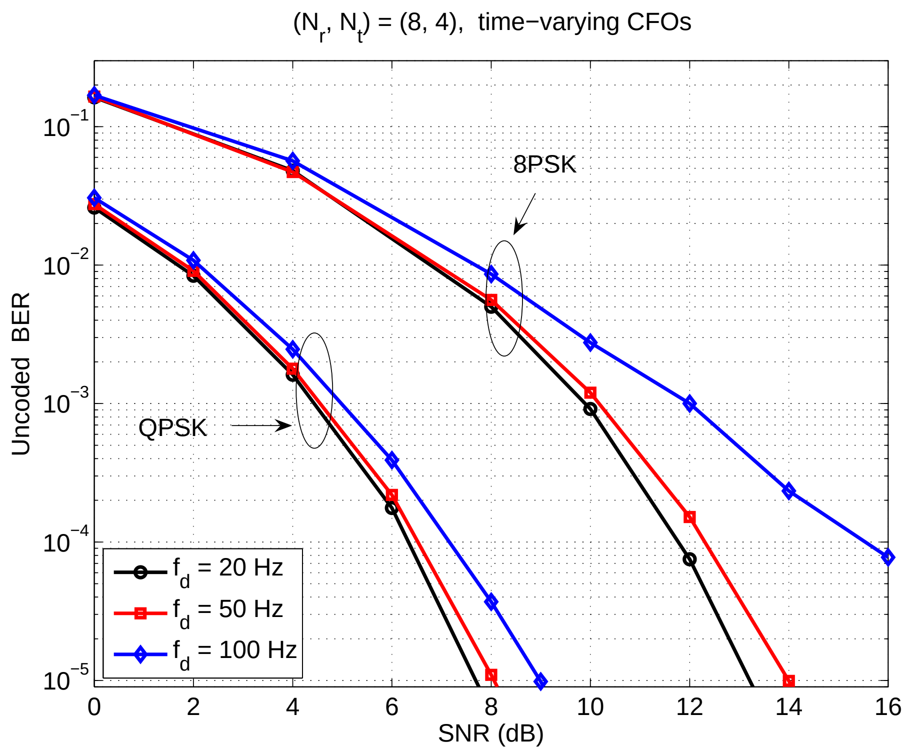

Figure 6 Uncoded bit error rate for time-varying CFOs for four transmitters.

antenna have the same time-varying CFOs, i.e., $f_{n,k}$=$\pm 100+10\sin\big(2\pi\cdot k/N+\phi_n+\theta\big)$, where $n=1,\ldots,4$; $k=1,\ldots,N$; $\phi_n=n\pi/2$ and θ is a random phase. The BER simulated under various maximum Doppler spreads are compared in Fig. 6. All these results are obtained by estimating channel in interpolation method and compensating CFOs via phase correction algorithm. It is observed that the algorithm works very well for the time-varying CFOs, implying it is robust to the CFO variation in each block. As we observe, the performance will degrade with the increase of Doppler spread. However, the BER of 8PSK modulation, as presented in Fig. 6, can still achieve approximately 10^{-4} for $f_d=100$ Hz at SNR=14 dB, which indicates the proposed receiver structure can be applicable for high speed mobility.

VII. CONCLUSION

In this paper, we demonstrated that multiple carrier frequency offsets (CFOs) in MIMO systems can be troublesome for single carrier frequency-domain equalization if the discrete Fourier transform block size is large and/or the constellation size of signal modulation is high. The multiple CFOs will cause the constellation of the equalized data to rotate, making reliable detection of the equalized data impossible if the effect of multiple CFOs is not mitigated. Instead of directly estimating the CFOs, which is very costly, we proposed a new method to estimate the rotated phases caused by the multiple CFOs, and then utilized the estimated phases to correct the phase rotation of the equalized data before performing the symbol detection. Numerical examples showed that the proposed method leads to very good results for a 4×2 wireless system with QPSK and 8PSK modulation over 75-tap Rayleigh fading channels, at a Doppler frequency of 50 Hz. The effect of various CFOs on the BER and the capability of tackling time-varying CFOs were evaluated by investigating a 8×4 system with 8PSK symbol mapping. The rotating phase estimation algorithm was proved to be not only computationally efficient, but also numerically robust over a wide range of signal-to-noise ratio values.

VIII. DERIVATION OF EQUALIZED BLOCK DATA

First, the matrix identity $\mathcal{H}^H(\mathcal{H}\mathcal{H}^H+\sigma^2\mathbf{I}_{N_rN})^{-1}\mathcal{H}=\mathbf{I}_{N_tN}-(\mathbf{I}_{N_tN}+\sigma^{-2}\mathcal{H}^H\mathcal{H})^{-1}$ can be proved by applying matrix inverse lemma. From this equation, we can observe that $\mathcal{H}^H(\mathcal{H}\mathcal{H}^H+$

$\sigma^2\mathbf{I}_{N_rN})^{-1}\mathcal{H}$ is approaching $\mathbf{I}_{N_tN}$ with high accuracy provided the signal-to-noise ratio (SNR) is high. Based on this approximation, we have the following equations

$$\left[\lambda_{1,p}^*\hat{\mathbf{H}}_{1,p}^H \cdots \lambda_{Nr,p}^*\hat{\mathbf{H}}_{Nr,p}^H\right]\left(\mathcal{H}\mathcal{H}^H+\sigma^2\mathbf{I}_{N_rN}\right)^{-1}\begin{bmatrix}\lambda_{1,p}\hat{\mathbf{H}}_{1,p}\\ \vdots \\ \lambda_{N_r,p}\hat{\mathbf{H}}_{N_r,p}\end{bmatrix}\simeq\mathbf{I}_N \tag{64}$$

$$\left[\lambda_{1,p}^*\hat{\mathbf{H}}_{1,p}^H \cdots \lambda_{Nr,p}^*\hat{\mathbf{H}}_{Nr,p}^H\right]\left(\mathcal{H}\mathcal{H}^H+\sigma^2\mathbf{I}_{N_rN}\right)^{-1}\begin{bmatrix}\lambda_{1,q}\hat{\mathbf{H}}_{1,q}\\ \vdots \\ \lambda_{N_r,q}\hat{\mathbf{H}}_{N_r,q}\end{bmatrix}=\mathbf{O}_N \tag{65}$$

where $p,\ q=1,\cdots,N_t$ and $p\neq q$.

Substituting (36) into (46), we have

$$\begin{aligned}\begin{bmatrix}\hat{\mathbf{X}}_1\\ \vdots \\ \hat{\mathbf{X}}_{N_t}\end{bmatrix} &= \mathcal{H}^H(\mathcal{H}\mathcal{H}^H+\sigma^2\mathbf{I}_{N_rN})^{-1}\cdot \\ &\quad\left(\begin{bmatrix}\mathbf{\Phi}_{1,1}\mathbf{H}_{1,1} & \cdots & \mathbf{\Phi}_{1,N_t}\mathbf{H}_{1,N_t}\\ \vdots & \ddots & \vdots \\ \mathbf{\Phi}_{N_r,1}\mathbf{H}_{N_r,1} & \cdots & \mathbf{\Phi}_{N_r,N_t}\mathbf{H}_{N_r,N_t}\end{bmatrix}\begin{bmatrix}\mathbf{X}_1\\ \vdots \\ \mathbf{X}_{N_t}\end{bmatrix}+\begin{bmatrix}\mathbf{V}_1\\ \vdots \\ \mathbf{V}_{N_r}\end{bmatrix}\right) \\ &= \begin{bmatrix}\lambda_{1,1}^*\hat{\mathbf{H}}_{1,1}^H & \cdots & \lambda_{N_r,1}^*\hat{\mathbf{H}}_{N_r,1}^H\\ \vdots & \ddots & \vdots \\ \lambda_{1,N_t}^*\hat{\mathbf{H}}_{1,N_t}^H & \cdots & \lambda_{N_r,N_t}^*\hat{\mathbf{H}}_{N_r,N_t}^H\end{bmatrix}(\mathcal{H}\mathcal{H}^H+\sigma^2\mathbf{I}_{NN_r})^{-1}\cdot \\ &\quad\begin{bmatrix}\mathbf{\Phi}_{1,1}\mathbf{H}_{1,1} & \cdots & \mathbf{\Phi}_{1,N_t}\mathbf{H}_{1,N_t}\\ \vdots & \ddots & \vdots \\ \mathbf{\Phi}_{N_r,1}\mathbf{H}_{N_r,1} & \cdots & \mathbf{\Phi}_{N_r,N_t}\mathbf{H}_{N_r,N_t}\end{bmatrix}\begin{bmatrix}\mathbf{X}_1\\ \vdots \\ \mathbf{X}_{N_t}\end{bmatrix}+\hat{\mathbf{V}}.\end{aligned} \tag{66}$$

where $\hat{\mathbf{V}}=\mathcal{H}^H(\mathcal{H}\mathcal{H}^H+\sigma^2\mathbf{I}_{N_rN})^{-1}\mathbf{V}$ and $\mathbf{V}=[\mathbf{V}_1^T,\cdots,\mathbf{V}_{N_r}^T]^T$.

Based on (64), (65) and $\mathbf{\Phi}_{m,n}$ being diagonally dominant, we have

$$
\begin{aligned}
\hat{\mathbf{X}}_n =& \left[\lambda^*_{1,n}\hat{\mathbf{H}}^H_{1,n}, \cdots, \lambda^*_{N_r,n}\hat{\mathbf{H}}^H_{N_r,n}\right](\mathcal{H}\mathcal{H}^H + \sigma^2\mathbf{I}_{N_rN})^{-1} \cdot \\
& \begin{bmatrix} \mathbf{\Phi}_{1,n}\mathbf{H}_{1,n} \\ \vdots \\ \mathbf{\Phi}_{N_r,n}\mathbf{H}_{N_r,n} \end{bmatrix} \mathbf{X}_n + \hat{\mathbf{V}}_n \\
\approx & [\lambda^*_{1,n}\hat{\mathbf{H}}^H_{1,n}, \cdots, \lambda^*_{N_r,n}\hat{\mathbf{H}}^H_{N_r,n}](\mathcal{H}\mathcal{H}^H + \sigma^2\mathbf{I}_{N_rN})^{-1} \cdot \\
& \begin{bmatrix} \mathbf{H}_{1,n}\mathbf{\Phi}_{1,n} \\ \vdots \\ \mathbf{H}_{N_r,n}\mathbf{\Phi}_{N_r,n} \end{bmatrix} \mathbf{X}_n + \hat{\mathbf{V}}_n \\
=& \left[\mathbf{G}_{1,n}, \cdots, \mathbf{G}_{N_r,n}\right] \begin{bmatrix} \mathbf{H}_{1,n}\mathbf{\Phi}_{1,n} \\ \vdots \\ \mathbf{H}_{N_r,n}\mathbf{\Phi}_{N_r,n} \end{bmatrix} \mathbf{X}_n + \hat{\mathbf{V}}_n \\
=& \sum_{m=1}^{N_r} \mathbf{G}_{m,n}\mathbf{H}_{m,n}\mathbf{\Phi}_{m,n}\mathbf{X}_n + \hat{\mathbf{V}}_n \\
=& \Big(\sum_{m=1}^{N_r} \mathbf{\Delta}_{m,n}\mathbf{\Phi}_{m,n}\Big)\mathbf{X}_n + \hat{\mathbf{V}}_n
\end{aligned} \tag{67}
$$

where $\mathbf{G}_{m,n} = [\lambda^*_{1,n}\hat{\mathbf{H}}^H_{1,n}, \cdots, \lambda^*_{N_r,n}\hat{\mathbf{H}}^H_{N_r,n}]\Xi[(mN-N+1):mN]$, in which $\Xi[(mN-N+1):mN]$ represents a matrix composed of the $(mN-N+1)$-th to (mN)-th column of $(\mathcal{H}\mathcal{H}^H + \sigma^2\mathbf{I}_{N_rN})^{-1}$.

IX. REFERENCES

[1] M. V. Clark, “Adaptive frequency-domain equalization and diversity combining for broadband wireless communications,” *IEEE J. Select. Areas Commun.*, vol.16, vol.16, pp.1385-1395, Oct. 1998.

[2] D. Falconer, S. L. Ariyavisitakul, A. Benyamin-Seeyar, and B. Eidson, “Frequency domain equalization for single-carrier broadband wireless systems,” *IEEE Commun. Mag.*, vol.40, no.4, pp.58-66, Apr. 2002.

[3] IEEE Std 802.16e-2005, “IEEE Standard for local and metroplolitan area networks, part 16: air interface for fixed and mobile broadband wireless access systems,” Feb. 2006.

[4] F. Pancaldi, G. M. Vitetta, R. Kalbasi, N. Al-Dhahir, M. Uysal, and H. Mheidat, “Single-carrier frequency domain equalization,” *IEEE Signal Proc. Mag.*, pp.37-56, Sept. 2008.

[5] B. Chen, "Maximum likelihood estimation of OFDM carrier frequency offset," *IEEE Signal Proc. Lett.*, vol.9, pp.123-126, Apr. 2002.

[6] M. Luise and R. Reggiannini, "Carrier frequency recovery in all-digital modems for burst-mode transmissions," *IEEE Trans. Commun.*, vol.43, pp.1169-1178, Feb.-Apr., 1995.

[7] J. Chen, Y. C. Wu, S. C. Chan, and T. S. Ng, "Joint maximum-likelihood CFO and channel estimation for OFDMA uplink using importance sampling," *IEEE Trans. Veh. Technol.*, vol.57, pp.3462-3470, Nov. 2008.

[8] E.Jeong, S. Jo, and Y. H. Lee, "Lease square frequency estimation in frequency-selective channels and its application to transmissions with antenna diversity," *IEEE J. Sel. Areas Commun.*, vol.19, pp.2369-2380, Dec. 2001.

[9] J. Van de Beek, M. Sandel, and P.O.Borjesson, "ML estimation of timing and frequency offset in OFDM systems," *IEEE Trans. Signal Process.*, vol.45, pp.1800-1805, Jul. 1997.

[10] D. Huang and K. B. Letaief, "Carrier frequency offset estimation for OFDM systems using null subcarriers," *IEEE Trans. Commun.*, vol.54, pp.813-823, May 2006.

[11] J. Zhu and W. Lee, "Carrier frequency offset estimation for OFDM systems with null subcarriers," *IEEE Trans. Veh. Technol.*, vol.55, pp.1677-1690, Sept. 2006.

[12] U. Tureli, H. Liu, and M. D. Zoltowski, "OFDM blind carrier offset estimation: ESPRIT," *IEEE Trans. Commun.*, vol.48, pp.1459-1461, Sep. 2000.

[13] A. Al-Dweik, A. Hazmi, S. Younis, B. Sharif, and C. Tsimenidis, "Carrier frequency offset estimation for OFDM system over mobile radio channels," *IEEE Trans. Veh. Technol.*, vol.59, pp. 974-979, Feb. 2010.

[14] Y. Wang and X. Dong, "Comparison of frequency offset and timing offset effects on the performance of SC-FDE and OFDM over UWB channels," *IEEE Trans. Veh. Technol.*, accepted for publication.

[15] M. Sabbaghian and D. Falconer, "Joint turbo frequency domain equalization and carrier synchronization," *IEEE Trans. Wireless Commun.*, vol.7, pp.204-212, Jan. 2008.

[16] J. Wu and C. Xiao, "Performance analysis of wireless systems with doubly selective Rayleigh fading," *IEEE Trans. Veh. Technol.*, vol.56, pp.721-730, March 2007.

[17] J. Siew, J. Coon, R. J. Piechocki, A. Dowler, A. Nix, M. Beach, S. Armour, and J. McGeehan, "A channel estimation algorithm for MIMO-SCFDE," *IEEE Commun. Lett.*, vol.8, pp.555-557, Sept. 2004.

[18] J. Coon, S. Armour, M. Beach, and J. MeGeehan, "Adaptive frequency-domain equalization for single-carrier multiple-input multiple-output wireless transmissions," *IEEE Trans. Signal Proc.*, vol.53, pp.3247-3256, Aug. 2005.

[19] D. C. Chu, "Polyphase codes with good periodic correlation properties," *IEEE Trans. Inform. Theory*, vol.IT-18, pp.531-532, July 1972.

[20] A. Chini, "Multicarrier modulation in frequency selective fading channels," Ph.D. dissertation, Carleton University, Ottawa, Canada, 1994.

[21] Y. R. Zheng and C. Xiao, "Channel estimation for frequency-domain equalization of single carrier broadband wireless communications," *IEEE Trans. Veh. Technol.*, vol.58, pp.815-823, Feb. 2009.

[22] Y. R. Zheng and J. Zhang, "Improved frequency-domain channel estimation for fast time-varying MIMO-SCFDE channels," in *Proc. IEEE ICC08*, Beijing, China, May 19-23, 2008, pp.5108-5112.

[23] Y. R. Zheng, C. Xiao, T. C. Yang, and W. B. Yang, "Frequency-domain channel estimation and equalization for single carrier underwater acoustic communications," in *Proc. IEEE/MTS OCEANS'07*, Vancouver, BC, Canada, Oct. 2007, pp.1-6.

[24] C. Xiao, J. Wu, S. Leong, Y. R. Zheng, and K. B. Letaief, "A discrete-time model for triply selective MIMO Rayleigh fading channels," *IEEE Trans. Wireless Commun.*, vol.3, pp.1678-1688, Sept. 2004.

[25] C. Xiao, Y. R. Zheng, and N. C. Beaulieu, "Novel sum-of-sinusoids simulation models for Rayleigh and Rician fading channels," *IEEE Trans. Wireless Commun.*, vol.5, pp.3667-3679, Dec. 2006.

3. LAYERED FREQUENCY-DOMAIN EQUALIZATION FOR SINGLE CARRIER MIMO SYSTEMS WITH MULTIPLE CARRIER FREQUENCY OFFSETS

Jian Zhang and Yahong Rosa Zheng

Abstract—In this paper, carrier frequency offsets (CFOs) are considered in a layered frequency-domain equalization (LFDE) architecture for a single carrier (SC) broadband wireless multiple-input multiple-output (MIMO) system. At each layer of detection, a group of best data streams are selected to be equalized and reliably detected via removing the phase and amplitude distortion caused by the multiple CFOs. The estimated phase rotations and amplitude scalars are required to be compensated to the detected data streams in order to reconstruct the interference signals which are canceled out from the received signals. Instead of direct estimation of CFOs, our algorithm is to estimate the phase rotations and amplitude scalars in a group-wise fashion, which dramatically reduces the computational complexity at receiver. Simulation results demonstrate that the proposed LFDE with phase compensation architecture can provide good performance for a MIMO system impaired by CFOs over unbalanced multi-path channels with long delay spread. We also show that the performance will be improved if more layers are used at receivers.

I. INTRODUCTION

Multiple-input and multiple-output (MIMO) systems applied in wireless communications have shown enormous potential in increasing capacity and the improving performance. A variety of techniques have been extensively investigated to exploit the advantages of MIMO to achieve high-data rate communications with low bit-error-rate (BER). Among these work, the layered detection architecture has been an active and interesting topic since the Vertical Bell Laboratories Layered Space-Time (V-BLAST) system was developed for flat fading channels [1]. In V-BLAST system, independent and equal-rate data streams are transmitted simultaneously from multiple antennas, and multi-layer detection with successive interference cancelation is performed at receivers. The extension of this technique to MIMO frequency selective fading channels brings in the issue of equalization combating the inter-symbol interference (ISI) and co-channel interference (CCI). A wide range of layered space-time equalization (LSTE) structures have been proposed to improve the performance, such as MIMO layered decision feedback equalizer (MIMO-LDFE) [2], [3] and MIMO delayed decision feedback sequence estimator (MIMO-DDFSE) [4]. However, the complexity of time-domain equalization is increased linearly with the memory length of the channel. To reduce the complexity in long delay spread channels, frequency-domain equalization (FDE) was applied to the layered architectures in [5], namely, layered space-frequency equalization (LSFE). It provides great tradeoffs between the performance and complexity.

However, all the work on the layered detection presented thus far do not take into account the effect of carrier frequency offset (CFO) which is typically caused by the local oscillator mismatch between transmitter and receiver. CFO is a popular problem studied in orthogonal frequency division multiplexing (OFDM) because it destroys the orthogonality of sub-carriers and introduces inter-carrier interference (ICI). For single carrier (SC) with FDE system, it is also definitely worth paying attention on this problem if the discrete Fourier transform (DFT) block size is large and/or the constellation size of modulation is high. In a MIMO system, the nonalignment of carrier frequency between multiple transmitters and receivers leads to multiple CFOs which can cause severe phase error on the received signals [7]. Hence, it is critical to estimate and correct the phase errors for phase coherent communications.

In this paper, we investigate a layered FDE architecture in presence of multiple CFOs. At each layer, the MIMO FDE designed by minimum mean square error (MMSE) criterion is performed, and a group of best data streams are selected to output. The phases of equalized symbols are rotated and the amplitudes are scaled due to the combining effect of CFOs, timing errors and estimated channels. A novel group-wise amplitude and phase correction (APC) algorithm is proposed to rectify the phase and amplitude distortion, and the corrected data are detected to recover the transmitted data. In order to cancel the contribution of the detected data streams, the estimated phases and scalars of amplitude should be compensated to the detected symbols before applying the estimated channels to reconstruct the received signals. Then the synthesized signals are considered as the interferences which are subtracted from the received signal delivered by the previous layer. The interference-canceled data will be the input of next layer. Our work differs from the previous work in that the CFOs need not to be estimated directly at receiver which saves much computation complexity, and the proposed algorithm is suitable to quadrature amplitude modulation (QAM) as well as phase-shift keying (PSK) modulation. Furthermore, the power levels of data stream from each transmitter are assumed to be unequal due to the power allocation or pre-coding schemes employed at transmitters, which is commom in practical communication systems. Moreover, the physical channel itself have difference on the power for different transmitter at some condition. It implies that the equivalent channel impulse response for each transmitter are unbalanced due to power allocation and physical channel unbalance. Simulation results show that the layered FDE with the phase compensation algorithm can achieve good performance for a MIMO system interfered with CFOs over unbalanced fading channels. It is also demonstrated that the performance will be enhanced when multiple layers are used in the detection.

Throughout the paper, we use $[\cdot]^T$, $[\cdot]^H$, $(\cdot)^{-1}$, and $\mathrm{Tr}(\cdot)$ to denote the matrix transpose, Hermitian transpose, inverse, and trace, respectively.

II. SYSTEM MODEL AND PRELIMINARIES

Consider an MIMO system with N_t transmit and N_r receive antennas. Let $\mathbf{x}_q = [x_q(1), \cdots, x_q(N)]$ denote the data block transmitted by the q-th transmitter. A copy of the last N_{cp} symbols which is termed as cyclic prefix (CP) is appended at the front of each block to avoid inter-block interference (IBI) and make the channels circulant. It is commonly required that $N_{cp} \geq M - 1$, where M is the maximum channel length. All the transmitters radiate data streams simultaneously and independently. The baseband equivalent signal collected by p-th receive antenna at time k is given by

$$y_p(k)=\sum_{q=1}^{N_t}\sum_{\nu=1}^{M}h_{p,q}(\nu,k)x_q(k+1-\nu)e^{j(2\pi f_{p,q}kT_s+\theta_{p,q})}+v_p(k) \tag{68}$$

where $h_{p,q}(\nu,k)$ is the impulse response of the frequency selective channel at time k between p-th receiver and q-th transmitter combining the effects of the transmit pulse-shape filter, physical channel and receiving filter, $f_{p,q}$ and $\theta_{p,q}$ are respectively the CFO and timing error phase, $v_p(k)$ is the additive white Gaussian noise with average power σ^2, and T_s is the symbol period. The fading channels are generally time-varying, but can be supposed to be invariant for one block if the block duration $(N+N_{cp})T_s$ is less than the channel coherence time. Therefore, the impulse response of the (p,q)-th subchannel can be denoted by the vector $\mathbf{h}_{p,q} = [h_{p,q}(1), \cdots, h_{p,q}(M)]^T$. The CPs are discarded at receivers to yield the signal vectors expressed by

$$\begin{bmatrix} \mathbf{y}_1 \\ \vdots \\ \mathbf{y}_{N_r} \end{bmatrix} = \begin{bmatrix} \mathbf{D}_{1,1}\mathbf{A}_{1,1} & \cdots & \mathbf{D}_{1,N_t}\mathbf{A}_{1,N_t} \\ \vdots & \ddots & \vdots \\ \mathbf{D}_{N_r,1}\mathbf{A}_{N_r,1} & \cdots & \mathbf{D}_{N_r,N_t}\mathbf{A}_{N_r,N_t} \end{bmatrix} \begin{bmatrix} \mathbf{x}_1 \\ \vdots \\ \mathbf{x}_{N_t} \end{bmatrix} + \begin{bmatrix} \mathbf{v}_1 \\ \vdots \\ \mathbf{v}_{N_r} \end{bmatrix} \tag{69}$$

where $\mathbf{A}_{p,q}$ is the (p,q)-th circulant matrix where the first column is defined as $\mathbf{h}_{p,q}$ padded with $N-M$ zeros, $\mathbf{y}_p$ and $\mathbf{v}_p$ are the overlap-added data block and noise block at the p-th receiver, and

$$\mathbf{D}_{p,q} = \mathrm{diag}\left\{ e^{j(2\pi f_{p,q}T_s+\theta_{p,q})}, \cdots, e^{j(2\pi f_{p,q}NT_s+\theta_{p,q})} \right\}. \tag{70}$$

Convert the discrete-time model into frequency-domain representation by multiplying block DFT matrix $\mathbf{F}_{N_r} = \mathbf{\Gamma}_N \otimes \mathbf{I}_{N_r}$ on both sides of (69), where $\mathbf{\Gamma}_N$ is normalized DFT matrix of size $N \times N$ and $\otimes$ represents Kronecker product.

$$\begin{bmatrix} \mathbf{Y}_1 \\ \vdots \\ \mathbf{Y}_{N_r} \end{bmatrix} = \begin{bmatrix} \mathbf{\Phi}_{1,1}\mathbf{H}_{1,1} & \cdots & \mathbf{\Phi}_{1,N_t}\mathbf{H}_{1,N_t} \\ \vdots & \ddots & \vdots \\ \mathbf{\Phi}_{N_r,1}\mathbf{H}_{N_r,1} & \cdots & \mathbf{\Phi}_{N_r,N_t}\mathbf{H}_{N_r,N_t} \end{bmatrix} \begin{bmatrix} \mathbf{X}_1 \\ \vdots \\ \mathbf{X}_{N_t} \end{bmatrix} + \begin{bmatrix} \mathbf{V}_1 \\ \vdots \\ \mathbf{V}_{N_r} \end{bmatrix} \tag{71}$$

where $\mathbf{Y}_p \triangleq \mathbf{\Gamma}_N \mathbf{y}_p$, $\mathbf{X}_q \triangleq \mathbf{\Gamma}_N \mathbf{x}_q$, $\mathbf{V}_p \triangleq \mathbf{\Gamma}_N \mathbf{v}_p$, $\mathbf{H}_{p,q} = \mathbf{\Gamma}_N \mathbf{A}_{p,q} \mathbf{\Gamma}_N^H$, and $\mathbf{\Phi}_{p,q} = \mathbf{\Gamma}_N \mathbf{D}_{p,q} \mathbf{\Gamma}_N^H$. $\mathbf{H}_{p,q}$ is a diagonal matrix whose diagonal elements are the N-point DFT of $\mathbf{h}_{p,q}$ due to the circulant property of $\mathbf{A}_{p,q}$. $\mathbf{\Phi}_{p,q}$ is generally a non-diagonal matrix, but its diagonal elements, $\{\mathbf{\Phi}_{p,q}(i,i)\}_{i=1}^N$, are identical and equal to

$$\lambda_{p,q} = \mathbf{\Phi}_{p,q}(i,i) = \frac{1}{N}\sum_{k=1}^{N} e^{j(2\pi f_{p,q}kT_s + \theta_{p,q})},\ i = 1, 2, \cdots, N. \tag{72}$$

If the block duration is smaller than one third of $1/\max(f_{p,q})$, $\mathbf{\Phi}_{p,q}$ will become a diagonal-dominant matrix, which implies that the non-diagonal elements are negligible compared to the diagonal elements. This property enables us to derive the approximate solutions for SC-FDE with CFOs in next section.

As a result, Equation (71) can be simplified and decomposed into each frequency tone represented as

$$\begin{bmatrix} \mathbf{Y}_1(m) \\ \vdots \\ \mathbf{Y}_{N_r}(m) \end{bmatrix} = \begin{bmatrix} \lambda_{1,1}\mathbf{H}_{1,1}(m) & \cdots & \lambda_{1,N_t}\mathbf{H}_{1,N_t}(m) \\ \vdots & \ddots & \vdots \\ \lambda_{N_r,1}\mathbf{H}_{N_r,1}(m) & \cdots & \lambda_{N_r,N_t}\mathbf{H}_{N_r,N_t}(m) \end{bmatrix} \begin{bmatrix} \mathbf{X}_1(m) \\ \vdots \\ \mathbf{X}_{N_t}(m) \end{bmatrix} + \begin{bmatrix} \mathbf{V}_1(m) \\ \vdots \\ \mathbf{V}_{N_r}(m) \end{bmatrix} \tag{73}$$
$$m = 1, \cdots, N.$$

where $\mathbf{H}_{p,q}(m)$ denotes the m-th tone of the (p,q)-th subchannel frequency response.

III. LFDE WITH PHASE CORRECTION

The proposed MIMO layered detection structure is illustrated in Fig. 1, where only the first two layers are shown in detail for brevity. The other layers will follow the same procedures. We assume the MIMO detection scheme consists of L layers in total. At the l-th layer, there are J_l undetected data streams remained and I_l data streams coming out after equalizing and phase correction. Hence, we have $\sum_{l=1}^{L} \mathrm{I}_l = N_t$, $\mathrm{J}_l = N_t - \sum_{j=1}^{l-1} \mathrm{I}_j$, and $\mathrm{I}_l \leq \mathrm{J}_l$. For the purpose of properly constructing the interference signals, the estimation of phase rotation and amplitude scalar caused by the combined CFOs are required to compensate the phase and amplitude of the detected data streams intentionally. The phase-amplitude-compensated signals pass through the estimated channels to generate the interference signals which are canceled out completely from the receiving signals. Then the substracted signals will be treated as the input for the next layer detection.

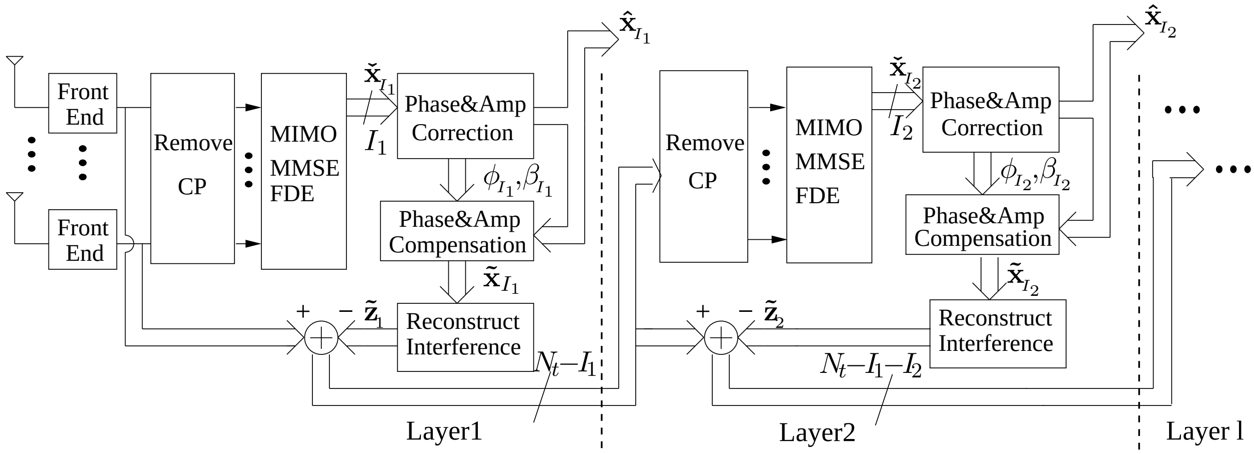

Figure 1 Layered FDE architecture with phase and amplitude correction and compensation

Practically, the power strength of transmitted signals for every antenna may be different from each other due to the power allocation or precoding employed at transmitter. It results in the equivalent MIMO channels appear unbalanced, which leads to different performance for different transmit antennas. In the layered detection structure, the strongest data stream(s) is extracted and canceled first and then the detection of remaining weak ones are proceeding in a sequential way. It has been demonstrated in [4] and [5] that this detection strategy can improve the performance significantly for MIMO communication systems. In this section, we will take into account the effects of multiple unknown CFOs in the layered detection for the MIMO long term evolution (LTE) system.

A. Layered Equalization with CFOs. We assume that the receiver architecture can be separated into L layers, and at the l-th layer, $l = 1, \cdots, L$, the remained received data which contain the information of J_l undetected data streams after succussive interference cancelation of the previous $l-1$ layers are provided to the equalizer and I_l equalized data streams are the output. In the description of layered equalization algorithm, without loss of generality, we use the $l_u^{(1)}, \cdots, l_u^{(\mathrm{J}_l)}$ to represent all the undetected transmit antennas, which is only a subset of all transmit antennas, and $l_d^{(1)}, \cdots, l_d^{(\mathrm{I}_l)}$ are used to denote the output data streams at the l-th layer. We also drop the notion of frequency bin m in equation (73) for convenience of description. The MMSE FDE for the l-th layer can be represented as follows:

$$\begin{bmatrix} \check{X}_{l_d^{(1)}} \\ \vdots \\ \check{X}_{l_d^{(\mathrm{I}_l)}} \end{bmatrix} = (\hat{\mathcal{H}}_l^{(\mathrm{I}_l)})^H \left(\hat{\mathcal{H}}_l \hat{\mathcal{H}}_l^H + \sigma^2 \mathbf{I}_{N_r}\right)^{-1} \begin{bmatrix} \check{Y}_{l,1} \\ \vdots \\ \check{Y}_{l,N_r} \end{bmatrix} \tag{74}$$

where

$$\hat{\mathcal{H}}_l = \begin{bmatrix} \lambda_{1,l_u^{(1)}} \hat{H}_{1,l_u^{(1)}} & \cdots & \lambda_{1,l_u^{(\mathrm{J}_l)}} \hat{H}_{1,l_u^{(\mathrm{J}_l)}} \\ \vdots & \ddots & \vdots \\ \lambda_{N_r,l_u^{(1)}} \hat{H}_{N_r,l_u^{(1)}} & \cdots & \lambda_{N_r,l_u^{(\mathrm{J}_l)}} \hat{H}_{N_r,l_u^{(\mathrm{J}_l)}} \end{bmatrix}, \tag{75}$$

$$\hat{\mathcal{H}}_l^{(\mathrm{I}_l)} = \begin{bmatrix} \lambda_{1,l_d^{(1)}} \hat{H}_{1,l_d^{(1)}} & \cdots & \lambda_{1,l_d^{(\mathrm{I}_l)}} \hat{H}_{1,l_d^{(\mathrm{I}_l)}} \\ \vdots & \ddots & \vdots \\ \lambda_{N_r,l_d^{(1)}} \hat{H}_{N_r,l_d^{(1)}} & \cdots & \lambda_{N_r,l_d^{(\mathrm{I}_k)}} \hat{H}_{N_r,l_d^{(\mathrm{I}_l)}} \end{bmatrix}, \tag{76}$$

and $\left[\check{Y}_{l,1} \cdots \check{Y}_{l,N_r}\right]^T$ represents the interference-canceled receive data which is the input at the l-th layer. Applying inverse DFT to $\check{X}_{l_d^{(1)}} \cdots \check{X}_{l_d^{(\mathrm{I}_l)}}$, we can obtain the time-domain equalized symbols corresponding to the I_l date streams. It has been proved in [7] that the equalized symbols are amplitude-scaled and phase-rotated version of the transmitted symbols. The rotated phases are determined by the CFOs $f_{p,q}$, timing-error phases $\theta_{p,q}$, and the channel transfer functions. As mentioned in [7], the rotating phase changes gradually in one block and can be regarded as a constant for a small number of N_s symbols. Hence, one data block can be decomposed into $N_g = N/N_s$ groups which are assumed to have constant phase deviations. The detail on the phase estimation will be discussed in subsection B. Here we assume the phase for each group in one block of q-th data stream has been estimated and denoted by $\phi_q^{(g)}, g = 1, \cdots, N_g, q = 1, \cdots, l_d^{(\mathrm{I}_l)}$. The estimated phases are applied on the equalized symbols to obtain the phase-corrected and detected data block $\hat{\mathbf{x}}_q$. This block is also separated into N_g groups and the g-th group $\hat{\mathbf{x}}_q^{(g)}$ is corresponding to the phase $\phi_q^{(g)}$. In order to cancel out the detected data completely, the distortion of phase and amplitude are ought to be first compensated to the detected data:

$$\tilde{\mathbf{x}}_q^{(g)} = \hat{\mathbf{x}}_q^{(g)} \cdot e^{j \cdot \phi_q^{(g)}} \cdot \beta_q^{(g)} \tag{77}$$

where $\beta_q^{(g)}$ is the amplitude scalar for the g-th group of the q-th data stream. Then the compensated data go through the estimated channels to construct the interference signals as

$$\tilde{\mathbf{z}}_{l,p} = \sum_{q=1}^{\mathrm{I}_l} \tilde{\mathbf{x}}_q \odot \hat{\mathbf{h}}_{p,q} \qquad p = 1, \cdots, N_r \tag{78}$$

where $\odot$ denotes the operation of convolution, $\tilde{\mathbf{z}}_{l,p}$ is the reconstructed interference signals at the l-th layer based on the phase-compensated data streams. The input for the next layer is expressed as

$$\check{\mathbf{y}}_{l+1} = \check{\mathbf{y}}_l - \tilde{\mathbf{z}}_l. \tag{79}$$

where $\tilde{\mathbf{z}}_l = [\tilde{\mathbf{z}}_{l,1}^T, \cdots, \tilde{\mathbf{z}}_{l,N_r}^T]^T$ and $\check{\mathbf{y}}_l = [\check{\mathbf{y}}_{l,1}^T, \cdots, \check{\mathbf{y}}_{l,N_r}^T]^T$

B. Amplitude and Phase Correction (APC). In this paper, a phase and amplitude correction algorithm is proposed to address the amplitude and phase distortion problem caused by multiple CFOs. The phase correction methods proposed in [6] and [7] for PSK modulations in SIMO and MIMO systems can be regarded as special application cases of the method introduced here which can also be applied to QAM modulations. Due to the nearly constant CFOs, the rotating phases of symbols in one block are slowly varying over time and can be treated as a constant for a small group of symbols. The phases of the adjacent groups have high correlation which allows the phases to be estimated progressively. Here, we assign N_w pilot symbols to estimate the initial rotating phase and amplitude distortion in each block. The equalized N-symbol block is partitioned into N_g groups and each group has $N_s = N/N_g$ symbols. Here we suppose N/N_g is an integer. Before introducing the algorithm, we denote $\mathcal{O}_{M_m}(\cdot)$ to be the hard decision function for an M_m-ary modulation scheme, $\angle(\cdot)$ and $|\cdot|$ represent the operations of calculating the angle and amplitude, respectively.

The group-wise phase estimation and amplitude scaler estimation algorithm is described in Table 1.

Table 1 The group-wise APC algorithm

(1)	Estimate the initial rotating phase and amplitude scalar $\phi_q^{(0)} = \frac{1}{N_w}\sum_{k=1}^{N_w} \angle\check{x}_q(k) - \angle x_q(k)$ $\beta_q^{(0)} = \frac{\sum_{k=1}^{k=N_w} \lvert\check{x}_q(k)\rvert}{\sum_{k=1}^{k=N_w} \lvert x_q(k)\rvert}$
(2)	Correct the phase and amplitude of the first group $\hat{x}_q^{(1)}(k) = \frac{1}{\beta_q^{(0)}} \cdot \check{x}_q(k)e^{-j\phi_q^{(0)}}, \quad k = 1, 2, \cdots, N_s$
(3)	Calculate the average phase deviation, the rotating phase and the amplitude scalar for the first group and then set $g = 2$ $\Delta\phi_q^{(1)} = \frac{1}{N_s}\sum_{k=1}^{N_s}\left(\angle\hat{x}_q^{(1)}(k) - \angle\mathcal{O}_{M_m}(\hat{x}_q^{(1)}(k))\right)$ $\phi_q^{(1)} = \phi_q^{(0)} + \Delta\phi_q^{(1)}$ $\beta_q^{(1)} = \frac{\sum_{k=1}^{k=N_s} \lvert\hat{x}_q^{(1)}(k)\rvert}{\sum_{k=1}^{k=N_s} \lvert\mathcal{O}_{M_m}(\hat{x}_q^{(1)}(k))\rvert}$
(4)	Correct the phase and amplitude of the g-th group $\hat{x}_q^{(g)}(k) = \frac{1}{\beta_q^{(g-1)}} \cdot \check{x}_q((g-1)N_s + k)e^{-j\phi_q^{(g-1)}}, \; k = 1, 2, \cdots, N_s$
(5)	Take the average on the phase deviation and recalculate the amplitude scalar for the g-th group $\Delta\phi_q^{(g)} = \frac{1}{N_s}\sum_{k=1}^{N_s}\left(\angle\hat{x}_q^{(g)}(k) - \angle\mathcal{O}_{M_m}(\hat{x}_q^{(g)}(k))\right)$ $\phi_q^{(g)} = \phi_q^{(g-1)} + \Delta\phi_q^{(g)}$ $\beta_q^{(g)} = \frac{\sum_{k=1}^{k=N_s} \lvert\hat{x}_q^{(g)}(k)\rvert}{\sum_{k=1}^{k=N_s} \lvert\mathcal{O}_{M_m}(\hat{x}_q^{(g)}(k))\rvert}$
(6)	Update $g = g + 1$ and repeat (4) $\sim$ (6) until $g = N_g$
(7)	Output the estimation of phases $\mathbf{\Phi}_q$ and scalars β_q $\mathbf{\Phi}_q = \left[\phi_q^{(1)}, \cdots, \phi_q^{(N_g)}\right]^T, \; \beta_q = \left[\beta_q^{(1)}, \cdots, \beta_q^{(N_g)}\right]^T$

IV. NUMERICAL RESULTS

We consider an MIMO communication system with 4 transmit and 4 receiver antennas. Each data block has a length of 1024, and the symbol period is $T = 0.25\mu$s. QPSK, 8PSK, and 16QAM are employed to map binary bits to symbols. A frequency-selective fading channel, which has exponential decay power delay profile with overall channel length of 11 is employed, which is generated by the improved Clark's model [8]. In order to simulate the unbalanced channel conditions, the power allocated to the first two antennas are four times of the other two antennas. However the total average power is normalized by $\mathrm{E}\{\mathrm{Tr}(\mathrm{H}(m)\mathrm{H}^H(m))\} = N_r N_t$. Therefore, the SNR is defined as the ratio of the total transmit power to the noise power, which is expressed as $\mathrm{SNR} = \frac{P_T}{\sigma^2}$, where P_T is the transmit power.

In the simulations, the frequency-domain channel estimation method presented in [9] was employed to estimate the MIMO channels by inserting frequency orthogonal pilot blocks between data frames. The estimated channels were used to equalize data and reconstruct the interference signals. As a benchmark, the performance of the proposed receiver scheme assuming perfect channel information were also provided for comparison. The multiple unknown CFOs which are invariant for the epoch of transmission were configured to random variables with constant means. The multiple CFOs corresponding to the first and third transmit antennas are assumed to follow the uniform distribution with the mean of -200 Hz, and the CFOs for the second and fourth transmit antennas are also distributed uniformly but with the mean of 200 Hz. In the second generation (2G) and the third generation (3G) wireless communication standards, it is specified that the maximum CFO of wireless systems must not beyond $\pm$ 200 Hz. The rotated phases for the PSK symbols were estimated via the proposed method introduced in section III. We chose N_w=8 pilot symbols to estimate the initial phase prior to every block transmission, and the group size is set to 16. To illustrate the effect of CFOs and necessity of amplitude-phase correction in the symbol detection, the performance of detection without applying APC algorithm is also provided. Moreover, we compared the performance in term of bit error rates (BERs) for one layer, two layers, and four layers to demonstrate the effectiveness of the layered detection algorithm. The one layer detection is actually equivalent to the classical MIMO MMSE FDE which separates all the data streams simultaneously. For the two layers structures, the best two data streams will be detected, and the interference contribution can be removed from the received signals before the detection of the other two data streams. In four layers scheme, the best data stream will be detected at one time after the processing of one layer.

The constellations of equalized and amplitude-phase-corrected 16QAM symbols for the first antenna is depicted in Fig. 2 and Fig. 3, respectively. From the two figures, it is sufficiently illustrated that the rotating phase and amplitude distortions can be corrected with the group-wise amplitude and phase correction (APC) algorithm so that the symbols can be reliably detected.

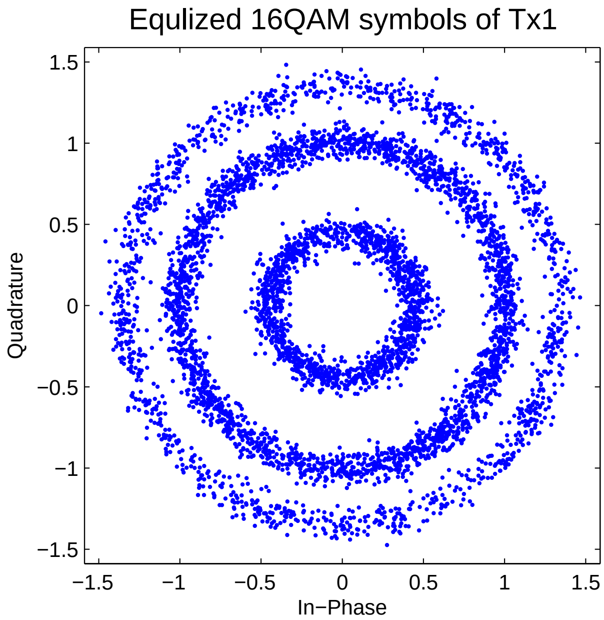

Figure 2 Scatter plot of equalized 16QAM symbols for the transmit antenna 1, SNR=24 dB

The BER performance for QPSK modulation, 8PSK modulation and 16QAM are shown in Fig. 4, Fig. 5, and Fig. 6, respectively. As shown in these figures, if APC algorithm is not applied, the equalized symbols are difficult to be completely detected at the receiver because of the effect of CFOs. Most equalized symbols are rotated and appear in wrong decision areas in the constellation plot. Also in the simulations, we employed 1 layer, 2 layers and 4 layers architectures to detect the data streams of four antennas. One layer detection is actually the traditional MIMO-FDE and all the data of the transmitters are detected instantaneously and concurrently. For multiple-layer detection, a strong subset of transmit data streams are squeezed out at each layer and canceled out to be prepared for the next layer. We compared the three architectures with phase estimation, correction and compensation by evaluating the uncoded BER in Fig. 4, Fig. 5 and Fig. 6. As expected, the 2-layer and 4-layer

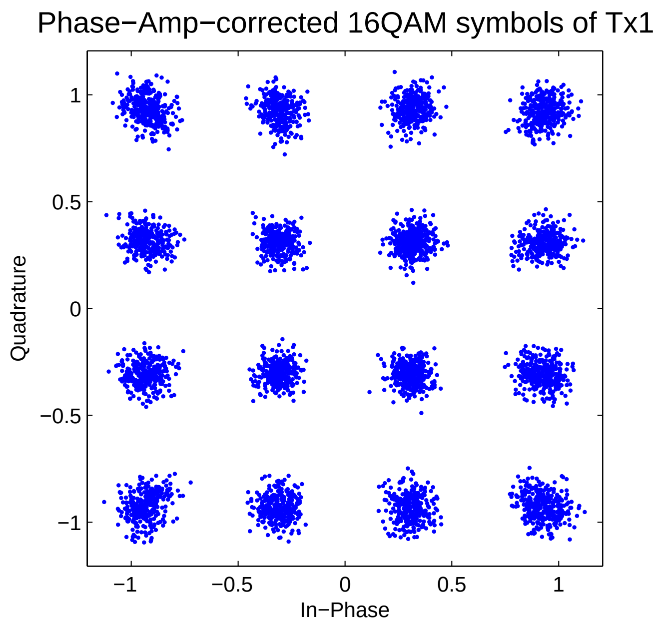

Figure 3 Scatter plot of phase-amplitude-corrected 16QAM symbols for the transmit antenna 1, SNR=24 dB

architectures outperform the 1-layer architecture significantly, and the 4-layer case has more performance gain than the 2-layer scheme. The estimated channels lead to degradation on the performance of about $2.5 \sim 3$ dB for all modulations as oppose to the case of perfect channel information with APC algorithm. To demonstrate the effectiveness of the proposed scheme, the performance for the ideal case of known CFOs and channels at receivers are also depicted in these three figures as the benchmark. The narrow gap between the ideal case and the proposed method indicates the LFDE with amplitude and phase correction can work well for SC MIMO system impaired by CFOs.

V. CONCLUSION

In this paper, we investigated a low-complexity LFDE architecture for SC-MIMO system in the case that multiple CFOs exist. Each layer has performed the MMSE equalization, phase-amplitude correction, and successive interference cancelation. A subset of data streams were extracted , and the phase-amplitude-compensated interference signals were canceled out thoroughly. Simulation results showed that the proposed method obtained good

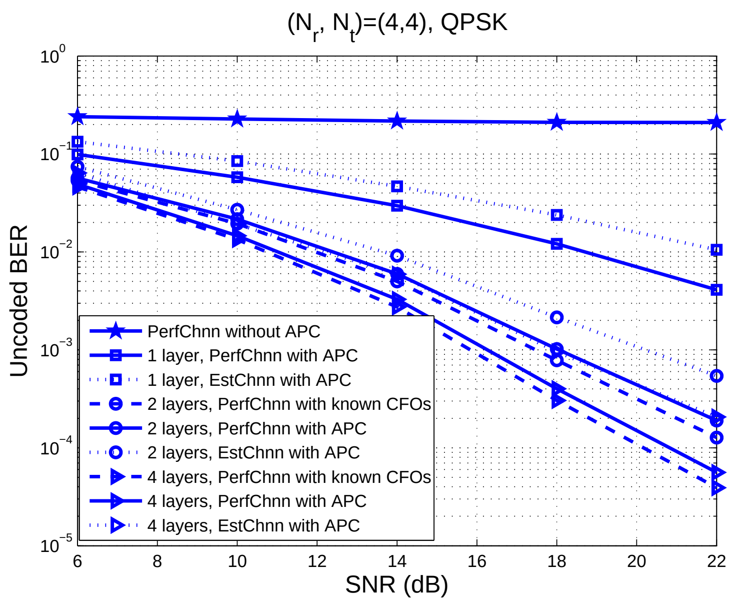

Figure 4 Uncoded bit error rate of equalized and phase-corrected QPSK by three detection schemes of 1 layer, 2 layers and 4 layers

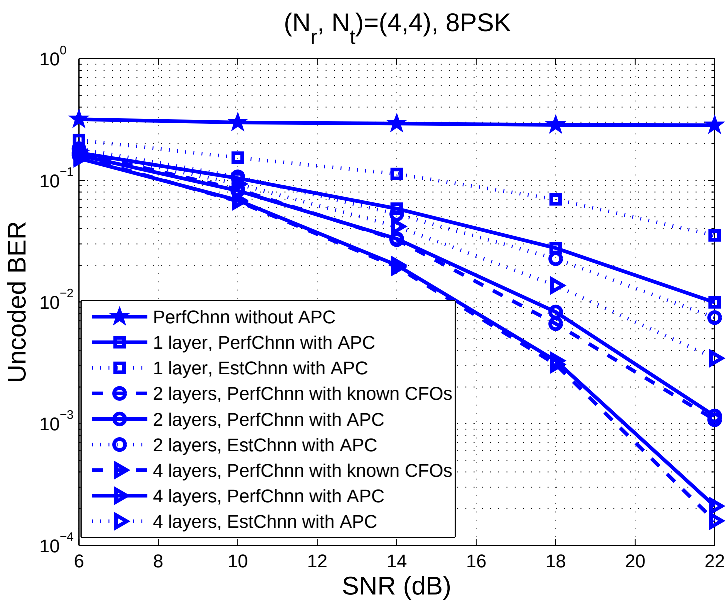

Figure 5 Uncoded bit error rate of equalized and phase-corrected 8PSK by three detection schemes of 1 layer, 2 layers and 4 layers

performance over MIMO frequency selective channels. It has also shown that the method can effectively cope with the multiple CFOs.

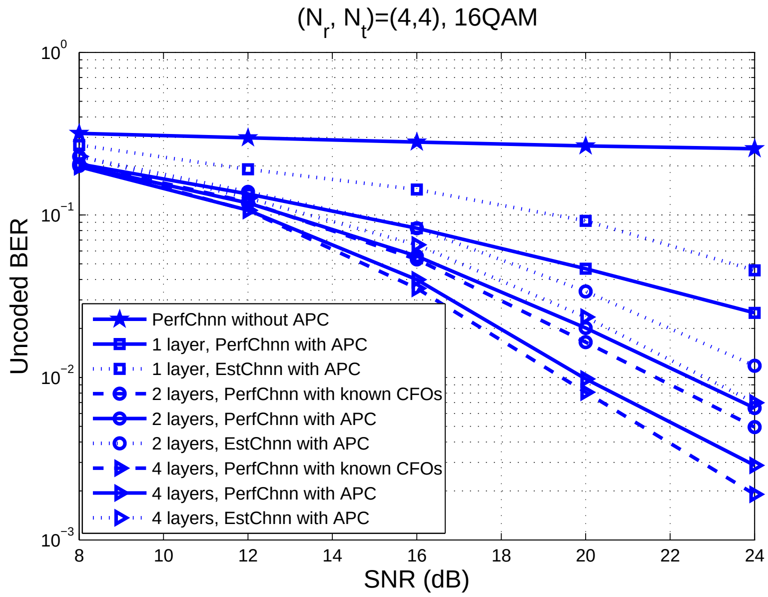

Figure 6 Uncoded bit error rate of equalized and phase-corrected 16QAM by three detection schemes of 1 layer, 2 layers and 4 layers

VI. REFERENCES

[1] G. J. Foschini, "Layered space-time architecture for wireless communication in a fading environment when using multi-element antennas," *Bell Labs Tech. J.*, vol.1, pp.41-59, Autunm 1996.

[2] A. Lozano and C. Papadias, "Layered space-time receivers for frequency-selective wireless channels," *IEEE Trans. Commun.*, vol.50, pp.65-73, Jan. 2002.

[3] X. Zhu and R. D. Murch, "MIMO-DFE based BLAST over frequency selective channels," in *Proc. IEEE GLOBECOM'01*, vol.1, San Antonio, Tx, Nov. 2001.

[4] X. Zhu and R. D. Murch, "Layered space-time equalization for wireless MIMO systems," *IEEE Trans. Wireless Commun.*, vol.2, pp.1189-1203, Nov. 2003.

[5] X. Zhu and R. D. Murch, "Layered space-frequency equalization in a single-carrier MIMO system for frequency-selective channels," *IEEE Trans. Wireless Commun.*, vol.3, pp.701-708, May 2004.

[6] Y. R. Zheng, C. Xiao, T. C. Yang, and W. B. Yang, "Frequency-domain channel estimation and equalization for single carrier underwater acoustic communications," in *Proc. IEEE/MTS OCEANS'07*, Vancouver, BC, Canada, Oct. 2007.

[7] C. Xiao and Y. R. Zheng, "Channel equalization and symbol detection for single carrier broadband MIMO systems with multiple carrier frequency offsets," in *Proc. IEEE ICC'08*, Beijing, China, May 19-23, 2008.

[8] C. Xiao, Y. R. Zheng, and N. C. Beaulieu, "Novel sum-of-sinusoids simulation models for Rayleigh and Rician fading channels," *IEEE Trans. Wireless Commun.*, vol.5, pp.3667-3679, Dec. 2006.

[9] Y. R. Zheng and C. Xiao, "Channel estimation for frequency-domain equalization of single carrier broadband wireless communications," *IEEE Trans. Veh. Technol.*, vol. 58, pp.815-823, Feb. 2009.

4. FREQUENCY-DOMAIN TURBO EQUALIZATION WITH SOFT-SUCCESSIVE INTERFERENCE CANCELLATION FOR SINGLE CARRIER MIMO UNDERWATER ACOUSTIC COMMUNICATIONS

Jian Zhang and Yahong Rosa Zheng

Abstract—A low-complexity frequency-domain turbo equalizer (FDTE) combined with phase rotation compensation and soft-successive interference cancellation (SSIC) is proposed for single carrier multiple-input multiple-output (MIMO) underwater acoustic (UWA) communications. Different from existing time-domain turbo equalizers in MIMO UWA systems, the proposed receiver implements low-complexity turbo equalization in the frequency domain to combat severe inter-symbol interference (ISI) and a layered structure to improve performance for unbalanced MIMO channel conditions. Soft SIC rather than hard SIC is employed in layered iterative turbo detection to alleviate co-channel interference (CCI). The proposed scheme is evaluated by both numerical simulations and the SPACE08 ocean experiment carried out in a shallow area of the Atlantic Ocean in October 2008. With a transmission bandwidth of 9.7656 kHz centered at 13 kHz and a transmission power of 185 dB re μPa @ 1 m, the 2-transducer and 12-hydrophone MIMO system communicated with QPSK and 8PSK modulation schemes over 200 m and 1000 m ranges. The data rate is approximately 20 kilo symbols/second. The bit error rates (BERs) achieved on the order of 10^{-5} (200 m) and 10^{-4} (1000 m) for QPSK with only two iterations. The 8PSK scheme has higher spectral efficiency and achieved average BERs on the order of 10^{-3} for the two ranges. Simulation results also demonstrated that the proposed FDTE-SSIC receiver provided lower BER with comparable complexity than the traditional FDTE receiver.

I. INTRODUCTION

Shallow underwater acoustic (UWA) channels present significant technical challenges for high data-rate robust UWA communication systems [3]- [6] due to the unique characteristics of underwater channels. In comparison to radio frequency (RF) wireless channels, UWA channels exhibit severe frequency-dependent attenuation, low acoustic wave propagation speed, excessive multipath delay spread, and severe Doppler spread and Doppler shift.

Frequency-dependent propagation loss leads to very limited transmission bandwidth for underwater channels, e.g., only a few tens of kHz for medium range communications (1-10 kilometers). The multipath delay spread is often on the order of tens to hundreds of millisecond for practical UWA channels due to reflection and scattering of shallow water ocean structures. This results in severe inter-symbol interference (ISI) for high data-rate transmission. Another obstacle imposed by UWA channels is the significant time-varying Doppler spread and drift caused by dynamic motion of waves and relative motion of transceivers. Since acoustic wave normally travels in underwater at the speed of 1500 m/s, relatively low motion also results in large Doppler spread. Therefore the Doppler-to-carrier ratio is usually on the order of 10^{-3} to 10^{-4} in underwater channels, in contrast to 10^{-7} to 10^{-9} in RF communications. Severe Doppler not only causes temporal dilation or compression of signal waveforms [4], but also leads to fast time-varying fading and phase rotation of coherent symbols [6]. If multiple transducers and multiple hydrophones are employed, strong spatial correlation of the MIMO channel also leads to large angular spread. All these features of UWA channels make it one of the most challenging physical links for high data-rate communications.

The current state-of-the-art UWA systems include noncoherent frequency-shift-keying (FSK) systems and single-carrier or multi-carrier coherent modulation systems [2]. The noncoherent FSK scheme can provide stable and reliable communications due to its low requirement on channel estimation and symbol synchronization, but its extremely low data-rate (< 100 bps) has been unendurable by the increasing demand of data transmission. Coherent UWA communications can provide better bandwidth and power efficiency and has been successfully demonstrated by [6] to achieve higher data rates. A special technique employing a time-domain decision feedback equalizer (DFE) with an embedded phase-locked loop (PLL) is used in [6] to mitigate severe ISI and obviate phase rotation. Following this success, [11] extends the DFE-PLL coherent structure to a MIMO system to achieve higher spectral efficiency and data rates. However, the time-domain equalizers encounter prohibitive complexity and instability if the channel length exceeds 50 taps. Recently, frequency-domain equalization (FDE) methods are extensively investigated for UWA communication systems, including multi-carrier and single carrier systems. For example, an orthogonal frequency-division multiplexing (OFDM) approach combined with two-stage Doppler compensation is discussed in [7], and a single carrier MIMO FDE with group-wise phase compensation is proposed in [16].

Iterative turbo detection methods have been intensively investigated in RF communication area in recent years. The MMSE-based time-domain turbo equalization is firstly proposed in [9] and then frequency-domain turbo equalization is discussed in [10]- [12]. All these work is for single-input single-output channels. The coded system is considered as a serially concatenated convolutional code (SCCC) where the encoder and the frequency-selective channel play the roles of constituent codes. At the receiver, the equalizer and decoders exchange soft information of the coded bits iteratively to improve the detection in severe ISI. Time-domain and frequency-domain turbo equalizers are also investigated in [13] and [14], respectively. More recently, the time-domain turbo equalization has been used in SISO and MIMO underwater communications [11,15] for performance improvement. Although the performance gain is demonstrated sucessfully, the computational complexity of the time-domain equalizer becomes prohibitive because UWA channels usually have memory length greater than 100 symbols, much more than the length of RF channels. In contrast, [16] applies a frequency-domain turbo equalization (FDTE) scheme for UWA MIMO channels to reduce the complexity, where further improvement of BER is achieved in the ocean experiment.

In this paper, we propose an improved FDTE structure combined with soft successive interference cancellation (SSIC) to achieve lower BER performance than the traditional FDTE in [16] with comparable complexity. Successive interference cancellation based on hard symbol decision has been applied to time-reversed UWA channels in [17] to improve the performance of MIMO UWA communication systems. The main contribution of this work lies in that the FDTE is embedded in a layered detection struction and soft symbols are used in the interference cancellation. Instead of simultaneously detecting data streams of all transducers by the traditional FDTE, the proposed structure divides the detection of all streams into multiple layers and each layer consists of an FDTE, a phase rotation compensator, and a soft interference canceler. In most situations, the underwater channels corresponding to different transducer are unbalanced, and the received signal streams have different power levels. The FDTE-SSIC scheme better copes with co-channel interference (CCI) in these unbalanced conditions than the traditional FDTE.

The proposed FDTE-SSIC algorithm is evaluated and verified by computer simulation first and then applied on the ocean experimental data. A simulated example with a 4×4 MIMO system and 8PSK modulation demonstrates the advantage of the FDTE-SSIC over the traditional FDTE. Extensive data were also recorded in the Surface Process and Acoustic Communications Experiment (SPACE) conducted at Martha's Vineyard cabled observatory (MVCO) of Woods Hole Oceanographic Institution (WHOI) in late Fall, 2008 [19]. The encoded data streams were transmitted over 200 m and 1000 m ranges at a carrier of 13 kHz and a bandwidth of 9.7656 kHz. Two pilot-based MIMO channel estimation methods were used in the experiment: time-domain least square (TD-LS) estimation and frequency-domain interpolation (FD-Interp) estimation. By applying the proposed algorithm with TD-LS channel estimation, the average bit error rates (BERs) for the 200 m system with 2×12 MIMO can achieve 5.6×10^{-5} for QPSK and 4.6×10^{-3} for 8PSK. For the 1000 m range system, the average BERs for QPSK and 8PSK are 1.7×10^{-4} and 5.5×10^{-3}, respectively. The FD-Interp method has less computational complexity but slightly higher BER than the TD-LS method. These experimental results demonstrate the effectiveness and robustness of the proposed single carrier UWA communication system.

In the rest of this paper, Section II describes the system model of the UWA and its frequency domain representation which differs from RF systems. Sections III details the proposed receiver structure with FDTE-SSIC and two channel estimation methods. Simulation results of a 4×4 MIMO example is given in Section IV to demonstrate the advantages of layered soft FDTE, and extensive results with data from real-world undersea experiments are presented in Section V to demonstrate the effectiveness of the proposed algorithm. Finally, our concluding remarks are drawn in Section VI. We use boldface letters to denote vectors and matrices, and the superscripts $[\cdot]^T$, $[\cdot]^H$, $[\cdot]^{-1}$, and $[\cdot]^\dagger$ to denote the matrix transpose, Hermitian transpose, inverse, and pseudo-inverse, respectively.

II. SYSTEM MODEL AND PRELIMINARIES

Consider a MIMO underwater acoustic communication system with P transducers at the transmitter and Q hydrophones at the receiver. The independent bit streams, $\mathbf{b}_p$, $p = 1, \cdots, P$, are encoded by separate channel encoders and permuted randomly by interleavers to yield the coded bit streams, $\mathbf{c}_p$. The interleaved coded bits are then mapped into 2^M-ary symbols based on a symbol alphabet set $\mathcal{S} = \{\alpha_1, \cdots, \alpha_{2^M}\}$, where α_m corresponds to the bit pattern denoted by $\mathbf{d}_m = [d_{m,0}, \cdots, d_{m,M}]$ and has unit average power. Let $x_p(k)$ denote the k-th symbol of the p-th transducer, then $x_p(k) = \alpha_m$ if the bit vector $[c_{p,Mk-M+1}, \cdots, c_{p,Mk}] = \mathbf{d}_m$. The modulated symbols are grouped into blocks with length N_d, and each block is appended with N_{zp} zeros to avoid inter-block interference (IBI) for SC-FDE systems. Hence, each zero-padded block has length $N = N_d + N_{zp}$ and all transducers transmit the data blocks simultaneously at the same carrier frequency over the UWA channels. At the receiver, the blockwise frequency-domain equalization is applied on the blocks by N-point FFT/IFFT. The first N_d elements of each block is extracted from the equalized N symbols as the estimate of $x_p(k)$ and the last N_{zp} symbols are discarded [18].

The baseband equivalent signal at the q-th hydrophone can be expressed in the discrete time domain as

$$y_q(k) = \sum_{p=1}^{P} \sum_{l=1}^{L} h_{q,p}(l,k) x_p(k+1-l) e^{j(2\pi k T f_{q,p,k} + \theta_{q,p})} + w_q(k), \tag{80}$$

where T is the symbol interval, L is the memory length of the channels, $h_{q,p}(l,k)$ represents the channel impulse response on the l-th tap at time k, $f_{q,p,k}$ is the instantaneous Doppler shift between the p-th transducer and the q-th hydrophone, $\theta_{q,p}$ is the initial phase error for the (p,q)-th subchannel after synchronization, and $w_q(k)$ is the white Gaussian noise at the q-th hydrophone with the probability density function (PDF) $\mathcal{N}(0, \sigma_w^2)$, where σ_w^2 is the variance.

Denote the received block at the q-th hydrophone after the front-end processing as $\mathbf{y}_q = [y_q(1), \cdots, y_q(N)]^T$. The concatenated receive vector for all hydrophones is represented as $\mathbf{y} = [\mathbf{y}_1^T, \cdots, \mathbf{y}_Q^T]^T$. A data block transmitted by the p-th transducer is represented as $\mathbf{x}_p = [x_p(1), \cdots, x_p(N)]^T$, where $x_p(k) = 0$ for $k \in \{N_d+1, \cdots, N\}$. The concatenated transmit vector of all transducers is $\mathbf{x} = [\mathbf{x}_1^T, \cdots, \mathbf{x}_P^T]^T$. The MIMO system can be modeled in matrix as

$$\mathbf{y} = \begin{bmatrix} \mathbf{y}_1 \\ \vdots \\ \mathbf{y}_Q \end{bmatrix} = \begin{bmatrix} \mathbf{D}_{1,1}\mathbf{h}_{1,1} & \cdots & \mathbf{D}_{1,P}\mathbf{h}_{1,P} \\ \vdots & \ddots & \vdots \\ \mathbf{D}_{Q,1}\mathbf{h}_{Q,1} & \cdots & \mathbf{D}_{Q,P}\mathbf{h}_{Q,P} \end{bmatrix} \begin{bmatrix} \mathbf{x}_1 \\ \vdots \\ \mathbf{x}_P \end{bmatrix} + \begin{bmatrix} \mathbf{w}_1 \\ \vdots \\ \mathbf{w}_Q \end{bmatrix}$$
$$= \mathbf{\Lambda}\cdot\mathbf{x} + \mathbf{w}, \tag{81}$$

where $\mathbf{D}_{q,p} = \mathrm{diag}\{e^{j(2\pi T f_{q,p,1}+\theta_{q,p})}, \cdots, e^{j(2\pi NT f_{q,p,N}+\theta_{q,p})}\}$, $\mathbf{w}_q = [w_q(1), \cdots, w_q(N)]^T$, for $q \in \{1, \cdots, Q\}$, and $\mathbf{w} = [\mathbf{w}_1^T, \cdots, \mathbf{w}_Q^T]^T$. The matrix $\mathbf{h}_{q,p}$ is the (p, q)-th channel impulse response (CIR) without the diagonal phase components, and it takes the format of (82).

$$\mathbf{h}_{q,p} = \begin{bmatrix} h_{q,p}(1,1) & 0 & \cdots & 0 & h_{q,p}(L, N_d+1) & \cdots & h_{q,p}(2, N_d+1) \\ h_{q,p}(2,2) & h_{q,p}(1,2) & 0 & \ddots & \ddots & \ddots & \vdots \\ \vdots & \ddots & \ddots & \ddots & \ddots & \ddots & h_{q,p}(L, N_d+L-1) \\ h_{q,p}(L,L) & \ddots & \ddots & h_{q,p}(1,L) & 0 & \ddots & 0 \\ 0 & h_{q,p}(L, L+1) & \ddots & \ddots & \ddots & \ddots & \vdots \\ \vdots & \ddots & \ddots & \ddots & \ddots & \ddots & 0 \\ 0 & \cdots & 0 & h_{q,p}(L,N) & \cdots & \cdots & h_{q,p}(1,N) \end{bmatrix} \tag{82}$$

Two assumptions are made for the UWA channel: A1) The block duration is less than the channel coherence time which implies that the channels are quasi-static, and the responses of the channels are time-invariant within one block. A2) The block duration is smaller than one third of the quantity $1/\max(f_{q,p,k})$, which is usually satisfied in fixed-to-fixed UWA channels.

To convert the block-wise time-domain model into frequency-domain representation, we define the normalized DFT matrix of size $N \times N$ as $\mathbf{F}$, whose (m, n)-th element is given by $\frac{1}{\sqrt{N}}\exp\left(\frac{-j2\pi(m-1)(n-1)}{N}\right)$. Thus, $\mathbf{F}\mathbf{F}^H = \mathbf{I}_N$ and $\mathbf{F}^H$ is the IDFT matrix. Denote the block DFT matrix as $\mathbf{F}_Q = \mathbf{I}_Q \otimes \mathbf{F}$, where $\otimes$ represents the Kronecker product of matrices.

Multiplying $\mathbf{F}_Q$ on both sides of (81) yields

$$\mathbf{Y} = \mathbf{F}_Q \mathbf{y} = \mathbf{F}_Q \mathbf{\Lambda} \mathbf{F}_P^H \mathbf{F}_P \mathbf{x} + \mathbf{F}_Q \mathbf{w} = \mathbf{H} \cdot \mathbf{X} + \mathbf{W}, \tag{83}$$

where $\mathbf{H}$ is defined as

$$\mathbf{H} \approx \begin{bmatrix} \lambda_{1,1}\mathbf{H}_{1,1} & \cdots & \lambda_{1,P}\mathbf{H}_{1,P} \\ \vdots & \ddots & \vdots \\ \lambda_{Q,1}\mathbf{H}_{Q,1} & \cdots & \lambda_{Q,P}\mathbf{H}_{Q,P} \end{bmatrix}, \tag{84}$$

where $\lambda_{q,p}$ is the diagonal elements of $\mathbf{F}\mathbf{D}_{q,p}\mathbf{F}^H$, and the matrices $\mathbf{H}_{q,p}$ are diagonal, whose diagonal elements are the frequency response of the (q,p)-th channel because $\mathbf{h}_{q,p}$ is a circulant matrix due to assumption A1). The second assumption, A2), guarantees that $\mathbf{F}\mathbf{D}_{q,p}\mathbf{F}^H$ is a diagonal dominant matrix and can be approximated as a diagonal matrix [21] with identical diagonal elements equal to $\lambda_{q,p} = \frac{1}{N}\sum_{k=1}^{N} e^{j(2\pi k T f_{q,p,k} + \theta_{q,p})}$. Note that this system model differs from conventional RF systems in that it singles out the fast rotating phase components in the channel because the equalizer often cannot deal with significant phase rotation caused by severe Doppler shift and extra care has to be taken to correct the phase after equalization.

III. JOINT FREQUENCY-DOMAIN TURBO EQUALIZATION WITH SOFT-SUCCESSIVE INTERFERENCE CANCELLATION

In this section, we propose a robust receiver structure for single carrier MIMO underwater systems, combing low-complexity FDTE with layered SSIC and group-wise phase correction. In the proposed structure, inter-symbol interferences (ISI) are effectively mitigated by FDTE with multiple iterations of detection, and CCI are alleviated by SSIC with multiple layers of detection.

The overall structure of the proposed receiver is depicted in Fig. 1, where $\mathcal{M}$ layers of detection are used but only the first two layers are sketched for illustration. Before the first layer of detection, a front-end module is employed to pre-process the data packets received by all hydrophones to synchronize, demodulate from passband to baseband, and compensate for dilation/compression. The average signal-to-noise ratios (SNR) of all data streams are also evaluated from the estimated channels to determine the number of layers and the order of detection. The channel impulse responses corresponding to all transducer-hydrophone pairs are estimated by pilot symbols. Assume that Δ_1 data streams with the strongest power among the undetected streams are selected for the first layer, and the r-th layer has Δ_r data streams. Therefore $\sum_{r=1}^{\mathcal{M}} \Delta_r = P$. Each layer consists of similar functional components, including an FDTE, a soft decision decoder, a phase correction module, and an SSIC module. The received signals at each layer are converted to the frequency domain and then equalized to estimate the transmitted symbols. The phase rotations of the equalized symbols are corrected, and the phase-corrected symbols are passed to the soft decision decoding module to yield the extrinsic information on the coded bits. The extrinsic information is fed back to the equalizers of both current layer and previous layers as the *a-priori* information for the next iteration. The *a-posteriori* information of the coded bits provided by soft decoding is delivered to the SSIC module to construct the interference signals with the phase distortion. The constructed interference signals are canceled from the received signals, and the interference-canceled signals are then transferred to the succeeding layer (Δ_{r+1}) for detection of other streams.

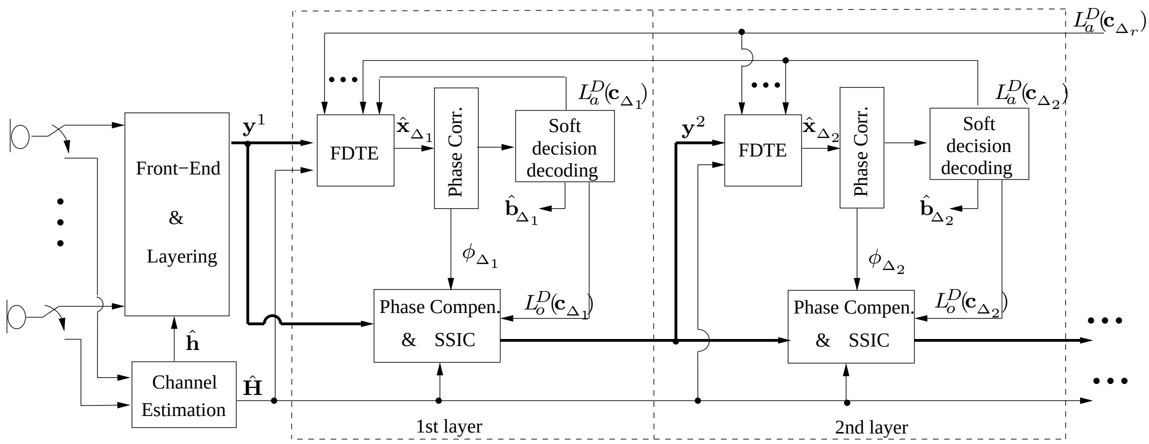

Figure 1 The receiver structure with FDTE-SSIC

The detailed algorithms of each functional module of each layer are described in the following subsections.

A. Pilot-Based Channel Estimation. Two pilot-based channel estimation methods are adopted for UWA receivers: time-domain least square (TD-LS) channel estimation and frequency-domain interpolation (FD-Interp) channel estimation. The data structures for these two channel estimation methods are shown in Fig. 2. In the TD-LS scheme, the pilot block with N_p symbols is enclosed in the data block and the payload of a length N block is $N - N_p$. A gap spanning N_g symbols is inserted between each block. In contrast, the FD-Interp scheme uses a length N_p pilot block before the payload block of length N with an extra gap inserted between the pilot and payload blocks. Both schemes have similar bandwidth efficiency, but the latter has less computation complexity than the former. However, the drawback of the FD-Interp scheme is its less capability to track fast time-varying channels due to the long gap needed between the pilot and payload blocks. As will be shown in Section , the performance of the FD-Interp method is inferior to that of the TD-LS method in underwater experiments. In the TD-LS channel estimation scheme, all transducers simulta-

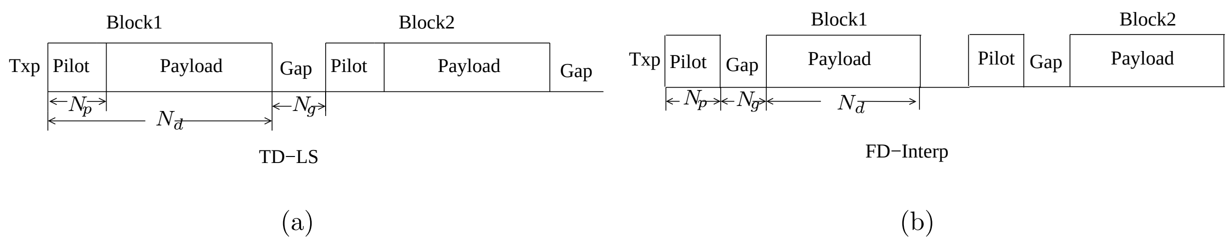

Figure 2 Data structure for channel estimation $N_d = 1024$, $N_g = 120$. (a) TD-LS channel estimation, $N_p = 300$. (b) FD-Interp channel estimation, $N_p = 240$

neously transmit N_p independent pilot symbols and the impulse responses of all subchannels are estimated for each block by the LS criterion. Let $\mathbf{y}_{tq}$ denote the received pilot symbols at the q-th hydrophone, and $\mathbf{x}_{tp}$ denote the pilot symbol matrix for the p-th transducer, which is given by

$$\mathbf{x}_{tp}=\begin{bmatrix} x_{tp}(L) & x_{tp}(L-1) & \cdots & x_{tp}(1) \\ x_{tp}(L+1) & x_{tp}(L) & \cdots & x_{tp}(2) \\ \vdots & \ddots & \ddots & \vdots \\ x_{tp}(N_p) & x_{tp}(N_p-1) & \cdots & x_{tp}(N_p-L+1) \end{bmatrix}. \tag{85}$$

The impulse responses of the subchannels related to the q-th hydrophone are denoted by $\hat{\mathbf{h}}_q = [\lambda_{q,1}\hat{\mathbf{h}}_{q,1}^T, \cdots, \lambda_{q,P}\hat{\mathbf{h}}_{q,P}^T]^T$, and estimated by

$$\hat{\mathbf{h}}_q = \mathbf{x}_t^{\dagger} \cdot \mathbf{y}_{tq}, \tag{86}$$

where $\mathbf{y}_{tq} = [y_{tq}(L), \cdots, y_{tq}(N_P)]^T$, and $\mathbf{x}_t = \begin{bmatrix}\mathbf{x}_{t1}, & \cdots, & \mathbf{x}_{tP}\end{bmatrix}$.

In the FD-Interp channel estimation scheme, the Chu sequences [22] with orthogonal frequency tones are adopted as the pilot blocks for multiple transducers. The pilot block for the p-th transducer is denoted by $\mathbf{C}_p$ which is the time-domain rotated version of $\mathbf{C}_1$, the pilot block of the first transducer. The k-th element of $\mathbf{C}_p$, denoted as $C_p(k)$, is obtained as

$$C_p(k) = C_1(k) \cdot e^{j2\pi(p-1)(k-1)/N_p}, \quad k = 1, \cdots, N_p. \tag{87}$$

Duplicating a length-(N_p/P) Chu sequence for P times yields a length-N_p pilot block $\mathbf{C}_1$. The spectrum of $\mathbf{C}_1$ exhibits periodic constant peaks with $(P-1)$ zeros in between. These pilot blocks, $\mathbf{C}_1, \cdots, \mathbf{C}_P$, are orthogonal to each other in the frequency domain although they are overlapped in the time domain. This FD-Interp channel estimation method is introduced in [28], and the details are omitted here for brevity.

B. Soft Decision Decoding. Soft decision decoding, depicted in Fig. 3, is an important part of turbo equalization and is employed at each layer for each transmitted data stream. It consists of an interleaver, Π, a de-interleaver, Π^{-1}, an extrinsic Log-likelihood ratios (LLRs) calculator, and a soft decision channel decoder. The equalized soft symbols and parameters ρ and σ_p (will be described in (103)) are used to compute the extrinsic LLRs of coded bits by Gaussian approximation, and then the extrinsic LLRs, $L_e^E(c_{p,k'})$, are passed via the de-interleaver to the channel decoder as the *a-priori* LLRs, $L_a^E(c_{p,k'})$. The decoder calculates the *a-posteriori* LLRs, $L_o^D(c_{p,k'})$, based on the coding structure. The extrinsic LLRs gleaned by the decoder, $L_e^D(c_{p,k'})$, are obtained by subtracting the *a-priori* LLRs from the *a-posteriori* LLRs. For trellis-based coding schemes, the Bahl-Cocke-Jelinek-Raviv (BCJR) algorithm [24] designed by maximum *a-posteriori* (MAP) criterion and soft output Viterbi algorithm (SOVA) based on maximum likelihood (ML) criterion [26] are often employed to produce the *a-posteriori* LLRs. The extrinsic LLRs are fed back to the equalizer via the interleaver as the *a-priori* LLRs, $L_a^D(c_{p,k'})$. for the next turbo iteration. Define the *a-priori*

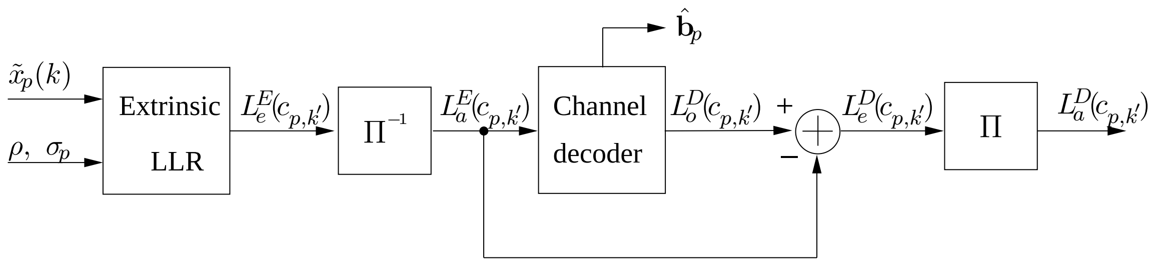

Figure 3 The block diagram for soft decision decoding

LLR and the *a-posteriori* LLR of the coded bit $c_{p,k'}$ as

$$\begin{aligned} L_a(c_{p,k'}) &\triangleq \ln\frac{\mathcal{P}(c_{p,k'}=0)}{\mathcal{P}(c_{p,k'}=1)} \\ L_o\big(c_{p,k'}|\hat{x}_p(k)\big) &\triangleq \ln\frac{\mathcal{P}\big(c_{p,k'}=0|\hat{x}_p(k)\big)}{\mathcal{P}\big(c_{p,k'}=1|\hat{x}_p(k)\big)}, \qquad k^{'}=(k-1)M+i, \quad i=1,\cdots,M. \end{aligned} \tag{88}$$

Using Bayes' rule, we can write (88) as

$$\begin{aligned} &L_o\big(c_{p,k'}|\hat{x}_p(k)\big) = \\ &\underbrace{\ln\frac{\sum_{\forall\alpha_m:d_{m,i}=0}\mathcal{P}\big(\hat{x}_p(k)|\alpha_m\big)\prod_{\forall j',j'\neq i}\mathcal{P}(c_{p,(k-1)M+j'}=d_{m,j'})}{\sum_{\forall\alpha_m:d_{m,i}=1}\mathcal{P}\big(\hat{x}_p(k)|\alpha_m\big)\prod_{\forall j',j'\neq i}\mathcal{P}(c_{p,(k-1)M+j'}=d_{m,j'})}}_{L_e(c_{p,k'})} \\ &\qquad + \underbrace{\ln\frac{\mathcal{P}(c_{p,k'}=0)}{\mathcal{P}(c_{p,k'}=1)}}_{L_a(c_{p,k'})}. \end{aligned} \tag{89}$$

From (89), the extrinsic LLR of the coded bit is associated with two probabilities $\mathcal{P}(c_{p,(k-1)M+j'} = d_{m,j'})$ and $\mathcal{P}\big(\hat{x}_p(k)|\alpha_m\big)$. The first probability is determined by

$$\mathcal{P}(c_{p,(k-1)M+j'} = d_{m,j'}) \;=\; \frac{(1-d_{m,j'})E_1 + d_{m,j'}E_2}{E_1+E_2}, \qquad d_{m,j'} \in \{0,1\}, \tag{90}$$

where $E_1 = e^{L_e^D(c_{p,(k-1)M+j'})/2}$, and $E_2 = e^{-L_e^D(c_{p,(k-1)M+j'})/2}$.

The second probability depends on the distribution of equalized symbols, $\hat{x}_p(k)$, conditioned on the transmitted symbols, α_m. It is commonly assumed that the equalized symbols are approximately Gaussian distributed for given transmitted symbols [16, 27]. Thus, the detected symbols can be approximated by

$$\hat{x}_p(k) = \rho_{p,k} x_p(k) + \eta_p(k), \tag{91}$$

where $\rho_{p,k}$ is a scalar and $\eta_p(k)$ is a complex white Gaussian noise with zero mean and variance σ_p^2. Thus, the conditional probability density function $\mathcal{P}(\hat{x}_p(k)|\alpha_m)$ is represented by

$$\mathcal{P}(\hat{x}_p(k)|\alpha_m) = \frac{1}{\pi\sigma_p^2}\exp\Big(-\frac{|\hat{x}_p(k)-\rho_{p,k}\alpha_m|^2}{\sigma_p^2}\Big), \tag{92}$$

where the calculation of $\rho_{p,k}$ and σ_p^2 will be given in (103).

C. Frequency-Domain Turbo Equalization. In the FDTE module of the receiver, the received data blocks $\mathbf{y}_p$ are first converted into the frequency domain by FFT yielding $\mathbf{Y}_p$. The means and variances of the transmit symbols are evaluated from the *a-priori* LLRs provided by the decoders. Using the minimum mean square error (MMSE) criterion, the FDTE adaptively computes its coefficients with the help of the *a-priori* mean and variance, $\mu_{p,k}$ and $\nu_{p,k}$, and estimates the soft symbols, $\hat{\mathbf{x}}_p$.

The mean and variance of $x_p(k)$ is calculated by

$$\begin{aligned} \mu_{p,k} &= \mathrm{E}[x_p(k)] = \sum_{\alpha_m \in \mathcal{S}} \alpha_m \cdot \mathcal{P}(x_p(k) = \alpha_m) \\ &= \sum_{\alpha_m \in \mathcal{S}} \alpha_m \prod_{k'=M(k-1)}^{Mk-1} \mathcal{P}(c_{p,k'+1} = d_{m,(k' \bmod M)+1}), \end{aligned} \tag{93}$$

$$\nu_{p,k} = \sum_{\alpha_m \in \mathcal{S}} |\alpha_m|^2 \mathcal{P}(x_p(k) = \alpha_m) - |\mu_{p,k}|^2, \tag{94}$$

where $d_{m,(k' \bmod M)+1} \in \{0,1\}$ is determined by α_m. For example, the alphabet of QPSK symbols is given by $\mathcal{S} = [1, j, -1, -j]$, and the corresponding bit patterns are $[d_{m,1}d_{m,2}] \in \{00, 01, 11, 10\}$. The alphabet of 8PSK symbols is defined by $\mathcal{S} = [1, \frac{1}{\sqrt{2}}(1+j), j, \frac{1}{\sqrt{2}}(-1+j), -1, \frac{1}{\sqrt{2}}(-1-j), -j, \frac{1}{\sqrt{2}}(1-j)]$ and the corresponding bit patterns are $[d_{m,1}d_{m,2}d_{m,3}] \in \{111, 110, 010, 000, 100, 101, 001, 011\}$. For QPSK alphabet, $\mu_{p,k}$ and $\nu_{p,k}$ are calculated by

$$\begin{aligned}
\mu_{p,k} &= \frac{1}{2}\Big(\tanh\big(\frac{1}{2}L_a^D(c_{p,2(k-1)+1})\big) + \tanh\big(\frac{1}{2}L_a^D(c_{p,2k})\big)\Big) \\
&\quad + j \cdot \frac{1}{2}\Big(\tanh\big(\frac{1}{2}L_a^D(c_{p,2(k-1)+1})\big) - \tanh\big(\frac{1}{2}L_a^D(c_{p,2k})\big)\Big) \\
\nu_{p,k} &= 1 - |\mu_{p,k}|^2.
\end{aligned} \tag{95}$$

For 8PSK alphabet, $\mu_{p,k}$ and $\nu_{p,k}$ are given by

$$\begin{aligned}
\mu_{p,k} &= 1/4 \cdot \big((l_1 - 1)\cdot(l_3 + l_2) - \sqrt{2}\cdot(l_2 + l_1 \cdot l_3)\big) \\
&\quad + j \cdot 1/4 \cdot \big((l_1 + 1)\cdot(l_3 - l_2) + \sqrt{2}\cdot(l_3 + l_1 \cdot l_2)\big) \\
\nu_{p,k} &= 1 - |\mu_{p,k}|^2
\end{aligned} \tag{96}$$

where $l_g = \tanh\big(L_a^D(c_{p,3(k-1)+g})/2\big)$, for $g = 1, 2, 3$.

By applying the MMSE criterion, the equalized symbols can be represented in the frequency domain as

$$\hat{\mathbf{X}}_p(k) = K_p^{-1} \cdot \mathbf{U}_p^H \cdot (\mathbf{Y} - \hat{\mathbf{H}} \cdot \bar{\mathbf{X}} + \mu_{p,k}\hat{\mathbf{H}}\mathbf{F}_P \mathbf{u}_{p,k}), \tag{97}$$

where $\hat{\mathbf{H}}$ is the estimated frequency-domain channel matrix, and $\mathbf{u}_{p,k}$ is a unit vector with length PN, whose $((p-1)N+k)$-th element is 1 and others are 0; The vector $\bar{\mathbf{X}}$ is the frequency-domain representation of the mean of the symbols, and it is given by

$$\bar{\mathbf{X}} = \mathbf{F}_P[\bar{\mathbf{x}}_1^T, \cdots, \bar{\mathbf{x}}_P^T]^T, \tag{98}$$

where $\bar{\mathbf{x}}_p = [\mu_{p,1}, \cdots, \mu_{p,N}]^T$. The equalizer coefficients $\mathbf{U}_p$ for the p-th data stream is computed as

$$\mathbf{U}_p = (\sigma_w^2 \mathbf{I}_{QN} + \hat{\mathbf{H}} \cdot \bar{\mathbf{V}} \cdot \hat{\mathbf{H}}^H)^{-1} \cdot \hat{\mathbf{H}} \cdot \begin{bmatrix} \mathbf{O}_{(p-1)N\times N} \\ \mathbf{I}_N \\ \mathbf{O}_{(P-p)N\times N} \end{bmatrix}, \tag{99}$$

where $\mathbf{O}_{m\times n}$ denotes an all-zero matrix of size $m \times n$, and $\bar{\mathbf{V}}$ is a diagonal matrix of size $(PN) \times (PN)$, defined by

$$\bar{\mathbf{V}} = \mathrm{diag}\{\bar{\nu}_1 \mathbf{I}_N, \quad \cdots \quad, \bar{\nu}_P \mathbf{I}_N, \}, \tag{100}$$

where $\bar{\nu}_p = \frac{1}{N}\sum_{k=1}^{N} \nu_{p,k}$. The scalar K_p is defined as

$$K_p = 1 + \frac{1-\bar{\nu}_p}{N} \mathrm{Tr}\{\hat{\mathbf{H}}^H_{(\bullet, pN-N+1:pN)} \mathbf{U}_p\}, \tag{101}$$

where $\hat{\mathbf{H}}_{(\bullet,i:j)}$ denotes the matrix composed of the i-th to j-th columns of $\hat{\mathbf{H}}$, and $\mathrm{Tr}\{\cdot\}$ represents the trace operation of a matrix.

With the frequency-domain estimation of the symbols for the p-th transducer in (97), the time-domain symbols are calculated by inverse DFT as

$$\hat{x}_p(k) = \mathbf{F}^H_{(\bullet,\ k)} \cdot \hat{\mathbf{X}}_p(k), \tag{102}$$

where $\mathbf{F}_{(\bullet,\ k)}$ represents the k-th column of the DFT matrix $\mathbf{F}$.

To calculate the extrinsic LLRs of coded bits, the scalar $\rho_{p,k}$ and average variance σ_p^2 in (92) are estimated by

$$\begin{aligned} \rho_{p,k} &= 1/K_p \cdot \mathbf{F}^H_{(\bullet,\ k)} \mathbf{U}_p^H \hat{\mathbf{H}} \mathbf{F}_P \mathbf{u}_{p,k} \\ \sigma_p^2 &= 1/K_p \cdot \frac{1}{N} \sum_{k=1}^{N} (|\rho_{p,k}| - \bar{\nu}_p |\rho_{p,k}|^2). \end{aligned} \tag{103}$$

Although the average symbol variance of each transducer is used in (100) to reduce the complexity of the FDTE, it is still costly due to the inversion of large matrices. As the block length N and the number of hydrophones Q increase, the computational complexity increases as $O(N^3Q^3)$. To further reduce computational complexity, we decompose the frequency-domain equalization into each frequency tone by taking advantage of the diagonal property of the channel matrix $\mathbf{H}_{q,p}$. As a result, a large matrix is partitioned into N small matrices – one per frequency tone. The channel responses on the i-th tone are extracted from the channel matrix $\hat{\mathbf{H}}$ to form a small matrix with size $Q \times P$ as

$$\mathcal{H}_i = \begin{bmatrix} \lambda_{1,1}\hat{H}_{1,1;i} & \cdots & \lambda_{1,P}\hat{H}_{1,P;i} \\ \vdots & \ddots & \vdots \\ \lambda_{Q,1}\hat{H}_{Q,1;i} & \cdots & \lambda_{Q,P}\hat{H}_{Q,P;i} \end{bmatrix}. \tag{104}$$

The equalization coefficients on the i-th frequency tone are then computed by

$$\mathbf{U}_p^i = (\sigma_w^2 \mathbf{I}_Q + \mathcal{H}_i \cdot \bar{V} \cdot \mathcal{H}_i^H)^{-1} \cdot \mathcal{H}_i \cdot \mathbf{e}_p, \qquad i = 1, \cdots, N, \tag{105}$$

where $\bar{V} = \mathrm{diag}\{\bar{\nu}_1, \cdots, \bar{\nu}_P\}$, and $\mathbf{e}_p$ is a length-P unit vector whose p-th entry is 1, and others are zeros.

Denote the received vector on the i-th frequency tone over all receive antennas as $\mathbf{Y}_i = [Y_{1,i}, \cdots, Y_{Q,i}]^T$ and the transmit vector of the i-th frequency tone as $\bar{\mathbf{X}}_i = [\bar{X}_{1,i}, \cdots, \bar{X}_{P,i}]^T$, then $\hat{X}_{p,i}$ is estimated by

$$\hat{X}_{p,i} = K_p^{-1} \cdot \mathbf{U}_p^{iH} \cdot (\mathbf{Y}_i - \mathcal{H}_i \cdot \bar{\mathbf{X}}_i + \mu_{q,k}\mathcal{H}_i \mathbf{s}_{p,i,k}), \tag{106}$$

where $\mathbf{s}_{p,i,k}$ is a length-P vector whose p-th element is $\mathrm{e}^{-\frac{j2\pi(k-1)(i-1)}{N}}$ and other elements are zeros; the matrix K_p can also be rewritten as $K_p = 1 + \frac{1-\hat{\nu}_p}{N}\sum_{i=1}^{N} \mathcal{H}_i^H(\bullet, p)\mathbf{U}_p^i$. It is noted from (105) that the matrix inversion is performed on a small matrix with size $Q \times Q$, and the equalization is performed on each frequency tone. Therefore, the computational complexity is significantly reduced from $O(N^3Q^3)$ to $N \cdot O(Q^3)$.

D. Phase Rotation Estimation and Correction. The equalized symbols are usually phase-rotated due to instantaneous Doppler shift, synchronization errors, temporal changes in the ocean, etc. If the phase rotation is significant, phase correction is required to be executed on the equalized symbols before soft decision decoding. Meanwhile, the phase rotation is also re-inserted when rebuilding the interference signals in the SSIC. Since the average phase rotation varies slowly with time and is more robust than per symbol phase rotation, a group-wise phase estimation algorithm is employed to estimate and correct phase distortions [15, 16], where the equalized data block is divided into many small groups, and the phase rotations are estimated group by group. The detailed algorithm is omitted here for brevity.

E. Soft-Successive Interference Cancellation. Interference signals formed by the detected data streams at the current layer are canceled out by the SSIC from the received signals in the frequency domain to reduce interference for the next layer. Here, the soft estimation of the symbol $\tilde{x}_p(k)$ is obtained by $\mu_{p,k}$ in (93), but with $\mathcal{P}(c_{p,k'}{=}0){=}\frac{e^{L_o^D(c_{p,k'})}}{1+e^{L_o^D(c_{p,k'})}}$ and $\mathcal{P}(c_{p,k'}{=}1){=}\frac{1}{1+e^{L_o^D(c_{p,k'})}}$, where $L_o^D(c_{p,k'})$ is the *a-posteriori* LLR for the coded bit $c_{p,k'}$ provided by soft decoding. In the r-th layer, we assume Δ_r data streams are to be detected and denote $\tilde{\mathbf{x}}_{r,i} = [\tilde{x}_{(r,i)}(1), \cdots, \tilde{x}_{(r,i)}(N)]$ as the phase-corrected soft symbol block of the (r,i)-th stream, for $i = 1, \cdots, \Delta_r$. To construct the interference, the phase rotation estimated by the group-wise phase estimation algorithm is compensated into the soft symbols to generate the phase-distorted symbol

$$\tilde{x}'_{(r,i)}(k) = \tilde{x}_{(r,i)}(k) \cdot e^{-j\phi_{(r,i),k}}, \tag{107}$$

where $\phi_{(r,i),k}$ represents the estimated phase rotation for the k-th symbol of the (r,i)-th data stream. The reconstructed interference is canceled in the frequency domain by passing the phase-distorted soft symbols through the estimated channels

$$\begin{bmatrix} \mathbf{Y}_1^{(r+1)} \\ \vdots \\ \mathbf{Y}_Q^{(r+1)} \end{bmatrix} = \begin{bmatrix} \mathbf{Y}_1^{(r)} \\ \vdots \\ \mathbf{Y}_Q^{(r)} \end{bmatrix} - \begin{bmatrix} \hat{\mathbf{H}}_{1,(r,1)} & \cdots & \hat{\mathbf{H}}_{1,(r,\Delta_r)} \\ \vdots & \ddots & \vdots \\ \hat{\mathbf{H}}_{Q,(r,1)} & \cdots & \hat{\mathbf{H}}_{Q,(r,\Delta_r)} \end{bmatrix} \begin{bmatrix} \tilde{\mathbf{X}}'_{(r,1)} \\ \vdots \\ \tilde{\mathbf{X}}'_{(r,\Delta_r)} \end{bmatrix}, \tag{108}$$

where $\tilde{\mathbf{X}}'_{(r,i)}$ is the frequency-domain representation of $\tilde{\mathbf{x}}'_{(r,i)}$, and $\mathbf{Y}_q^{(r)}$ and $\mathbf{Y}_q^{(r+1)}$ are the received signal represented in the frequency domain for the r-th and $(r+1)$-th layer, respectively.

IV. NUMERICAL RESULTS BY MONTE-CARLO SIMULATIONS

We conducted computer simulation for the proposed receiver algorithm and verified its effectiveness and superior performance by the simulation results. In the simulation, a MIMO 4×4 system was considered and the UWA channels were assumed to be 80-taps frequency-selective channels following Rayleigh distribution [25]. Based on the estimation of practical underwater channels, the power delay profile (PDP) is specified to ramp up and down exponentially, where the first 20 taps have the power as $1/P_n \cdot e^{0.1 \cdot l}$ and the last 60 taps have the power as $1/P_n \cdot e^{-0.03 \cdot l}$. The constant P_n normalizes the PDP to yield a total power of 1. The maximum Doppler spread is set at $f_d = 1$ Hz. In order to make the MIMO channels unbalanced, we assume the subchannels related to the first and second transmit antennas have twice the power of the other two antennas. The average SNR at the receiver is defined as

$$\mathrm{SNR} = \frac{P_T \cdot \sum_{q,p} \sum_{(l)} |h_{q,p}(l)|^2}{P \cdot Q \cdot \sigma_w^2} \tag{109}$$

where P_T is the total transmit power.

Binary information bits were encoded by a rate-1/2 convolutional encoder with a coding generator $(1 + D + D^2 + D^3, 1 + D^2 + D^3)$, and the encoded bits are interleaved randomly and mapped into 8PSK symbols with a symbol period $T = 0.1$ ms. For each SNR, 1600 blocks are transmitted for BER evaluation and each block contains $N_d = 1024$ symbols. We applied the proposed receiver algorithm to detect the data streams transmitted from all antennas. The performance of FDTE with one layer and two layers detection is evaluated for comparison. In the FDTE with one layer detection, the soft information for all data streams is generated at the same time for detection and no interference cancellation is performed. Therefore, the FDTE with one layer detection is equivalent to the traditional frequency-domain turbo equalization. In the FDTE with two layer detection, the data streams from the first two transmit antennas are detected in the first layer and the other two weaker streams are detected in the second layer. The BER performance is depicted in Fig. 4.

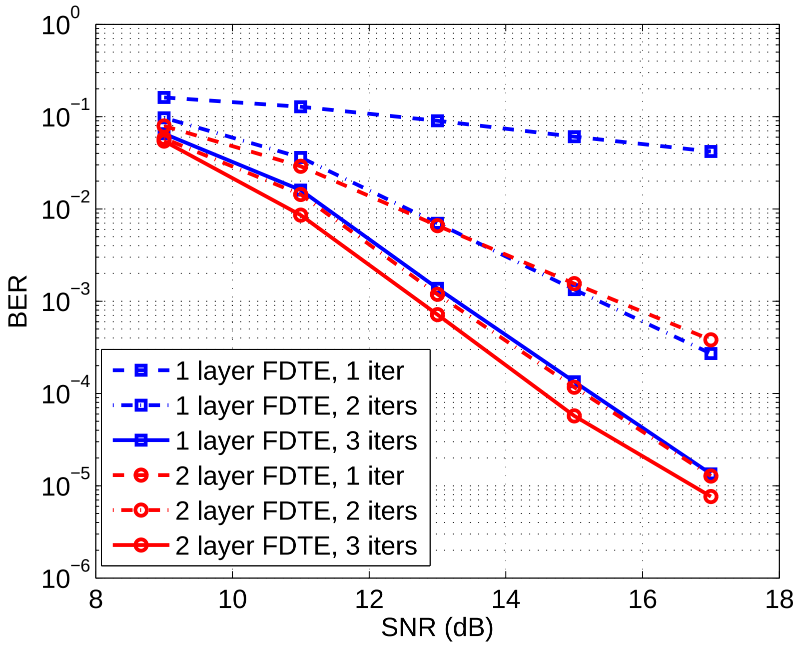

Figure 4 BER performance for FDTE with one and two layers, respectively. Simulated MIMO 4×4, 80-tap channels, $f_d T_s = 1 \times 10^{-4}$

We can see that under the same turbo iterations, the two-layer FDTE outperforms one layer detection and more turbo iterations lead to BER performance improvement. The performance gain due to turbo iterations is significant between the first and second iterations, but tends to decrease with the increase of the number of iterations. The diminishing gain reaches a low bound due to an approximation in each iteration, that is that the average symbol variance, rather than the individual symbol variance, is used in the equalizer for each block of symbols. It is also observed that FDTE with two layers and one iteration can achieve similar performance as the FDTE with one layer and two iterations. The same trend is also observed between the FDTE with two layers and two iterations and the FDTE with one layer and three iterations. It implies that the same performance can be obtained by increasing layers with less number of iterations or increasing the number of iterations with less layers.

It is worth noting that the proposed FDTE-SSIC receiver has similar complexity on computing the equalization coefficients in the turbo iterations compared to the traditional FDTE structure. Due to the frequency-domain interference cancellation in the layered structure, extra FFT and multiplication should be performed at each layer, which results in slightly increased complexity for the proposed algorithm. In addition, unlike the traditional FDTE, the proposed receiver detects data layer by layer, which introduces extra detection delay. Tradeoff between processing delay and receiver performance should be considered in practical implementation.

V. EXPERIMENTAL PERFORMANCE RESULTS

In this section, we present comprehensive performance results obtained by applying the proposed FDTE-SSIC algorithm to the real-world undersea experimental data collected during the Surface Process and Acoustic Communications Experiment (SPACE) in late fall, 2008. This experiment was conducted by Wood Hole Oceanographic Institution in a shallow area of the Atlantic Ocean, south of Cape Cod in Massachusetts [19]. The average water depth was less than 15 m, and the communication ranges between the transceivers were 200 m and 1000 m. The transmitter was fixed on a stationary tripod with multiple transducers deployed, and the source power level was set at 185 dB re μPa @ 1 m. The top transducer was approximately 3 m above the ocean bottom, and the spacing between neighboring transducers was 50 cm. The sampling frequency F_s was 39.0625 kHz, and the bandwidth F_b was 9.7656 kHz ($F_s/4$) centered at the carrier of 13 kHz. The square root raised cosine pulse with a roll-off factor 0.2 was used as the pulse shaping filter. For each transducer branch, information bits were encoded by the same convolutional encoder used in simulations. The coded bits were permuted by random interleavers and then mapped into QPSK or 8PSK symbols. At the receiver end, the hydrophone arrays were also mounted on fixed tripods with the top of each array located 3.25 m above the sea floor. The array at the 200 m range deployed 24 hydrophones vertically with a uniform-spacing space of 5 cm between adjacent elements, and the array at the 1000 m range had 12 hydrophones with 12 cm spacing between adjacent elements. During the experiment, data packets with a duration of 60 seconds were transmitted from multiple transducers every two hours. Each data packet consisted of a leading linearly frequency modulated (LFM) signal followed by a small gap, a 511-bit m-sequence with gap, and data blocks with QPSK and 8PSK modulation schemes. The received data of 12 hydrophones was recorded in one data file for each transmission. For FD-Interp channel estimation, Chu sequence blocks with length of 240 symbols were used and a gap with 120 zeros was inserted between blocks. For TD-LS channel estimation, pilot blocks with 300 symbols were used in each data block of length 1024. The environment condition was mild, with average wind speed of 2.5 m/s, wave height of 1.5 m and wave period of 8 seconds. More details on the environment can be found in [19]. In the following subsections, we present the results for the 200 m and 1000 m systems which had 60 and 24 received packets, respectively.

A. Channel Estimation. The receiver performed frame synchronization at the front-end module before channel estimation and equalization. In the experiment, two LFM signals were transmitted before and after the data packet and synchronization was achieved by correlating the received packet with a local replica of the LFM signal. The channel length was also approximated as the time span of the most of energy in the LFM correlation output. The channel of the 200 m system had larger delay spread of 9.2 ms than the 8.2 ms of the 1000 m system. Thus, for estimating channel impulse response (CIR), we assume that the channels of the 200 m system had 90 taps, and the channels of the 1000 m system spanned 80 symbols.

The received signals were demodulated and sampled at 2 samples/symbol to facilitate $2N$-point FFT in the equalizers. We employed the two methods described in Section III-A to estimate the time-varying, frequency-selective underwater channels. The amplitudes of CIRs corresponding to one hydrophone-transducer pair estimated by these two methods are shown in Fig. 5 for the 200 m and 1000 m systems. The amplitudes of CIRs were normalized by the maximum amplitude of the 200 m channels. In the 200 m channels, the CIRs of Transducer 2 had higher average power (0.0709 W) than those of Transducer 1 (0.0385 W). In contrast, the power distribution of the 1000 m channels was different. The CIRs of the Transducer

1 have more average power (5.6×10^{-3} W) than those of Transducer 2 (1.5×10^{-3} W). It is clear that the underwater MIMO channels exhibited unbalanced characteristics and unequal channel powers. Consequently, the data stream with larger channel power had higher SNR and was detected first in the layered detection. The channels of the 200 m system were spikier and had more dominant propagation paths than those of the 1000 m system.

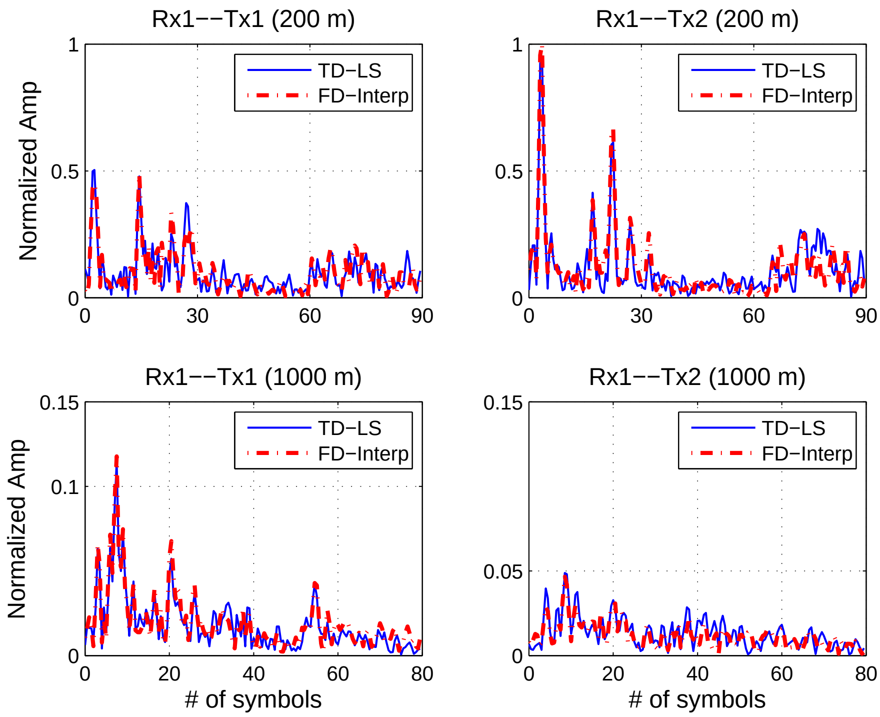

Figure 5 Normalized amplitudes of CIRs for the 200 m and 1000 m systems estimated by TD-LS and FD-Interp methods

Based on the estimated channels, the average SNR for one hydrophone was calculated by (109) or by estimating the signal-plus-noise power in the received data blocks and the noise-only power in the gaps of received packets. The average SNR per hydrophone was around 14 dB for the 1000 m system and 20 dB for the 200 m system.

B. Transceiver Performance. The proposed FDTE-SSIC scheme was used to process the received packets of the 200 m and 1000 m systems. In each packet, there were totally 14480 and 21720 information bits for QPSK and 8PSK, respectively. The duration of each packet was approximately equal to 1.34 seconds, taking into account both payload data and overhead including LFM, m-sequence, gaps and training symbols. Therefore, the information bit rate achieves 10.8 kbps for QPSK and 16.2 kbps for 8PSK.

To illustrate the iterative detection, the scatter plots of soft QPSK and 8PSK symbols after soft decision decoding for different turbo iterations are shown in Fig. 6. It is clearly seen that turbo equalization and detection gradually separated the soft symbols and pushed them closer to valid constellation points. The BERs of QPSK corresponding to one, two, and three iterations are 1.4×10^{-3}, 6.9×10^{-4}, and 0. The BERs of 8PSK for one, two, and three iterations are 0.0138, 8.3×10^{-3}, and 4.2×10^{-3}, respectively.

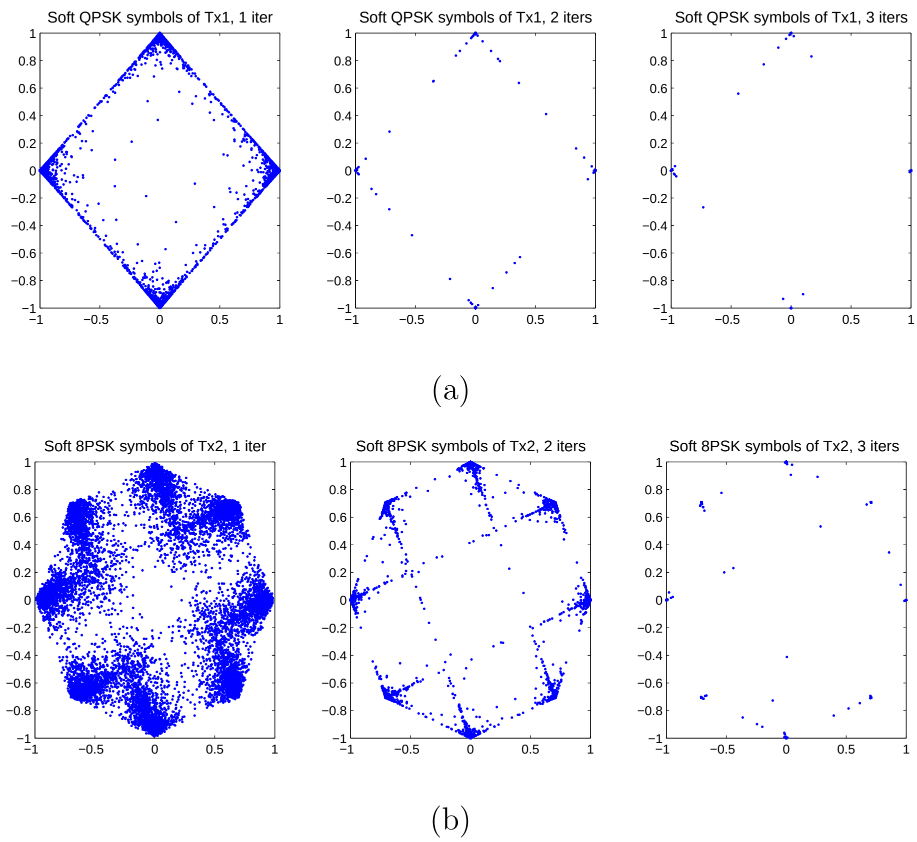

Figure 6 Scatter plots of soft symbols for different iterations. (a) QPSK. The BERs for one, two, and three iterations are 1.4×10^{-3}, 6.9×10^{-4}, and 0, respectively. (b) 8PSK. The BERs for one, two, and three iterations are 0.0138, 8.3×10^{-3}, and 4.2×10^{-3}, respectively.

From the scatter plots, we can also see that the QPSK and 8PSK soft symbols appear to be bounded by straight lines between neighboring constellation points and are concentrated along lines linking the constellation points. This pattern is inherited from the calculation of soft symbols in (14) because turbo equalization takes advantage of the interaction between coded bits and symbol mapping. Taking QPSK for example, the hard symbols are $\{1, j, -1, -j\}$, corresponding to bit patterns $\{00, 01, 11, 10\}$. Since $\mathcal{P}(c_{p,k'} = 0) + \mathcal{P}(c_{p,k'} = 1) = 1$ and based on (14), the soft symbol $\tilde{x}(k) = \mu_{p,k}$ satisfies $-1 \leq \text{Real}(\tilde{x}(k)) + \text{Imag}(\tilde{x}(k)) \leq 1$. Therefore, the soft symbols are bounded by the square area formed by the four lines. As the number of iteration increases, the soft symbols become focused on the constellation symbols gradually. Similarly for 8PSK, the soft symbols are bounded by the octagon formed by the eight constellation points.

The detailed BER performance is shown in Table 1 – 4, where Table 1 shows the BERs of 10 representative packets randomly selected from all packets. The BERs were achieved by the proposed FDTE-SSIC algorithm, compared with those by the FDTE without SSIC and by the non-iterative FDE with Viterbi soft decision (SD) decoding algorithm. Both iterative detection schemes, FDTE and FDTE-SSIC, significantly outperformed the non-iterative scheme, and the proposed FDTE-SSIC algorithm outperformed the traditional FDTE, especially in tough UWA channels.

Table 2 compares the BERs of the proposed FDTE-SSIC algorithm with different channel estimation methods. If the channels are estimated by the FD-Interp method, then the number of error bits in all packets were larger than or equal to those obtained by using the TD-LS method, although the FD-Interp method requires less computational complexity than the TD-LS method. The BERs of five representative packets are shown in Table 2 to demonstrate the performance difference between the two methods.

The performance difference of the proposed FDTE-SSIC with and without phase correction was also investigated, and the BERs of five representative packets are shown in Table 3. It is seen that the FDTE-SSIC with phase correction achieves better, or no worse, performance than that without phase correction. Checking all the data, we found that the phase rotation were insignificant for most packets because the transceivers were fixed during the experiments, and small Doppler spread between ± 1 Hz were estimated. For a small number of packets that did experience high Doppler spread, the performance without phase correction is inferior to that with phase compensation.

Table 4 provides the overall BER statistics for the 200 m and 1000 m systems with QPSK and 8PSK, respectively. The bit error rates of the 200 m system averaged over all 60 packets achieved 5.6×10^{-5} for QPSK and 4.6×10^{-3} for 8PSK. For the 1000 m system, the BERs averaged over 24 packets were 1.7×10^{-4} for QPSK and 5.5×10^{-3} for 8PSK. The majority of the packets achieved zero bit error for QPSK in both 200 m and 1000 m systems. However, for 8PSK, most packets had BERs in the range of 10^{-3} to 10^{-2}. This performance difference between 8PSK and QPSK is mainly due to the smaller decision distance of 8PSK than that of QPSK with the same SNR.

Table 1 Comparison of BERs of 10 packets obtained by non-iterative FDE-Viterbi-SD, FDTE without SSIC, and FDTE-SSIC, QPSK, $N = 1024$, two iterations, CIRs estimated by the TD-LS method

Index of packet	FDE Viterbi SD	FDTE (2 iters)	FDTE-SSIC (2 iters)
II.1	1.5×10^{-3}	0	0
II.2	7.76×10^{-2}	2.4704×10^{-4}	0
II.3	8.48×10^{-2}	2.964×10^{-4}	1.976×10^{-4}
II.4	7.9051×10^{-4}	0	0
II.5	7.7075×10^{-3}	2.9644×10^{-4}	0
II.6	6.0×10^{-2}	2.4704×10^{-4}	9.8814×10^{-5}
II.7	7.4111×10^{-4}	0	0
II.8	8.0534×10^{-3}	3.9526×10^{-4}	1.9763×10^{-4}
II.9	3.4585×10^{-4}	0	0
II.10	5.32×10^{-2}	2.4704×10^{-4}	0

Figure 7 shows the average BER performance of MIMO systems with different number of hydrophones for these two range systems. Given the space between adjacent hydrophones, more hydrophones deployed at the receiver obtain higher order of diversity gain, and the average BER performance tends to be better. While increasing the hydrophone numbers from six to eight, the BERs can be improved from 5×10^{-3} to 5×10^{-4}, which is ten times performance gain by augmenting two hydrophones.

Table 2 Comparison of BERs of 5 packets under the channel estimated by FD-Interp and TD-LS, two iterations

Index of packet	FDTE-SSIC 2 iters (FD-Interp)	FDTE-SSIC 2 iters (TD-LS)
III.1	4.447×10^{-4}	9.8814×10^{-5}
III.2	0	0
III.3	2.0257×10^{-3}	0
III.4	1.6798×10^{-3}	0
III.5	1.67×10^{-2}	0

Table 3 Comparison of BERs of 5 packets for with/without phase correction module, QPSK, $N = 1024$, two iterations, CIRs estimated by TD-LS

Index of packet	FDTE-SSIC (without phase correction)	FDTE-SSIC (with phase correction)
IV.1	3.953×10^{-4}	1.976×10^{-4}
IV.2	2.900×10^{-3}	1.300×10^{-3}
IV.3	8.399×10^{-4}	4.447×10^{-4}
IV.4	2.0257×10^{-3}	1.976×10^{-4}
IV.5	1.976×10^{-4}	0

Table 4 BER statistics of the 200 m and 1000 m systems for QPSK and 8PSK, $N = 1024$, two iterations, CIRs estimated by TD-LS

	200 m (60 packets)		1000 m (24 packets)	
BER	# of packets (QPSK)	# of packets (8PSK)	# of packets (QPSK)	# of packets (8PSK)
0	54	6	20	2
1e-5 $\sim$ 1e-4	2	2	1	0
1e-4 $\sim$ 1e-3	3	7	2	4
1e-3 $\sim$ 1e-2	1	33	1	15
1e-2 $\sim$ 1e-1	0	12	0	3
Avg. BER	5.6×10^{-5}	4.6×10^{-3}	1.7×10^{-4}	5.5×10^{-3}

VI. CONCLUSION

We have proposed a turbo detection scheme integrating the frequency-domain turbo equalization and soft successive interference cancellation for single carrier underwater acoustic MIMO communications. To achieve reliable UWA communications with high data-rate and low error-rate, the severe ISIs caused by the long-delay-spread UWA channels are iteratively mitigated by a low-complexity FDTE cooperating with soft decision channel decoders.

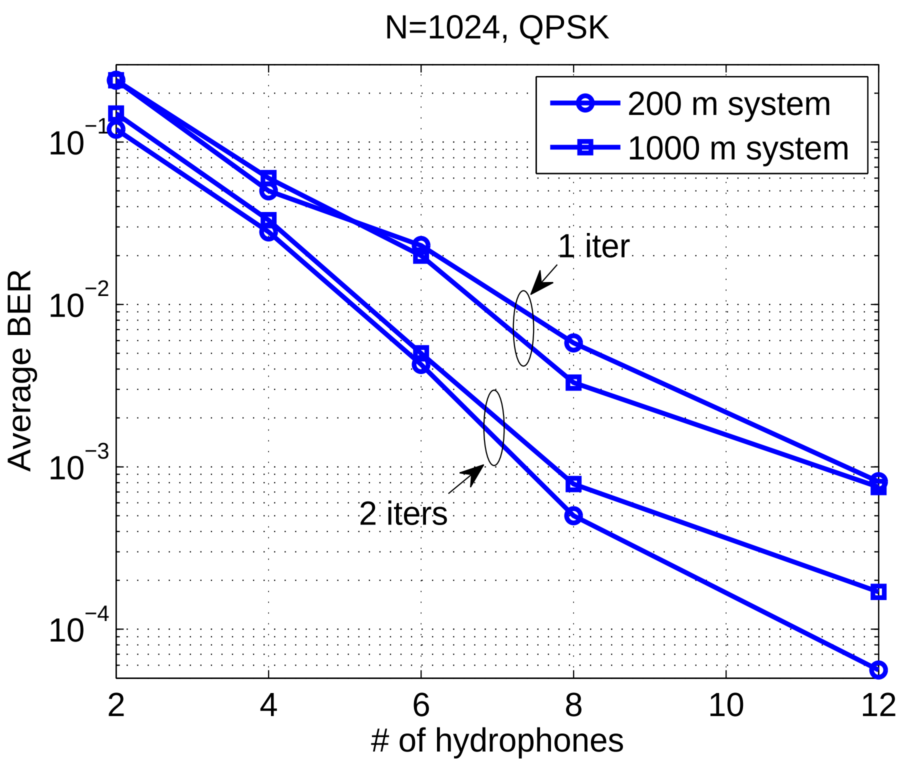

Figure 7 Experimental results for average BER performance for two transducers and different numbers of hydrophones

The CCIs caused by multiple transducers are also combatted by a layered detection structure based on SSIC. Excellent performance has been achieved by applying the proposed algorithm to real-world undersea data collected in SPACE08 experiment, which demonstrates that the proposed UWA communication system can offer reliable and high speed UWA data transmission.

VII. REFERENCES

[1] M. Stojanovic and J. Preisig, “Underwater acoustic communication channels: propagation models and statistical characterization,” *IEEE Commun. Mag.*, pp.84-89, Jan. 2009.

[2] A. C. Singer, J. K. Nelson, S. S. Kozat, “Signal processing for underwater acoustic communications,” *IEEE Commun. Mag.*, pp.90-96, Jan. 2009.

[3] D. B. Kilfoyle and A. B. Baggeroer, “The state of the art in underwater acoustic telemetry,” *IEEE J. Ocean. Eng.*, vol.25, pp.4-27, Jan. 2000.

[4] T. H. Eggen, A. B. Baggeroer, and J. C. Preisig, “Communication over Doppler spread channels – Part I: channel and receiver presentation,” *IEEE J. Ocean Eng.*, vol.25, pp.62-71, Jan. 2000.

[5] M. Stojanovic, J. Catipovic, and J. Proakis, "Phase-coherent digital communicaitons for underwater acoustic channels," *IEEE J. Ocean. Eng.*, vol.19, pp.100-111, Jan. 1994.

[6] S. Roy, T. M. Duman, V. McDonald, and J. Proakis, "High rate communication for underwater acoustic channels using multiple transmitters and space-time coding: receiver structures and experimental results," *IEEE J. Ocean. Eng.*, vol.32, pp.663-688, July 2007.

[7] B. Li, S. Zhou, M. Stojanovic, L. Freitag, and P. Willett, "Multicarier communication over underwater acoustic channels with nonuniform Doppler shift," *IEEE J. Ocean Eng.*, vol. 33, pp. 198-209, April 2008.

[8] J. Zhang, Y. R. Zheng, and C. Xiao, "Frequency-domain equalization for single carrier MIMO underwater acoustic communications," in *Proc. IEEE OCEANS'08*, Quebec city, Canada, Sept.15-18, 2008.

[9] M. Tüchler, A. C. Singer, and R. Koetter, "Minimum mean squared error equalization using a priori information," *IEEE Trans. Signal Proc.*, vol.50, pp.673-683, Mar. 2002.

[10] B. Ng, C. Lam, and D. Falconer, "Turbo frequency domain equalization for single-carrier broadband wireless systems," *IEEE Trans. Wireless Commun.*, vol.6, pp.759-767, Feb. 2007.

[11] M. Sabbaghian and D. Falconer, "Joint turbo frequency domain equalization and carrier synchronization," *IEEE Trans. Wireless Commun.*, vol.7, pp.204-212, Jan. 2008.

[12] H. Liu and P. Schniter, "Iterative frequency-domain channel estimation and equalization for single-carrier transmissions without cyclic-prefix," *IEEE Trans. Wireless Commun.*, vol.7, pp.3686-3691, Oct. 2008.

[13] T. Abe and T. Matsumoto, "Space time turbo equalization in frequency-selective MIMO channels," *IEEE Trans. Veh. Technol.*, vol.52, no.3, pp.469-475, May 2003.

[14] Y. Wu, X. Zhu, and A. K. Nandi, "Low complexity adaptive turbo space-frequency equalization for single-carrier multiple-input multiple-output systems," *IEEE Trans. Wireless Commun.*, vol.7, pp.2050-2056, June 2008.

[15] R. Otnes and T. H. Eggen, "Underwater acoustic communications: long-term test of turbo equalization in shallow water," *IEEE J. Ocean. Eng.*, vol.33, pp.321-334, July 2008.

[16] J. Zhang, Y. R. Zheng, and C. Xiao, "Frequency-domain turbo equalization for MIMO underwater acoustic communications," in *Proc. IEEE OCEANS'09*, Bremen, Germany, May 11-14, 2009.

[17] S. Cho, H. C. Song, and W. S. Hodgkiss, "Successive interference cancellation for time-reversed underwater acoustic channels," in *Proc. IEEE OCEANS'09*, Biloxi, USA, Oct. 2009.

[18] Y. R. Zheng, "Channel Estimation and Phase-Correction for Robust Underwater Acoustic Communications,"IEEE Military Communications Conf. (MilCom07), Orlando, USA, Oct. 2007, pp. 1-6.

[19] L. Freitag and S. Singh, "Performance of micro-modem PSK signaling under variable conditions during the 2008 RACE and SPACE experiments," in *Proc. IEEE OCEANS'09*, Biloxi, USA, Oct. 2009.

[20] N. Benvenuto, R. Dinis, D. Falconer, and S. Tomasin, "Single carrier modulation with nonlinear frequency domain equalization: an idea whose time has come-again,"*Proceedings of the IEEE*, vol.98, pp.69-96, 2010.

[21] J. Zhang, Y. R. Zheng, C. Xiao, and K. B. Lataief, "Channel equalization and symbol detection for single carrier MIMO systems in the presence of multiple carrier frequency offsets," *IEEE Trans. Veh. Technol.*, vol.59, pp.2021-2030, May 2010.

[22] D. C. Chu, "Polyphase codes with good periodic correlation properties," *IEEE Trans. Inform. Theory*, vol.IT-18, pp.531-532, July 1972.

[23] J. Zhang and Y. R. Zheng, "Improved frequency domain channel estimation and equalization for MIMO wireless communications" *Int. J. Wireless Inf. Networks*, vol. 16, pp.12-21, June 2009.

[24] L. R. Bahl, J. Cocke, F. Jelinek, and J. Raviv, "Optimal decoding of linear codes for minimizing symol error rate," *IEEE Trans. Info. Theory*, pp.284-287, March 1974.

[25] M. Chitre, "A high-frequency warm shallow water acoustic communications channel model and measurements," *J. Acoust. Soc. America*, vol.122, pp.2580-2586.

[26] J. Hagenauer, "A viterbi algorithm with soft-decision outputs and its application," in *Proc. IEEE GLOBECOM'89*, Dallas, USA, Nov. 1989, pp. 1680-1686.

[27] A. Dejonghe and L. Vandendorpe, "Turbo-equalization for multilevel modulation: an efficient low complexity scheme," in *Proc. IEEE Int. Conf. Commun.*, New York, USA, May 2002, pp. 1863-1867.

5. BANDWIDTH-EFFICIENT FREQUENCY-DOMAIN EQUALIZATION FOR SINGLE CARRIER MULTIPLE-INPUT MULTIPLE-OUTPUT UNDERWATER ACOUSTIC COMMUNICATIONS

Jian Zhang and Yahong Rosa Zheng

Abstract—This paper proposes a single carrier (SC) receiver scheme with bandwidth-efficient frequency-domain equalization (FDE) for underwater acoustic (UWA) communications employing multiple transducers and multiple hydrophones. Different from the FDE methods that perform FDE on a whole data block, the proposed algorithm implements an overlapped-window FDE by partitioning a large block into small subblocks. A decision-directed channel estimation scheme is incorporated with the overlapped-window FDE to track channel variations and improve the error performance. The proposed algorithm significantly increases the length of each block and keeps the same number of training symbols per block, hence achieving better data efficiency without performance degradation. The proposed scheme is tested by the undersea data collected in the Rescheduled Acoustic Communications Experiment (RACE) in March 2008. Without coding, the 2-by-12 MIMO overlapped-window FDE reduces the average bit error rate (BER) over traditional SC-FDE schemes by 74.4% and 84.6% for the 400 m and 1000 m range systems, respectively, at the same data efficiency. If the same BER performance is required, the proposed algorithm has only 8.4% transmission overhead, comparing to over 20% overhead in other existing UWA OFDM and SC-FDE systems. The improved data efficiency and/or error performance of the proposed FDE scheme is achieved by slightly increased computational complexity over traditional SC-FDE schemes.

I. INTRODUCTION

High data-rate shallow underwater acoustic (UWA) communications are challenging due to the hostile underwater propagation environment [1, 2]. An UWA communication system equipped with multiple transducers and multiple hydrophones usually experiences triply selective fading channels. First, the excessively long multi-path delay spread leads to severely frequency-selective channels causing excessive inter-symbol interference (ISI) [3, 4]. For example, UWA channels for medium communication ranges (1-10 km) usually have delay spread on the order of tens of millisecond, spanning several tens to hundreds of symbols. Second, the relative motion between transceivers and the dynamic motion of water media result in fast time-varying fading and significant time-varying Doppler spread, causing temporal dilation or compression of received signal waveforms and severe phase rotation of detected symbols. Furthermore, employing MIMO systems in UWA, which can improve data rate, imposes significant technical challenges in transceiver design due to co-channel interference (CCI) and angular spread among multiple transducers or multiple hydrophones.

To mitigate ISI and Doppler effect, a variety of time-domain and frequency-domain equalizers combined with Doppler compensation methods have been investigated for UWA communications [5] - [17]. Time-domain decision feedback equalization (TD-DFE) with a second-order digital phase-locked loop (PLL) has been successfully applied in single-input single-output (SISO) [6], single-input multiple-output (SIMO) [5], and multiple-input multiple output (MIMO) [11] UWA communications. However, due to long channel length and fast time-varying fading, the TD-DFE with PLL is often unstable, difficult to converge to optimal coefficients, and computationally prohibitive for long delay spreads. In contrast, frequency-domain equalization (FDE) can provide lower complexity and better robustness in severe ISI and Doppler fading channels. The common FDE schemes, multicarrier [12], orthogonal frequency division multiplexing (OFDM), and single carrier FDE (SC-FDE), have recently been applied to UWA communications successfully with excellent performance tested in real-world undersea experiments. In particular, the OFDM technique [13,14] employs a two-step Doppler mitigation method to combat severe UWA channels; and the SC-FDE [15–17] utilizes a group-wise phase correction method to combat fast phase rotation in equalized symbols.

However, the challenge of the current frequency-domain (FD) methods (OFDM and SC-FDE) is the conflicting goal of improving bandwidth efficiency and tracking channel variations. To utilize discrete Fourier transformation (DFT) at receiver, the FD methods require block transmission as well as zero padding (ZP) or cyclic prefix (CP) [18] between blocks to avoid interblock interference (IBI). The length of ZP or CP has to be greater than the channel memory length, resulting in large overhead in high date-rate UWA communications, because the UWA channel length is often on the order of a hundred taps [3]. Meanwhile, the channel coherent time only spans about a couple of hundred symbols and the data block length is limited by channel coherent time to effectively track the channel variation. In addition, pilot-assisted channel estimation often requires that the pilot block length to be larger than the channel length, further increasing the overhead. Therefore, conventional FDE schemes with a small block length can track channel variation and ensure good BER performance but suffering from low data efficiency. Increasing data block length may improve bandwidth efficiency but suffering from reduced performance due to poor channel estimation and tracking.

To solve the dilemma between the data efficiency and performance of FDE, an iterative CP-reconstruction and IBI-cancellation algorithm [19, 20] has been proposed to increase the bandwidth efficiency by using less CPs. However, this method demands considerably high computation due to its iterative process, and still suffers high overhead for channel estimation. Besides, compressive sensing techniques are also applied to channel estimation of OFDM systems to reduce pilot overhead [21,22]. However, the complexity of compressive sensing is prohibitively high for real-time communication systems.

This paper proposes a bandwidth-efficient SC-FDE scheme incorporated with decision-directed channel estimation for UWA MIMO communication systems. The proposed FDE is based on the overlap-save method [23, 24] for frequency domain filtering. A large data block is divided into small subblocks and an overlapped window is formed for the FDE input by the current subblock and small parts of the previous and subsequent subblocks. The parts of previous and subsequent subblocks are included in the equalization for cancellation of precursor and postcursor interference caused by the channels. After equalization, the desired subblock data is obtained by discarding the precursor and postcursor parts of the equalized data window. Before making decisions on the equalized symbols, the phase rotation caused by the Doppler spread is corrected by a group-wise phase correction algorithm. The UWA channels are initially estimated by pilot symbols and re-estimated by the detected subblock symbols. The time variation of the channels is effectively tracked by this decision-directed channel estimation approach, and the BER performance is significantly improved.

The novelty of the proposed FDE scheme lies in that a block with a length much larger than the channel coherence time can be equalized by FDE with only one pilot block without performance degradation, thus, improving the data efficiency at the cost of slightly increased computational complexity.

The proposed algorithms have been tested by real-world undersea data collected in the Reschedule Acoustic Communication Experiment (RACE) conducted in Narragansett Bay, Rhode Island from March 1st to March 17th, 2008. This experiment was designed for 400 m and 1000 m ranges, with 2 transducers at the transmitter and 12 hydrophones at the receiver. The quadrature phase-shift keying (QPSK) modulation with a bandwidth of 3.90625 kHz and a carrier frequency of 11.5 kHz was employed. Experimental results show that the proposed scheme effectively tracks the time-varying UWA channels, and the average uncoded BER over 30 data packets achieves 1.4% for the 400 m system and 0.6% for the 1000 m system when the length of subblock is set at 200 while a block length was 2048. The proposed algorithm significantly outperforms the traditional SC-FDE with more than 70% reduced bit errors under the same bandwidth efficiency. The transmission overhead, considering both the lengths of padding zeros and pilot symbols, is only 8.4%, which is a significant reduction compared with more than 20% overhead of other existing UWA OFDM and SC-FDE systems.

The remainder of this paper is organized as follows. Section II describes the system model and develops the frequency representation for the overlapped-window FDE. Section III presents the channel estimation, equalization, and phase correction algorithms. Section IV presents the experimental results. Finally, our conclusions are drawn in Section V. We use boldface letters to denote vectors and matrices, and the superscripts $[\cdot]^T$, $[\cdot]^H$, $[\cdot]^{-1}$, and $[\cdot]^\dagger$ to denote the matrix transpose, Hermitian transpose, inverse, and pseudo-inverse, respectively.

II. SYSTEM MODEL AND PRELIMINARIES

A MIMO system employing spatial multiplexing (SM) structure with N_t transducers and N_r hydrophones is considered with its baseband equivalent system model shown in Fig. 1. At the transmit end, one bit stream is split into N_t branches by a serial-to-parallel

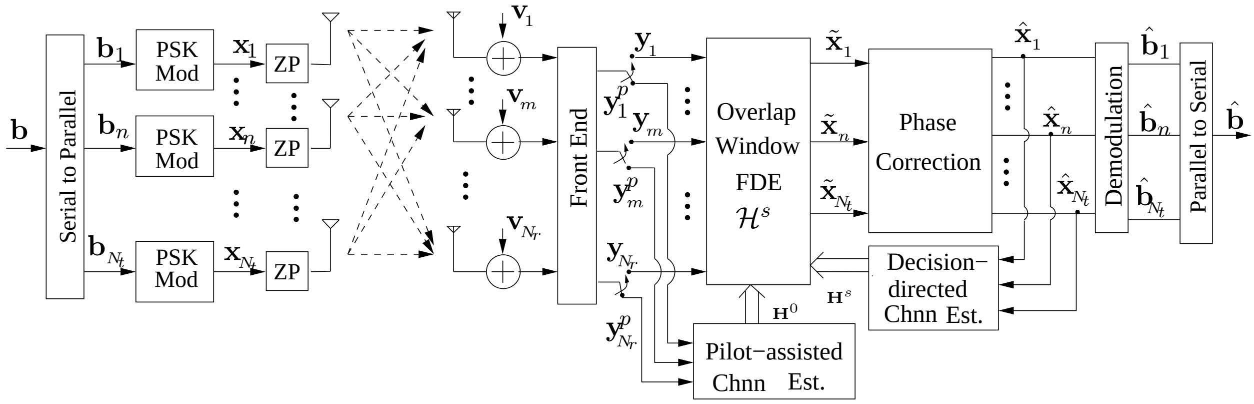

Figure 1 The diagram for the proposed MIMO UWA SC-FDE system with SM architecture.

(S/P) converter, and the bit stream of each branch is mapped to phase shift keying (PSK) modulated data symbols grouped into data blocks. Generally, in radio frequency communications, either CP or pseudo noise (PN) sequence is appended for each block to avoid IBI and make channel matrices circulant. However, in UWA communications, padding zeros to each block is usually adopted to play the same role and to save transmit power [18]. The zero-padded N_t data streams are transmitted simultaneously and independently over the underwater acoustic channels at the same carrier frequency. At the receiver end, the received signals are first pre-processed by a front-end component which consists of a bandpass filter to remove out-of-band noise, a synchronizer to locate the start of the packet and compensate compression/dilation of waveform, and a demodulator to down-convert the passband signals to baseband signals. Next, the bandwidth-efficient MIMO frequency-domain equalization is performed to mitigate the ISI and cochannel interference (CCI). The phase rotation caused by Doppler spread is compensated by a group-wise phase rotation algorithm. The UWA channels are initially estimated by known pilot symbols and then tracked by a decision-directed method. Finally, the estimated data symbols are demapped to the information bits which are converted to a serial stream by a parallel-to-serial (P/S) converter.

Assuming an oversampling factor γ, the baseband equivalent signals received at the m-th hydrophone are described in (T_s/γ)-spaced sampling (where T_s is the symbol period) as

$$y_m(k) = \sum_{n=1}^{N_t} \sum_{l=1}^{L} h_{m,n}(l,k) x_n(k-l+1) e^{j(2\pi f_{m,n,k} k T_s/\gamma + \theta_{m,n})} + v_m(k), \tag{110}$$

where $y_m(k)$ is the received sample of the m-th hydrophone, $v_m(k)$ is the additive Gaussian noise with an average power of σ^2, and $h_{m,n}(l,k)$ is the composite impulse response of the baseband equivalent channel linking the n-th transducer and the m-th hydrophone, combining the effects of the transmit pulse-shaping filter, the physical time-varying channel response, and the receive matched filter [26]; L is the channel memory length in terms of sample period, $x_n(k)$ is the transmitted signal from the n-th transducer at sampling time instant k, $f_{m,n,k}$ is the time-varying instantaneous Doppler drift, and $\theta_{m,n}$ is the phase error after symbol synchronization.

Let N and N_{zp} denote the payload data block length and zero padding length, respectively. At the receiver, discrete Fourier transform (DFT) with the size $\gamma N_x = \gamma(N + N_{zp})$ is performed to convert the time-domain signal to frequency domain. Define two length-(γN_x) vectors $\mathbf{y}_m$ and $\mathbf{v}_m$ as the received signal and the additive noise at the m-th hydrophone, respectively,

$$\mathbf{y}_m = \begin{bmatrix} y_m(1) & \cdots & y_m(\gamma N) & y_m(\gamma N+1) & \cdots & y_m(\gamma N_x) \end{bmatrix}^T \tag{111}$$

$$\mathbf{v}_m = \begin{bmatrix} v_m(1) & \cdots & v_m(\gamma N) & v_m(\gamma N+1) & \cdots & v_m(\gamma N_x) \end{bmatrix}^T \tag{112}$$

Correspondingly, the length-(γN_x) oversampled and zero-padded signal vector of the n-th transducer is defined as

$$\mathbf{x}_n = \begin{bmatrix} x_n(1) & \underbrace{0\cdots0}_{\gamma-1} & x_n(2) & \underbrace{0\cdots0}_{\gamma-1} & \cdots & x_n(N) & \underbrace{0\cdots0\;0\cdots0}_{\gamma(N_{zp}+1)} \end{bmatrix}^T. \tag{113}$$

Then the system model is approximately expressed in matrix format as

$$\begin{bmatrix} \mathbf{y}_1 \\ \vdots \\ \mathbf{y}_{N_r} \end{bmatrix} = \begin{bmatrix} \mathbf{C}_{1,1}\mathbf{h}_{1,1} & \cdots & \mathbf{C}_{1,N_t}\mathbf{h}_{1,N_t} \\ \vdots & \ddots & \vdots \\ \mathbf{C}_{N_r,1}\mathbf{h}_{N_r,1} & \cdots & \mathbf{C}_{N_r,N_t}\mathbf{h}_{N_r,N_t} \end{bmatrix} \begin{bmatrix} \mathbf{x}_1 \\ \vdots \\ \mathbf{x}_{N_t} \end{bmatrix} + \begin{bmatrix} \mathbf{v}_1 \\ \vdots \\ \mathbf{v}_{N_r} \end{bmatrix}, \tag{114}$$

where $\mathbf{C}_{m,n}$ is a diagonal matrix with phase rotation on its diagonal entries

$$\mathbf{C}_{m,n}{=}e^{j(\theta_{m,n})} \cdot \mathrm{diag}\Big\{e^{j2\pi f_{m,n,1}(T_s/\gamma)}, \quad \cdots, \quad e^{j2\pi f_{m,n,\gamma N_x}(N_x T_s)}\Big\}, \tag{115}$$

and $\mathbf{h}_{m,n}$ is a matrix of size $(\gamma N_x) \times (\gamma N_x)$ corresponding to the (m,n)-th channel impulse response which is given by (116).

If the block time duration $T_b = N_x T_s$ is less than the channel coherence time τ_c, then the time variation of CIR is negligible within the block and $\mathbf{h}_{m,n}$ approximates a circulant matrix.

Define the block DFT matrix $\mathbf{B}_{N_r} = \mathbf{I}_{N_r} \otimes \mathbf{F}_{\gamma N_x}$, where $\otimes$ denotes the Kronecker product, and $\mathbf{F}_{\gamma N_x}$ represents the normalized DFT matrix of size $(\gamma N_x)\times(\gamma N_x)$. Multiplying $\mathbf{B}_{N_r}$ on both sides of (114), we obtain the FD representation as (117).

$$\mathbf{h}_{m,n}{=} \begin{bmatrix} h_{m,n}(1,1) & 0 & \cdots & 0 & h_{m,n}(L,1) & \cdots & h_{m,n}(2,1) \\ h_{m,n}(2,2) & h_{m,n}(1,2) & 0 & \ddots & \ddots & \ddots & \vdots \\ \vdots & \ddots & \ddots & \ddots & \ddots & \ddots & h_{m,n}(L,L-1) \\ h_{m,n}(L,L) & \ddots & \ddots & h_{m,n}(1,L) & 0 & \ddots & 0 \\ 0 & h_{m,n}(L,L{+}1) & \ddots & \ddots & \ddots & \ddots & \vdots \\ \vdots & \ddots & \ddots & \ddots & \ddots & \ddots & 0 \\ 0 & \cdots & 0 & h_{m,n}(L,\gamma N_x) & \cdots & \cdots & h_{m,n}(1,\gamma N_x) \end{bmatrix} \tag{116}$$

$$\begin{bmatrix} \mathbf{Y}_1 \\ \vdots \\ \mathbf{Y}_{N_r} \end{bmatrix} {=} \begin{bmatrix} \mathbf{G}_{1,1}\mathbf{H}_{1,1} & \cdots & \mathbf{G}_{1,N_t}\mathbf{H}_{1,N_t} \\ \vdots & \ddots & \vdots \\ \mathbf{G}_{N_r,1}\mathbf{H}_{N_r,1} & \cdots & \mathbf{G}_{N_r,N_t}\mathbf{H}_{N_r,N_t} \end{bmatrix} \begin{bmatrix} \mathbf{X}_1 \\ \vdots \\ \mathbf{X}_{N_t} \end{bmatrix} + \begin{bmatrix} \mathbf{V}_1 \\ \vdots \\ \mathbf{V}_{N_r} \end{bmatrix}, \tag{117}$$

where $\mathbf{Y}_m = \mathbf{F}_{\gamma N_x}\mathbf{y}_m$, $\mathbf{X}_n = \mathbf{F}_{\gamma N_x}\mathbf{x}_n$, $\mathbf{V}_m = \mathbf{F}_{\gamma N_x}\mathbf{v}_m$, $\mathbf{H}_{m,n} = \mathbf{F}_{\gamma N_x}\mathbf{h}_{m,n}\mathbf{F}^H_{\gamma N_x}$, and $\mathbf{G}_{m,n} = \mathbf{F}_{\gamma N_x}\mathbf{C}_{m,n}\mathbf{F}^H_{\gamma N_x}$. The frequency-domain channel response matrix $\mathbf{H}_{m,n}$ is diagonal due to the circulant property of $\mathbf{h}_{m,n}$, and the i-th diagonal component is calculated by $H_{m,n}(i) = \sum_{l=1}^{L} h_{m,n}(l, \frac{\gamma N_x}{2})\exp\Big(- \frac{j2\pi(l-1)(i-1)}{\gamma N_x}\Big)$. Although $\mathbf{G}_{m,n}$ is generally a non-diagonal matrix, the diagonal elements of $\mathbf{G}_{m,n}$ are significant comparing to the non-diagonal elements if the block duration T_b is less than one third of the quantity $1/\max(f_{m,n,k})$. This condition is satisfied if $T_b < \tau_c$ because $\tau_c \ll 1/\max(f_{m,n,k})$ for fixed-to-fixed UWA channels. Hence, $\mathbf{G}_{m,n}$ is a diagonally dominant matrix which can be approximated as a diagonal matrix with identical diagonal elements being

$$\mathbf{G}_{m,n}(i,i) = \frac{1}{\gamma N_x} \sum_{k=1}^{\gamma N_x} e^{j(2\pi f_{m,n,k} k T_s/\gamma + \theta_{m,n})}, \quad i = 1, 2, \cdots, \gamma N_x. \tag{118}$$

III. CHANNEL ESTIMATION, EQUALIZATION AND PHASE CORRECTION

A. Channel Estimation and Tracking. The accuracy of channel estimation and the capability of tracking the time-varying channels have significant impact on the performance of receiver. To achieve accurate channel estimation, fixed-length pilot symbols are inserted at the beginning of each large data block to provide initial estimation of channel impulse responses, and the estimated channel CIR is used to detect a small subblock of data following the pilot block. To track the channel variations, the CIRs are then re-estimated by the detected symbols in every subblock without inserting additional known pilot symbols. Both pilot-assisted and decision-directed channel estimation use the time-domain least square (TD-LS) method. Zero padding and pilot block are inserted in every large block to avoid error propagation.

Let the pilot samples of the n-th transducer be $x_{t_n}(1), \cdots, x_{t_n}(i), \cdots, x_{t_n}(\gamma N_p - L + 1)$, where N_p is the number of transmitted pilot symbols per block. The time-domain channel impulse response for the m-th hydrophone can be estimated as

$$\hat{\mathbf{g}}_m = \mathbf{x}_p^{\dagger} \cdot \mathbf{y}_{mp} = [\hat{\mathbf{g}}_{m,1}^T, \hat{\mathbf{g}}_{m,2}^T, \cdots, \hat{\mathbf{g}}_{m,N_t}^T]^T \tag{119}$$

where $\hat{\mathbf{g}}_{m,n} = [\hat{h}_{m,n}(1), \cdots, \hat{h}_{m,n}(L)]^T$, $\mathbf{x}_p = [\mathbf{P}_1 | \mathbf{P}_2 | \cdots | \mathbf{P}_{N_t}]$ with

$$\mathbf{P}_n = \begin{bmatrix} x_{t_n}(L) & x_{t_n}(L-1) & \cdots & x_{t_n}(1) \\ x_{t_n}(L+1) & x_{t_n}(L) & \cdots & x_{t_n}(2) \\ \vdots & \ddots & \ddots & \vdots \\ x_{t_n}(\gamma N_p) & x_{t_n}(\gamma N_p - 1) & \cdots & x_{t_n}(\gamma N_p - L + 1) \end{bmatrix} \tag{120}$$

and $\mathbf{y}_{mp} = [y_{mp}(L), \cdots, y_{mp}(\gamma N_p)]^T$ is the corresponding MIMO channel output vector.

For channel tracking, the detected symbols, rather than additional pilot symbols, are used to re-estimate the CIRs using the same LS method. Just replace the pilot symbols $x_{t_n}(i)$ in (120) by the detected symbols after channel equalization and phase rotation.

B. Overlapped-Window Frequency-Domain Equalization. In this section, we introduce the overlapped-window frequency-domain equalization which is implemented based on the overlap-save method, and the detailed processing strategy is shown in Fig. 2. The data block with a large block size N is divided into small subblocks, and each subblock has a length N_s. Thus, there are totally $M = \lceil N/N_s \rceil$ subblocks for one data block. If N/N_s is not an integer, then zeros are padded to the last subblock to make its size to be N_s. An overlapped data window is used to compose the input data for the equalization. It contains the last K_1 points of the previous subblock, the N_s points of the current subblock, and the first K_2 points of the subsequent subblock. The K_1 points of the previous subblock and the K_2 points of the subsequent subblock are saved in the overlap window to mitigate the precursor and postcursor interference. The size of FFT is the length of overlapped window $N_f = N_s + K_1 + K_2$. After performing the FDE on the overlapped window, the desired equalized subblock data $\tilde{\mathbf{x}}_n^s, \;\; n = 1, \cdots, N_t, \; s = 1, \cdots, M$, are obtained by discarding the first K_1 and the last K_2 symbols of the overlap window. It is assumed that the channel frequency responses keep invariant in the duration of overlapped window because $N_f T_s$ is smaller than the channel coherence time. As a result, the frequency-domain channel matrices of all the sub-channels for the s-th subblock $\mathbf{H}_{m,n}^s, \; m = 1, \cdots, N_r,$ and $n = 1, \cdots, N_t$, are diagonal matrices. We also define $\lambda_{m,n}^s = \frac{1}{\gamma N_f} \sum_{k=1}^{\gamma N_f} e^{j(2\pi f_{m,n,k}^s k T_s/\gamma + \theta_{m,n})}$ as the phase distortion caused by Doppler drift and synchronization, which is a complex-valued unknown parameter with its amplitude close to one. Now, based on the estimated channel transfer functions, we define $\mathcal{H}^s$ as

$$\mathcal{H}^s = \begin{bmatrix} \lambda_{1,1}^s \hat{\mathbf{H}}_{1,1}^s & \cdots & \lambda_{1,N_t}^s \hat{\mathbf{H}}_{1,N_t}^s \\ \vdots & \ddots & \vdots \\ \lambda_{N_r,1}^s \hat{\mathbf{H}}_{N_r,1}^s & \cdots & \lambda_{N_r,N_t}^s \hat{\mathbf{H}}_{N_r,N_t}^s \end{bmatrix}. \tag{121}$$

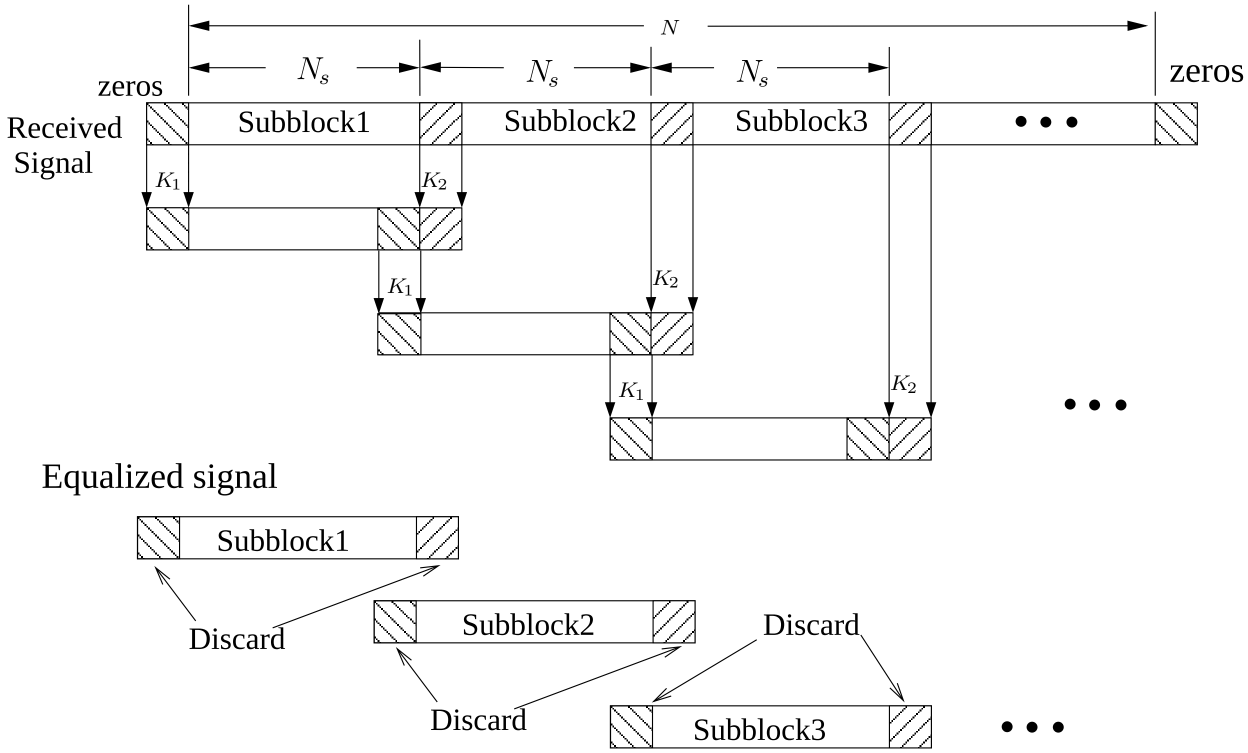

Figure 2 Data structure for overlapped-window FDE

Applying the linear minimum mean square error (LMMSE) criterion, we obtain the frequency-domain equalized subblock data as

$$\begin{bmatrix} \check{\mathbf{X}}_{1,s} \\ \vdots \\ \check{\mathbf{X}}_{N_t,s} \end{bmatrix} = \mathcal{H}^{s^H} (\mathcal{H}^s \mathcal{H}^{s^H} + \sigma^2 \mathbf{I}_{\gamma N_f N_r})^{-1} \begin{bmatrix} \mathbf{Y}_{1,s} \\ \vdots \\ \mathbf{Y}_{N_r,s} \end{bmatrix}, \tag{122}$$

where the $\mathbf{I}_{\gamma N_f N_r}$ is an unit matrix with size $\gamma N_f N_r \times \gamma N_f N_r$, (γN_f)-point vector $\mathbf{Y}_{m,s}$ is the frequency-domain representation of the s-th subblock of the current block received at the m-th hydrophone, and $\check{\mathbf{X}}_{n,s}$ is the estimation of $\mathbf{X}_{n,s}$ which is the frequency-domain representation of the corresponding subblock at the n-th transducer. Since received data is sampled at the γ/T_s rate, the time-domain symbols at the $1/T_s$ sampling rate are obtained by aliasing in frequency domain as

$$\check{\mathbf{X}}_{n,s}^{'} = \mathcal{O}(\check{\mathbf{X}}_{n,s}) = \sum_{\mu=1}^{\gamma} \mathbf{A}_{n,s}^{\mu}, \tag{123}$$

where $\mathcal{O}(\cdot)$ denotes aliasing function, and $\mathbf{A}^{\mu}_{n,s} = \check{\mathbf{X}}_{n,s}(\mu N_f - N_f + 1 : \mu N_f)$ which represents a vector consisting of the $(\mu N_f - N_f + 1)$-th to the (μN_f)-th row of $\check{\mathbf{X}}_{n,s}$. It has been demonstrated [28] that the equalized data $\check{\mathbf{X}}_{n,s}$ can be represented in frequency domain as

$$\check{\mathbf{X}}_{n,s} \approx \Big(\sum_{m=1}^{N_r} \boldsymbol{\Delta}^s_{m,n} \mathbf{G}^s_{m,n}\Big) \mathbf{X}_{n,s} + \hat{\mathbf{V}}_{n,s}, \tag{124}$$

where $\boldsymbol{\Delta}^s_{m,n}$ is approximately a diagonal matrix related to the channel response and equalizer coefficients, and $\mathbf{G}^s_{m,n}$ is a diagonal dominant matrix defined in (117). Then applying the N_f-point IFFT to the aliased equalized data vector $\check{\mathbf{X}}^{'}_{n,s}$ yields the time-domain data vector $\check{\mathbf{x}}^{'}_{n,s}$ as

$$\begin{aligned}
\check{\mathbf{x}}^{'}_{n,s} &= \mathbf{F}^H_{N_f} \check{\mathbf{X}}^{'}_{n,s} = \sum_{m=1}^{N_r} \mathbf{F}^H_{N_f} \mathcal{O}\big(\boldsymbol{\Delta}^s_{m,n} \mathbf{G}^s_{m,n} \mathbf{X}_{n,s}\big) + \mathbf{F}^H_{N_f} \mathcal{O}(\hat{\mathbf{V}}_{n,s}) \\
&= \sum_{m=1}^{N_r} \mathbf{F}^H_{N_f} \mathcal{O}\big(\boldsymbol{\Delta}^s_{m,n} \mathbf{G}^s_{m,n}\big) \mathcal{O}\big(\mathbf{X}_{n,s}\big) + \mathbf{F}^H_{N_f} \mathcal{O}(\hat{\mathbf{V}}_{n,s}) \\
&= \sum_{m=1}^{N_r} \mathbf{F}^H_{N_f} \mathcal{O}\big(\boldsymbol{\Delta}^s_{m,n} \mathbf{G}^s_{m,n}\big) \mathbf{F}_{N_f} \mathbf{x}^{'}_{n,s} + \hat{\mathbf{v}}^{'}_{n,s},
\end{aligned} \tag{125}$$

where $\mathbf{x}^{'}_{n,s}$ and $\hat{\mathbf{v}}^{'}_{n,s}$ are the T_s-spaced transmitted signal vector and error vector, respectively. By discarding the first K_1 symbols and the last K_2 symbols of the equalized overlapped window, the desired equalized symbols of the s-th subblock for the n-th antenna, denoted by $\tilde{\mathbf{x}}_{n,s}$, can be obtained by

$$\tilde{\mathbf{x}}_{n,s} = \check{\mathbf{x}}^{'}_{n,s}(K_1 + 1 : N_f - K_2). \tag{126}$$

Since $\mathcal{O}(\boldsymbol{\Delta}^s_{m,n} \mathbf{G}^s_{m,n})$ is a diagonal-dominant matrix and the subblock length is much smaller than the channel coherence time, all the non-diagonal elements of $\mathbf{F}^H_{N_f} \mathcal{O}\big(\boldsymbol{\Delta}^s_{m,n} \mathbf{G}^s_{m,n}\big) \mathbf{F}_{N_f}$ are insignificant comparing to its diagonal elements. Therefore, the k-th equalized data symbol in the s-th subblock of the n-th transducer is expressed by

$$\begin{aligned}
\tilde{x}_{n,s}(k) = & \left[\sum_{m=1}^{N_r} |\beta^s_{m,n}(k)| e^{j\angle \beta^s_{m,n}(k)}\right] x^{'}_{n,s}(k) + \hat{v}^{'}_{n,s}(k) \\
= & \; |\alpha_{n,s}(k)| e^{j\angle \alpha_{n,s}(k)} x^{'}_{n,s}(k) + \hat{v}^{'}_{n,s}(k), \qquad k = 1, \cdots, N_s,
\end{aligned} \tag{127}$$

where $\alpha_{n,s}(k) = \sum_{m=1}^{N_r} \beta_{m,n}^s(k)$ with $\beta_{m,n}^s(k)$ being the kth diagonal element of the matrix $\mathbf{F}_{N_f}^H \mathcal{O}\big(\boldsymbol{\Delta}_{m,n}^s \mathbf{G}_{m,n}^s\big)\mathbf{F}_{N_f}$, and k is the time index in T_s spaced.

From (127), we can conclude that the equalized data symbol $\tilde{x}_{n,s}(k)$ is approximately an amplitude-scaled and phase-rotated version of the transmitted data symbol $x_{n,s}^{'}(k)$. When $x_{n,s}^{'}(k)$ is a PSK-modulated symbol, the time-varying rotating phase $\angle\alpha_{n,s}(k)$ must be compensated before detection.

As shown in equation (122), the computation of the LMMSE frequency-domain equalizer becomes difficult as the subblock length N_f and the number of receiver antennas N_r increase because it requires the inverse of a large matrix with size $(\gamma N_r N_f) \times (\gamma N_r N_f)$. However, utilizing the diagonal property of $\mathbf{H}_{m,n}^s$ and taking into account that $\mathbf{G}_{m,n}^s$ is diagonal dominant, we can obtain a much more computationally efficient LMMSE frequency-domain equalization as

$$\begin{bmatrix} \check{X}_{1,s}(i) \\ \vdots \\ \check{X}_{N_t,s}(i) \end{bmatrix} = \mathcal{H}_i^{s^H} (\mathcal{H}_i^s \mathcal{H}_i^{s^H} + \sigma^2 \mathbf{I}_{N_r})^{-1} \begin{bmatrix} Y_{1,s}(i) \\ \vdots \\ Y_{N_r,s}(i) \end{bmatrix}, \tag{128}$$

where $i = 1, \cdots, \gamma N$ and

$$\mathcal{H}_i^s = \begin{bmatrix} \lambda_{1,1}^s H_{1,1}^s(i) & \cdots & \lambda_{1,N_t}^s H_{1,N_t}^s(i) \\ \vdots & \ddots & \vdots \\ \lambda_{N_r,1}^s H_{N_r,1}^s(i) & \cdots & \lambda_{N_r,N_t}^s H_{N_r,N_t}^s(i) \end{bmatrix}. \tag{129}$$

It is noted from (128) that the matrix inversion of an $\gamma N_r N_f \times \gamma N_r N_f$ matrix is decomposed into the matrix inversions of γN_f matrices with size of $N_r \times N_r$, so that the LMMSE frequency-domain equalization can be employed on each frequency bin. The computational complexity is significantly reduced from $O(\gamma^3 N_f^3 N_r^3)$ to $\gamma N_f \cdot O(N_r^3)$. This is also the computational savings of FDE over time-domain equalization.

C. The Group-wise Phase Correction Algorithm. As described in (127), the rotating phase $\angle\alpha_{n,s}(k)$ represents a nonlinearly composite effect of Doppler spreads and channel impulse responses, which is very difficult to estimate directly. A common approach of correcting the phase rotation adopted in UWA communications is to track the phase symbol by symbol using a second-order PLL or delay-locked loop (DLL) combined with a decision feedback equalizer (DFE). However, this approach is usually sensitive to channels and noise. Here, we present an effective and robust algorithm based on groups of symbols when correcting the phase rotations $\angle\alpha_{n,s}(k)$. Since the phase rotations are estimated by taking average on the phase deviation in group-wise way, the algorithm is less sensitive to noise perturbations.

Since the instantaneous Doppler shift $f_{m,n,k}$ varies gradually over a short period of time, the rotating phase also changes slowly and smoothly over time. Each equalized subblock is partitioned into N_g groups, and each group has $N_b = N_s/N_g$ symbols. The initial phase rotation for the subblock is same as the phase rotation of the last group of the previous subblock. For the first subblock, the initial phase rotation is obtained by the P pilot symbols. Let $\psi_{n,s}^{p-1}$ denote the average phase rotation for the $(p-1)$-th group of the s-th subblock, then correcting the phase rotation for the p-th group as

$$\hat{x}_{n,s}^{p}(k) = \tilde{x}_{n,s}((p-1)N_b + k)e^{-j\psi_{n,s}^{p-1}}, \quad k = 1, \cdots, N_b. \tag{130}$$

Let $\Delta\psi_{n,s}^{p}$ denote average phase deviation between the equalized symbols and modulated symbols for the p-th group, then the phase rotation for the p-th group of the s-th subblock is estimated in a decision-directed way given by

$$\psi_{n,s}^{p} = \psi_{n,s}^{p-1} + \Delta\psi_{n,s}^{p} = \psi_{n,s}^{p-1} + \frac{1}{N_b}\sum_{k=1}^{N_b}(\angle\tilde{x}_{n,s}^{p}(k) - \mathcal{Q}[\angle\tilde{x}_{n,s}^{p}(k)]) \tag{131}$$

where $\mathcal{Q}[\phi]$ is defined as a phase quantization function for Q-ary PSK modulation

$$\mathcal{Q}[\phi] = \frac{(q-1)2\pi}{Q}, \quad \text{if} \quad \frac{q2\pi - 3\pi}{Q} \leq \phi \leq \frac{q2\pi - \pi}{Q}, \quad q = 1, \cdots, Q. \tag{132}$$

The phase correction algorithm is proceeding until the last group, and the phase rotation for the last group is recorded for the phase correction of the next subblock. Finally, the phase corrected data symbols are demodulated by the maximum likelihood (ML) detector to recover the binary information bit. At the same time, the phase corrected data symbols are also used to re-estimate the channel impulse responses which are provided to the equalization of the next subblock.

IV. FIELD TEST RESULTS FROM THE RACE08 EXPERIMENT

The proposed bandwidth-efficient receive algorithm has been tested by the real-word experimental data and the results are presented here. The experimental data was collected during RACE in Narragansett Bay, Rhode Island, conducted by Woods Hole Oceanographic Institution (WHOI), in March 2008. Two receivers were located at 400 meters and 1000 meters away from the transmitter. The receivers were equipped with 12 hydrophones, located two meters above the bottom of sea, and the transmitter was mounted with two transducers, located four meters above the bottom of sea. The water depth varied between 9 to 14 meters. The carrier frequency $f_c = 11.5$ kHz, the sampling rate $f_s = 39.0625$ kHz, and the bandwidth $B = f_s/10 = 3.90625$ kHz. Binary information bits without coding schemes were mapped into QPSK symbols which were grouped into blocks with a size of $N = 2048$ and $N_{zp} = 40$ zeros are padded to each block. The frame structure for each transducer is shown in Fig. 3, where the m-sequence with a length of 511 was adopted to synchronize the data frames. The received data were downsampled at the rate $\gamma = 2$ after down-converting passband to baseband signals. Hence, the accuracy of synchronization was increased due to the multiple samples per symbol, and $2N_f$-point FFT was employed in the equalizer to improve the BER performance [27]. A pilot block with length $N_p = 150$ at the beginning of each data

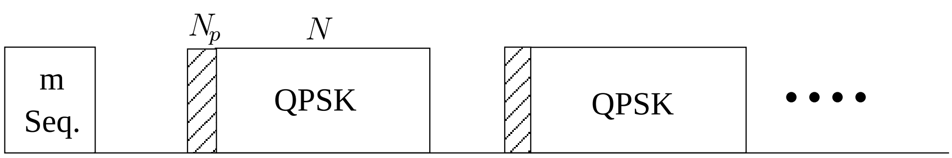

Figure 3 Frame structure of the transmitted data

block was used to initially probe the channels. The transmission overhead is defined as $\frac{N_{zp}+N_p}{N+N_{zp}+N_p} \times 100\%$. Therefore, the overhead of the proposed FDE scheme is only 8.4%, which is significantly reduced compared with more than 20% overhead of other UWA OFDM and SC-FDE systems.

To accurately track the channel variation, the proposed scheme set the length of each subblock to $N_s = 200$, thus, one data block was separated into 11 subblocks. The channels spanned 25 symbol periods, and the lengths of precursor and postcursor of the overlapped window were selected as $K_1 = K_2 = 40$ symbols. The time-varying channel impulse responses (CIRs) of the 1000 m system over long term and short term (one block duration) are shown in Fig. 4. In Fig. 4(a) and Fig. 4(c), the 2-dimensional time-varying CIRs within five seconds are depicted for the subchannels linking two transducers with one hydrophone. As seen from the two figures, the position of the dominant path component changes with time, and the amplitudes of CIRs also changes significantly with time. Fig. 4(b) and Fig. 4(d) show the amplitudes of CIRs of the 5-th and 10-th subblocks, respectively, which are estimated by pilot symbols. It is seen that the amplitude of CIRs varies fasteven within one data block duration. Similarly, in Fig. 5, the amplitudes of CIRs for the 400 m system are depicted over long term and short term, and they all exhibit fast time-varying property of the channels. Due to less attenuation caused by the shorter range communications, the amplitudes of CIRs of the 400 m system are larger than that of the 1000 m system. For both systems, our decision-directed channel estimation method effectively tracks the variations of the channels.

Applying the estimated channels in FDE, scatter plots of the equalized and phase corrected data symbols for one block are shown in Fig. 6. The channels estimated by pilot symbols are used in Fig. 6(a), and the equalized symbols can not be separated well in the scatter plot. The phases of equalized symbols are slightly rotated due to the small Doppler spread. During the processing of the experimental data, we found that the instantaneous Doppler spread in the received data is not significant (-1.5 Hz $\sim$ 1.5 Hz), which results in small phase rotations on the equalized symbols. However, the phase correction algorithm was still applied to correct some phase errors to further lower decision errors. Fig. 6(b) shows the phase corrected symbols, where the channels are estimated by the proposed method. There are clear boundary between modulated symbols to make decisions. We can see that

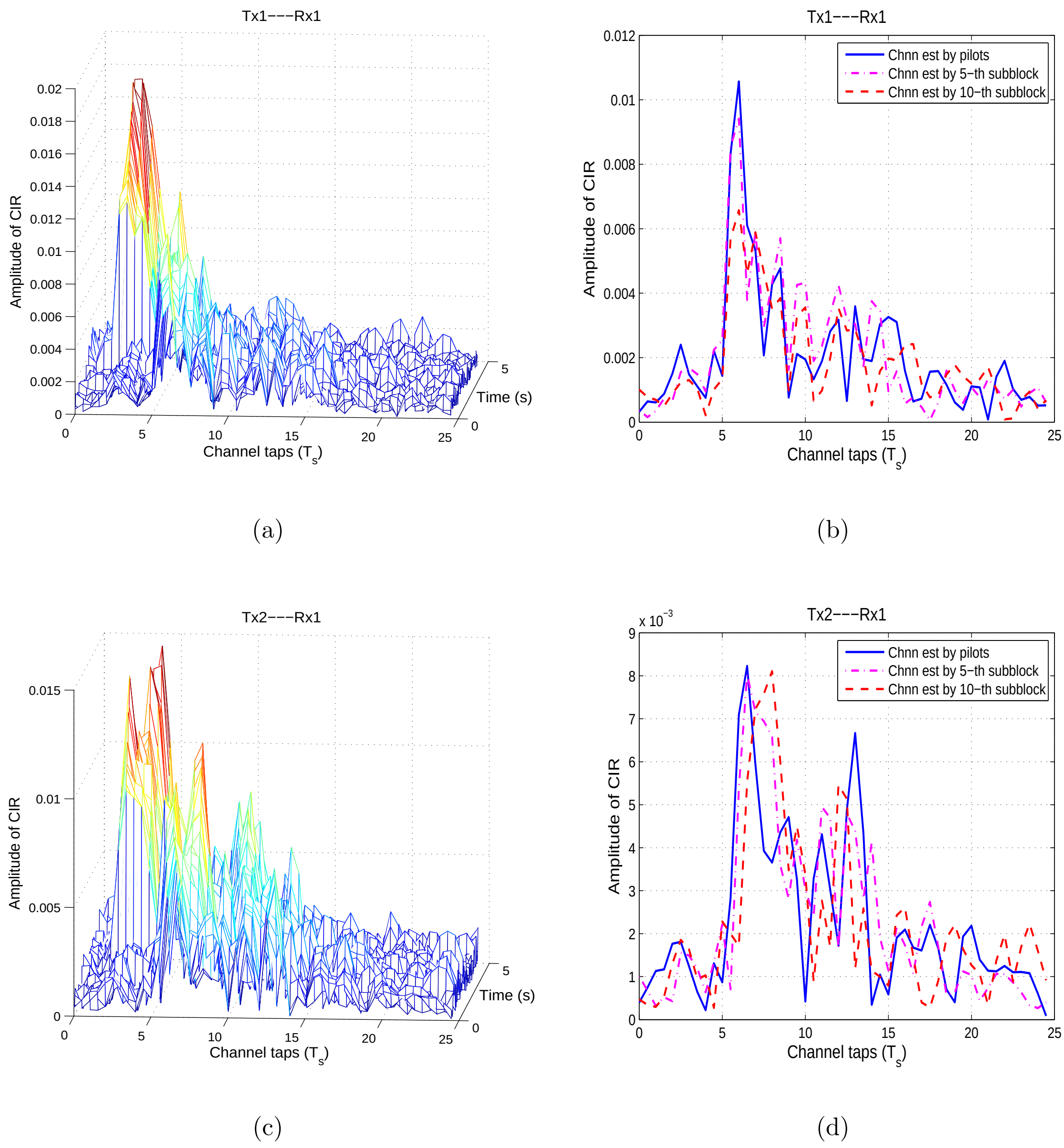

Figure 4 Amplitude of time-varying CIRs for the 1000 m system. (a) The 2D CIR for the subchannel Tx1—Rx1. (b) The CIRs in one block duration for the subchannel Tx1—Rx1. (c) The 2D CIR for the subchannel Tx2—Rx1. (d) The CIRs in one block duration for the subchannel Tx2—Rx1.

the time-varying channels have more effect on the equalized symbols than the time-varying Doppler spread in this experiment.

The uncoded bit error rates (BERs) and error reduction rate of the proposed receive algorithm are shown in Table 1 for the 400 m system and Table 2 for the 1000 meter system. For each system, 10 representative data packets were processed, and each packet had totally

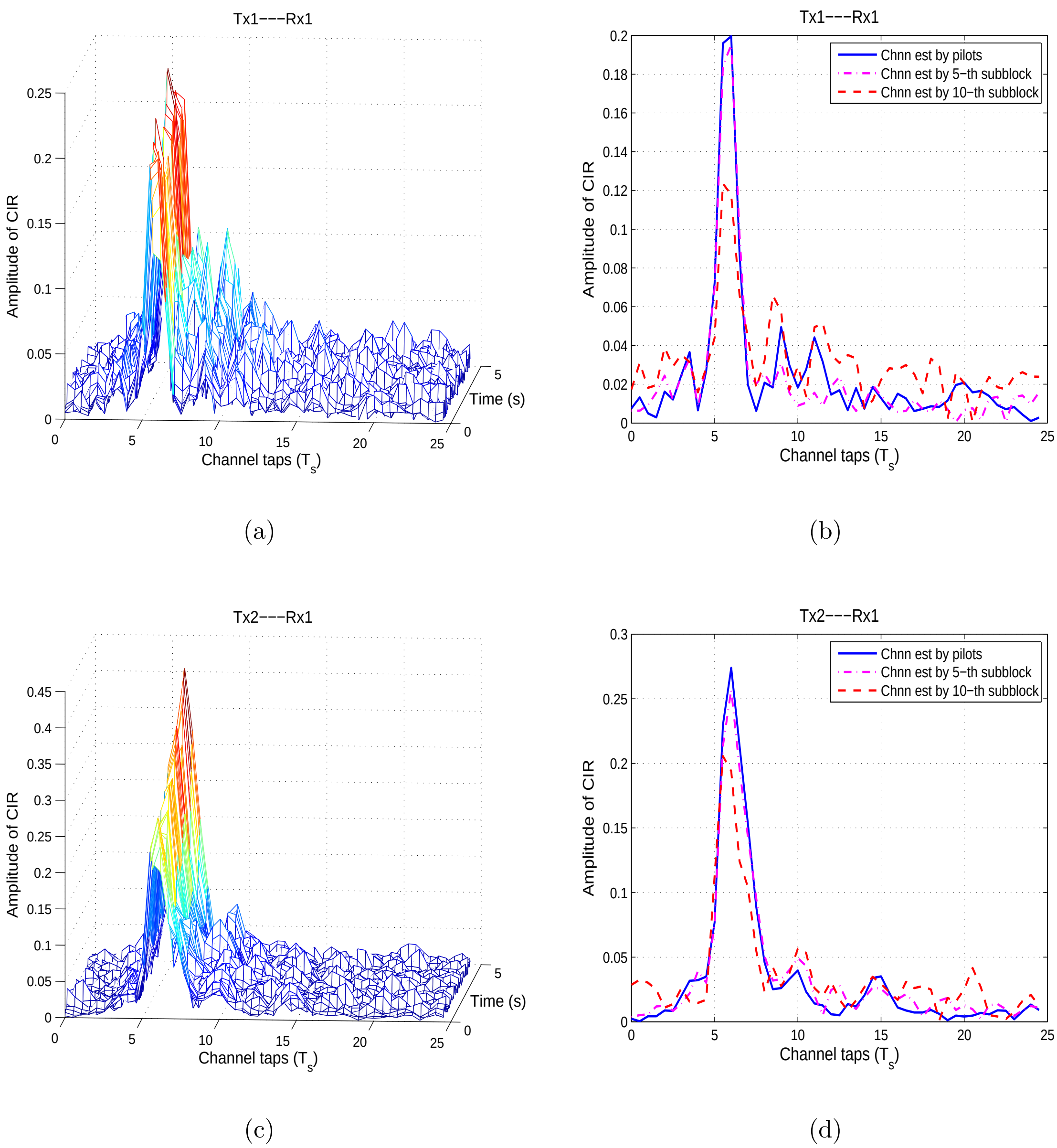

Figure 5 Amplitude of time-varying CIRs for the 400 m system. (a) The 2D CIR for the subchannel Tx1—Rx1. (b) The CIRs in one block duration for the subchannel Tx1—Rx1. (c) The 2D CIR for the subchannel Tx2—Rx1. (d) The CIRs in one block duration for the subchannel Tx2—Rx1.

65536 information bits transmitted. For comparison, the performance of the traditional FDE method which performs FDE on the whole data block using the channels estimated by pilot symbols were also included. We can see that the proposed algorithm outperforms the traditional FDE method with more than 70% reduction of average bit errors for these two range systems.

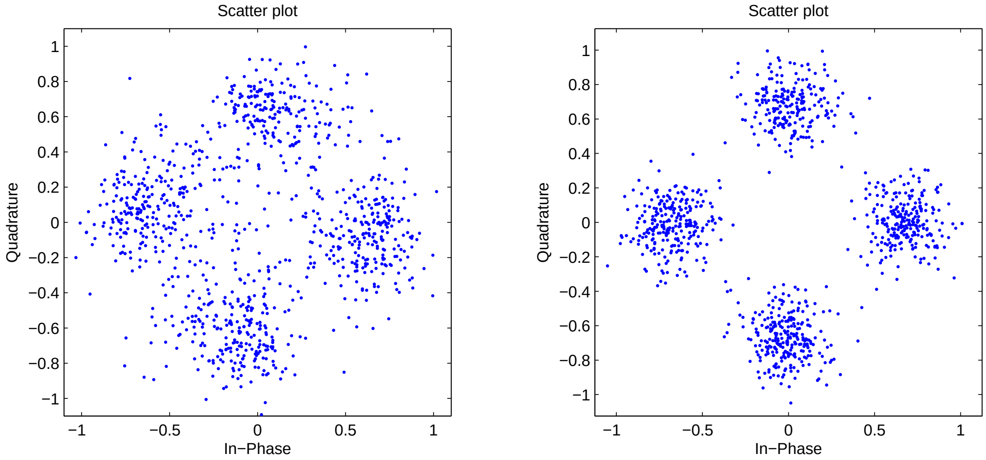

(a) (b)

Figure 6 (a) Scatter plot of equalized symbols (b) Scatter plot of equalized and phase-corrected symbols.

Table 1 Uncoded BER of QPSK-2048 blocks for 400 m system

Identifier of packet	Traditional FDE method	Proposed FDE method	Error Reduction
0791756F06_C0_S4	0.0836	0.0189	77.4%
0791756F06_C1_S4	0.1081	0.0199	81.6%
0792156F06_C0_S4	0.0487	0.0112	77.0%
0800156F06_C1_S4	0.0855	0.0269	68.5%
0800556F06_C0_S4	0.0154	0.0042	72.7%
0800556F06_C1_S4	0.0194	0.0051	73.7%
0801356F06_C1_S4	0.0920	0.0341	63.0%
0810956F06_C0_S4	0.0229	0.0069	69.8%
0811356F06_C0_S4	0.0890	0.0159	82.1%
0821756F06_C1_S4	0.0060	0.0013	78.3%
Avg.	0.0563	0.0144	74.4%

Figure 7 shows the scatter plots of phase-corrected symbols for one block at different subblock sizes. It is seen that the phase-corrected symbols cannot be separated clearly for large subblock size. However, when smaller subblock sizes are employed, the symbols much more focus the transmitted symbols and have distinct boundaries to make decision. It is understandable because using smaller size of subblock tracks the time-varying channels better than large subblock size. Besides, the average uncoded BERs under different subblock

Table 2 Uncoded BERs of QPSK-2048 blocks for 1000 m system

Identifier of packet	Traditional FDE method	Proposed FDE method	Error Reduction
0791355F06_C0_S6	0.0792	0.0085	89%
0800158F06_C0_S6	0.0559	0.0078	86%
0801355F06_C0_S6	0.0345	0.0025	92.7%
0791755F06_C0_S6	0.1006	0.0183	81.8%
0810955F06_C0_S6	0.0224	0.0031	86.1%
0820155F06_C0_S6	0.0399	0.0070	82.4%
0840955F06_C0_S6	0.0002	$3.0518e-5$	84.7%
0810155F06_C0_S6	0.0415	0.0083	80%
0810955F06_C0_S6	0.0216	0.0027	87.5%
0841755F06_C0_S6	0.0076	0.0018	76.3%
Avg.	0.0403	0.0060	84.6%

sizes were also evaluated for the two range systems, depicted in Fig. 8. There were 30 successfully received data packets for each range system, and the average uncoded BER over all available packets is calculated as the performance index. As expected, the performance becomes worse as the subblock size N_s increases. When $N_s = N$, the algorithm is equivalent to the traditional FDE, which has inferior performance. Small size of subblock leads to better performance for fast time-varying channels at expense of complexity of re-estimating channels. In practice, the size of subblock can be determined by the channel coherence time which reflects time-varying rate of channels, while taking account of complexity issues.

V. CONCLUSION

A bandwidth-efficient FDE scheme with decision-directed channel estimation has been proposed for SC MIMO UWA communications. The proposed scheme greatly increases the data efficiency by employing large transmission blocks with low overhead on pilot block and zero padding and improves symbol detection and channel tracking by the overlapped-window FDE method and decision-directed channel estimation. This FDE scheme significantly improves the system performance with slightly increased computational complexity. The scheme has been applied to process undersea data collected during the RACE08 ocean experiments conducted in March 2008. The average uncoded BER of QPSK modulation and 2048 block length achieves 1.4% for the 400 m range system and 0.6% for the 1000 m

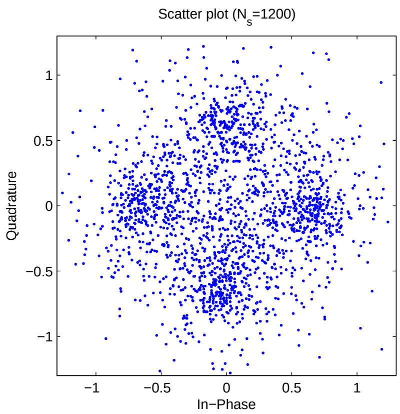

(a) $N_s = 1200$

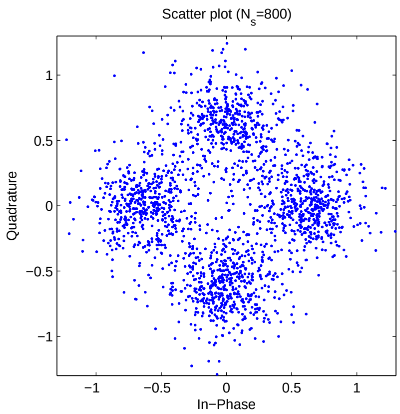

(b) $N_s = 800$

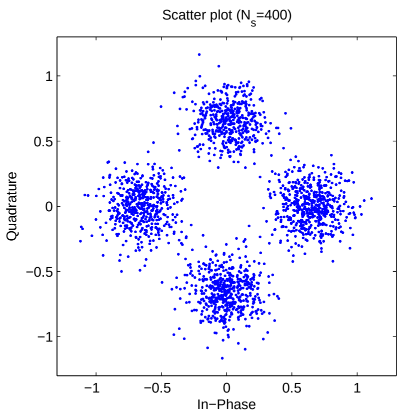

(c) $N_s = 400$

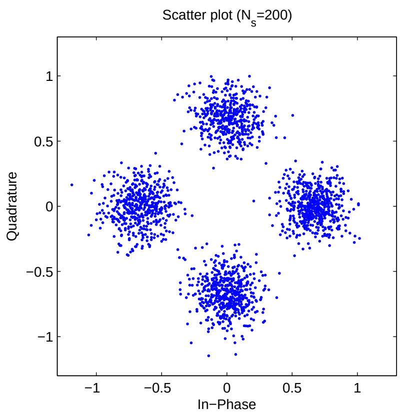

(d) $N_s = 200$

Figure 7 Scatter plots for the overlapped-window FDE scheme with different subblock sizes. The smaller the subblock size, the better the performance demonstrating better channel tracking and equalization.

range system with approximately one third of transmission overhead of traditional FDEs. Compared with traditional FDEs with the same bandwidth efficiency, the proposed scheme achieves error reduction rates from 63% to 93%.

VI. REFERENCES

[1] M. Stojanovic, "Recent advances in high-speed underwater acoustic communications," IEEE J. Ocean. Eng. **21**, 125-136 (1996).

[2] D. B. Kilfoyle and A. B. Baggeroer, "The state of the art in underwater acoustic telemetry," IEEE J. Ocean. Eng. **25**, 4-27 (2000).

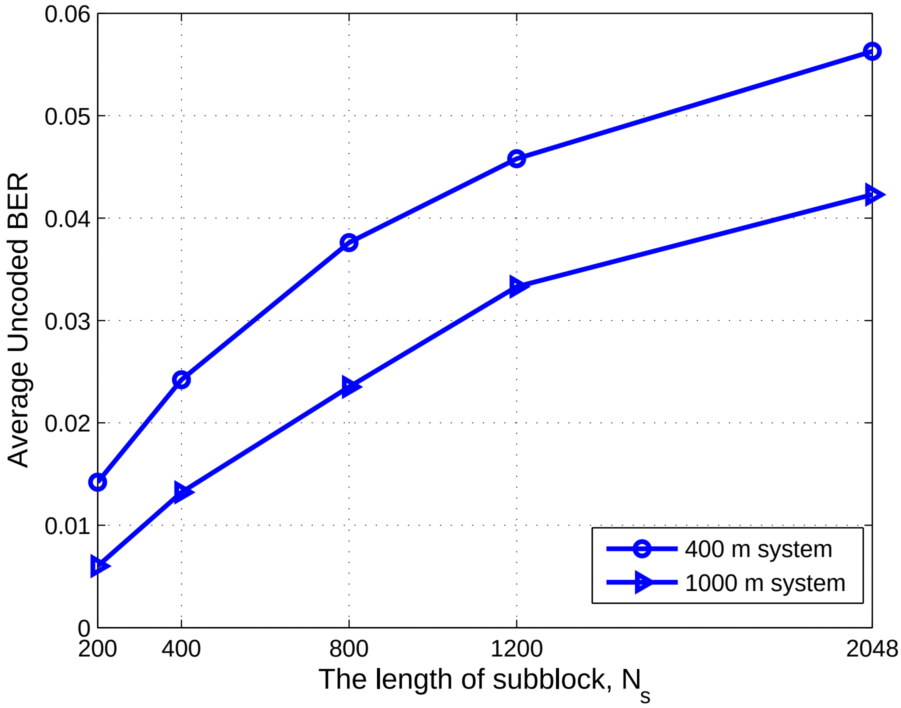

Figure 8 Average uncoded BER v.s. subblock size N_s

[3] M. Stojanovic and J. Preisig, "Underwater acoustic communication channels: propagation models and statistical characterization," IEEE Commun. Mag., 84-89 (2009).

[4] A. C. Singer, J. K. Nelson, S. S. Kozat, "Signal processing for underwater acoustic communications," IEEE Commun. Mag. 90-96 (2009).

[5] M. Stojanovic, J. Catipovic, and J. Proakis, "Adaptive multichannel combining and equalization for underwater acoustic communication signals," J. Acoust. Soc. America **94**, 1621-1631 (1993).

[6] M. Stojanovic, J. Catipovic, and J. Proakis, "Phase-coherent digital communicaitons for underwater acoustic channels," IEEE J. Ocean. Eng. **19**, 100-111 (1994).

[7] M. Stojanovic, J. Catipovic, and J. Proakis, "Reduced comlexity spatial and temporal processing of underwater acoustic communication signals," J. Acoust. Soc. America **98**, 961-972 (1995).

[8] J. C. Preisig, "Performance analysis of adaptive equalization for coherence acoustic communications in the time-varying ocean environment," J. Acoust. Soc. America **118**, 263-278 (2005).

[9] T. C. Yang, "Performance comparisons between passive-phase conjugation and decision-feedback equalizer for underwater acoustic communications," J. Acoust. Soc. America **115**, 2505-2506 (2004).

[10] J. C. Preisig, "Coherent equalization for underwater acoustic communications: a performance evaluation of adaptive MMSE and time-reversal techniques,"J. Acoust. Soc. America **112**, 2420 (2002).

[11] S. Roy, T. M. Duman, V. McDonald, and J. Proakis, "High rate communication for underwater acoustic channels using multiple transmitters and space-time coding: receiver structures and experimental results," IEEE J. Ocean. Eng. **32**, 663-688 (2007).

[12] J.P.Gomes and M.Stojanovic, "Performance Analysis of Filtered Multitone Modulation Systems for Underwater Communication," Proceedings of IEEE Oceans'09 (2009), Biloxi, Mississippi, USA.

[13] B. Li, S. Zhou, M. Stojanovic, L. Freitag, and P. Willet, "Multicarrier communication over underwater acoustic channels with nonuniform Doppler shifts," IEEE J. Ocean. Eng. **33**, 198-209 (2008).

[14] B. Li, S. Zhou, M. Stojanovic, L. Freitag, J. Huang, and P. Willett, "MIMO-OFDM over an underwater acoustic channel," Proceedings of IEEE Oceans'07 (2007).

[15] Y. R. Zheng, C. Xiao, T. C. Yang, and W. B. Yang, "Frequency-domain channel estimation and equalization for single carrier underwater acoustic communications," MTS/IEEE Int. Oceans Conf. (2007), Vancouver, Canada.

[16] J. Zhang, Y. R. Zheng, and C. Xiao, "Frequency-domain equalization for single carrier MIMO underwater acoustic communications," Proceedings of IEEE OCEANS'08 (2008), Quebec city, Canada.

[17] Y. R. Zheng, "Channel estimationg and phase-correction for robust underwater acoustic communictions," Proceedings of IEEE Military Commun. Conf. (2007), Orlando.

[18] N. Benvenuto, R. Dinis, D. Falconer, and S. Tomasin, "Single carrier modulation with nonlinear frequency domain equalization: an idea whose time has come-again," Proceedings of the IEEE **98**, 69-96 (2010).

[19] D. Kim and G. Stüber, "Residual ISI cancellation for OFDM with applications to HDTV broadcasting," IEEE J. Sel. Areas in Commun. **16**, 1590-1599, (1998).

[20] H. Liu and P. Schniter, "Iterative frequency-domain channel estimation and equalization for single-carrier transmission without cyclic-prefix," IEEE Trans. on Wireless Commun. **7**, 3686-3691, (2008).

[21] B. Li, J. Huang, S. Zhou, K. Ball, M. Stojanovic, L. Freitag, and P. Willett, "MIMO-OFDM for high rate underwater acoustic communications," *IEEE J. Ocean. Eng.*, **34**, 634–644, Oct. (2009).

[22] C. R. Berger, S. Zhou, J. C. Preisig, and P. Willett, "Sparse channel estimation for multicarrier underwater acoustic communicatioin: From subspace methods to compressed sensing," *IEEE Trans. Signal Proc.*, **58**, 1708–1721, Mar. (2010).

[23] J. G. Proakis, C. M. Rader, F. Ling, C. L. Nikias, M. Moonen, and I. K. Proudler, *Algorithms for statistical signal processing*, Prentice Hall (2002).

[24] A. V. Oppenheim and R. W. Schafer, *Digital signal processing*, New Jersey: Prentice-Hall (1975).

[25] C. Xiao and Y. R. Zheng, "Channel equalization and symbol detection for single carrier broadband MIMO systems with multiple carrier frequency offsets," Proceedings of IEEE ICC08 (2008), Beijing, China.

[26] C. Xiao, J. Wu, S.-Y. Leong, Y. R. Zheng, and K. B. Letaief, "A discrete-time model for triply selective MIMO Rayleigh fading channels," IEEE Trans. Wireless Commun.**3**, 1678-1688 (2004).

[27] M. V. Clark, "Adaptive frequency-domain equalization and diversity combining for broadband wireless communications," IEEE J. Select Areas Commun. **16**, 1385-1395 (1998).

[28] J. Zhang, Y. R. Zheng, C. Xiao, and K. B. Lataief, "Channel Equalization and Symbol detection for single carrier MIMO systems in the presence of multiple carrier frequency offsets," IEEE Trans. Veh. Technol. **59**, 2021-2030 (2010).

SECTION

2. CONCLUSIONS

This dissertation solves four key problems in single carrier frequency-domain equalization for MIMO communication systems: FD channel estimation, CFO mitigation, iterative FD turbo equalization, and bandwidth-efficient FDE. These algorithms have been demonstrated not only by computer simulations, but also by ocean experiments. acoustic communications and tested in practical experimental environment. They achieve excellent performance in estimation of time-varying channels and elimination of CFOs induced by Doppler shift and mismatch of local oscillator, implement a low bit error rate underwater receiver robust to noise and bad channel conditions, and implement an underwater SC-FDE system with high data transmission efficiency.

The contributions of all my research work during PhD study are summarized in five journal papers and eight conference papers, among which, four journal papers and one conference paper are included in this dissertation. The complete publication list is included in Section

Future work may lie in the following several aspects: (1) analyze the statistical characteristics of underwater acoustic channels, including the PDF of channel coefficients, inter-tap correlation and spatial correlation, etc, and evaluate the effect of these statistics of channels on the system performance. (2) employ more powerful channel coding schemes, e.g. low-density parity-check (LDPC) code and turbo trellis coded modulation (TTCM) in the turbo equalization to improve the performance. (3) investigate adaptive channel estimation algorithms with fast convergence rate and good performance and apply these adaptive algorithms to estimate underwater channels to reduce the length of training sequence and achieve good BER performance.

3. PUBLICATIONS

[1] J. Zhang, Y. R. Zheng, C. Xiao, and K. B. Letaief, "Channel equalization and symbol detection for single carrier MIMO systems in the presence of multiple carrier frequency offsets," *IEEE Transaction on Vehicular Technology*, vol.59, pp.2021-2030, May 2010.

[2] J. Zhang and Y. R. Zheng, "Improved frequency domain channel estimation and equalization for MIMO wireless communications," *International Journal of Wireless Information Networks*, vol.16, pp.12-21, June 2009.

[3] J. Zhang and Y. R. Zheng, "Bandwidth-Efficient Frequency-domain equalization for single carrier MIMO underwater acoustic communications," will be published by *Journal of the Acoustic Society of America*, Oct. 2010.

[4] J. Zhang and Y. R. Zheng, "Frequency-domain turbo equalization with soft-successive interference cancellation for single carrier MIMO underwater acoustic communications," *IEEE Transaction Wireless Communication*, in revision, June 2010.

[5] J. Zhang and Y. R. Zheng, "Joint frequency-domain multiuser turbo equalization with successive interference cancellation for triply-selective fading channels," submitted to *Wireless Personal Communications*.

[6] J. Zhang, J. Cross, and Y. R. Zheng, "Statistical characteristics of underwater acoustic channel impulse response,"*IEEE MilCom'10*, Oct. 2010, San Jose, CA, USA.

[7] J. Zhang and Y. R. Zheng, "Bandwidth efficient frequency-domain equalization for MIMO underwater acoustic communications," in *Proc. MTS/IEEE Oceans'10*, May 2010, Sydney, Australia.

[8] J. Zhang and Y. R. Zheng, "Layered frequency-domain turbo equalization for single carrier broadband MIMO systems," in *IEEE International Conference on Communications (ICC'10)*, May 2010, Cape Town, South Africa.

[9] J. Zhang and Y. R. Zheng, "Layered frequency-domain equalization for single carrier MIMO systems with multiple carrier frequency offsets," in *Proc. IEEE GlobeCom'09*, Hawaii, USA, Dec. 2009.

[10] J. Zhang, Y. R. Zheng, and C. Xiao, "Frequency-domain turbo equalization for MIMO underwater acoustic communications," in *Proc. MTS/IEEE OCEANS'09*, Bremen, Germany, May 11-14, 2009.

[11] J. Zhang, Y. R. Zheng, and C. Xiao, "Frequency-domain equalization for single carrier MIMO underwater acoustic communications," in *Proc. MTS/IEEE OCEANS'08*, Quebec City, Canada, Sep. 2008.

[12] Y. R. Zheng and J. Zhang, "Improved frequency-domain channel estimation for fast time-varying MIMO-SCFDE channels," in *IEEE International Conference on Communications (ICC'08)*, May 2008, Beijing, China.

[13] Y. Liu, J. Zhang, and Y. R. Zheng, "Simulation of doubly-selective compound K fading channels for mobile-to-mobile communications," in *IEEE Wireless Communications and Networking Conference (WCNC'08)*, Las Vegas, USA, Mar. 2008.

VITA

Jian Zhang was born January 18, 1980 in Taiyuan, Shanxi Province, China. He received his B.S. degree in 2002 and M.S. degree in 2005, both in Electrical Engineering from University of Electronic Science and Technology of China, Chengdu, Sichuan Province, China. He began Ph.D. study in January 2007 at the Department of Electrical and Computer Engineering at Missouri University of Science and Technology. His research interests include radio frequency/underwater acoustic wireless communications, channel coding theory, and digital signal processing. He is expected to receive his Ph.D. degree in Electrical Engineering from Missouri University of Science and Technology in December 2010.